

© 2014 by Osman Sarood. All rights reserved.

OPTIMIZING PERFORMANCE UNDER THERMAL AND POWER CONSTRAINTS  
FOR HPC DATA CENTERS

BY

OSMAN SAROOD

DISSERTATION

Submitted in partial fulfillment of the requirements  
for the degree of Doctor of Philosophy in Computer Science  
in the Graduate College of the  
University of Illinois at Urbana-Champaign, 2014

Urbana, Illinois

Doctoral Committee:

Professor Laxmikant V. Kalé, Chair

Professor Tarek Abdelzaher

Professor Maria Garzaran

Doctor Bronis de Supinski, Lawrence Livermore National Laboratory

# Abstract

Energy, power and resilience are the major challenges that the HPC community faces in moving to larger supercomputers. Data centers worldwide consumed energy equivalent to 235 billion kWh in 2010. A significant portion of that energy and power consumption is devoted to cooling. This thesis proposes a scheme based on a combination of limiting processor temperatures using Dynamic Voltage and Frequency Scaling (DVFS) and frequency-aware load balancing that reduces cooling energy consumption and prevents hot spot formation. Recent reports have expressed concern that reliability at the exascale level could degrade to the point where failures become a norm rather than an exception. HPC researchers are focusing on improving existing fault tolerance protocols to address these concerns. Research on improving hardware reliability has also been making progress independently. A second component of this thesis tries to bridge this gap and explore the potential of combining both software and hardware aspects towards improving reliability of HPC machines. Finally, the 10MW consumption of present day HPC systems is certainly becoming a bottleneck. Although energy bills will significantly increase with machine size, power consumption is a hard constraint that must be addressed. Intel's Running Average Power Limit (RAPL) toolkit is a recent feature that enables power capping of CPU and memory subsystems on modern hardware. The ability to constrain the maximum power consumption of the subsystems below the vendor-assigned Thermal Design Point (TDP) value allows us to add more nodes in an overprovisioned system while ensuring that the total power consumption of the data center does not exceed its power budget. The final component of this thesis proposes an interpolation scheme that uses an application profile to optimize the number of nodes and distribution of power between CPU and memory subsystems that minimizes execution time under a strict power budget. We also present a resource management scheme including a scheduler that uses CPU power capping, hardware overprovisioning, and job malleability to improve the throughput of a data center under a strict power budget.

*To my parents and wife for their continuous support.*

# Acknowledgments

*Both of you can not do PhD and raise kids.* This is what most people told my wife and I when we started doing PhD and had kids. My super-wife is the sole reason behind my PhD. How many wives have completed a PhD, took care of a husband and raised 2 kids all at the same time? I remember her taking care of our new born and our 2 year old daughter immediately after her C-section while I had to go for work. I would never be able to repay her for that!

It was my parents determination that brought me to the US to pursue higher studies. I still remember their kind words that made me believe in myself. My father sacrificed his career in order to spare time for me, while my mother would spend her nights praying to Allah (God) for my success. I still remember her standing with me on my PhD defense and saying: *6 saal sey iss din ka intezar kiya* (I have waited 6 years for this day). My grand father, Prof. Anjum Roomani, also played a very vital role in my studies and upbringing. May he rest in peace. I would also thank my brother, Omer Sarood, for supporting me to go for graduate studies. I also owe a lot to my sister, Amna Sarood, who has been praying for both my wife and I throughout our PhD. I like to thank my friends Musa, Rana, and Ghufraan for taking care of my parents while I was in the US.

I thank Prof. Laxmikant Kalé for being a generous and helping advisor. He taught me so many things from paper writing to exploring groundbreaking ideas. His emphasis on experimental work is something that greatly contributed to the quality of my work. Besides my advisor, I thank Prof. Bronis de Supinski and Prof. Maria Garzaran for serving on my doctoral committee and providing valuable perspectives on improving the dissertation.

I would like to thank my internship supervisor Barry Rountree, who played a key role towards the end of my thesis. Barry introduced me to the wonderful world of mathematical modeling and linear programming which facilitated the latter part of my research.

I would sincerely like to thank Prof. Tarek Abdelzaher for allowing us to use the Power

and Energy clusters. Without getting access to these clusters this thesis would not have been possible.

I am privileged to have worked with some of the most competent people in the world, i.e. my lab mates. I spent hours talking to most of them and learnt a lot from them. Esteban is a very good team player and I loved discussing my work with him. Some of our discussions led to very good projects. Akhil is a very smart person and would point out problems that most people would fail to identify. I owe a lot of credit to Phil for helping me out with my experimental work. Jonathan and Nikhil are both very competent and wonderful people to interact with. I enjoyed co-authoring a lot of papers with Abhishek due to his reliability. Lukasz, Dave, Abhinav, Eric, Isaac, and Pritish helped me during my initial days at the PPL. Harshitha and Ram were gentle colleagues with whom I had a lot of discussions about raising kids. I will miss discussing my power related work with Ehsan. The new generation of PPLers, Mike, Ronak, Bilge remind me of my early days. I would like to thank JoAnne for writing all those numerous HR related letters for me.

During my stay at Urbana-Champaign I was blessed to have the company of some amazing people. This town won't have been so much fun for me without Azeem *bhai* and Qazi *bhai*. I would miss all those night-long discussions we had. Syed Usman Ali is the most lively person I have ever met. I would miss playing cricket in the South Quad, especially alongside Ahmad Qadir.

Last but not least, I would like to thank everyone I met at Urbana during my stay. I may not remember their names but they made a difference in one of the most exciting adventures of my life.

# Grants

This work was partially supported by the following sources:

- **HPC Colony II.** This project is funded by the US Department of Energy under grant DOE DE-SC0001845. The Principal Investigator of this project is Terry Jones.
- **Simplifying Parallel Programming for CSE Applications using a Multi-Paradigm Approach.** This project is funded by the National Science Foundation (NSF) under grant NSF ITR-HECURA-0833188. It is a collaborative work between Prof. Laxmikant Kalé, Prof. David Padua and Prof. Vikram Adve.
- **Power/Energy Cluster.** This project is funded by the National Science Foundation (NSF) under grant NSF CNS 09- 58314. The Principal Investigator of this project is Prof. Tarek Abdelzaher.

# Table of Contents

List of Figures . . . . .	ix
List of Tables . . . . .	xii
List of Algorithms . . . . .	xiii
CHAPTER 1 Introduction . . . . .	1
1.1 Thesis Organization . . . . .	3
CHAPTER 2 Thermal Restraint Using Migratable Objects . . . . .	5
2.1 Related Work . . . . .	6
2.2 Limiting Temperatures . . . . .	8
2.3 Charm++ and Load Balancing . . . . .	10
2.4 ‘Cool’ Load Balancer . . . . .	12
2.5 Experimental Setup . . . . .	15
2.6 Constraining Core Temperatures and Timing Penalty . . . . .	17
2.7 Energy Savings . . . . .	23
2.8 Tradeoff in Execution Time and Energy Consumption . . . . .	32
CHAPTER 3 Thermal Restraint and Reliability . . . . .	35
3.1 Related Work . . . . .	36
3.2 Implications of Temperature Control . . . . .	37
3.3 Approach . . . . .	42
3.4 Experiments . . . . .	47
3.5 Projections . . . . .	55
CHAPTER 4 Optimizing Performance Under a Power Budget . . . . .	60
4.1 Related Work . . . . .	62
4.2 Approach . . . . .	62
4.3 Setup . . . . .	65
4.4 Case Study: Lulesh . . . . .	65
4.5 Results . . . . .	69



CHAPTER 5	Job Scheduling Under a Power Budget . . . . .	79
5.1	Related work . . . . .	80
5.2	Data Center and Job Capabilities . . . . .	81
5.3	The Resource Manager . . . . .	82
5.4	Strong Scaling Power Aware Model . . . . .	87
5.5	Experimental Results . . . . .	90
5.6	Large Scale Projections . . . . .	97
CHAPTER 6	Concluding Remarks . . . . .	107
6.1	Thermal Restraint . . . . .	107
6.2	Power Constraint . . . . .	109
APPENDIX A	Machine Descriptions . . . . .	112
APPENDIX B	Benchmark Descriptions . . . . .	114
REFERENCES	. . . . .	117

# List of Figures

1.1	Mean Time Between Failures (MTBF) for different numbers of sockets using different MTBF per socket. . . . .	2
1.2	Power consumption and theoretical peak performance for supercomputers from the Top500 (blue circles). The proposed Exascale machine under a power budget of 20MW (red square). . . . .	3
2.1	Average core temperatures and maximum difference of any core from the average for <i>Wave2D</i> . . . . .	9
2.2	Execution time and energy consumption for <i>Wave2D</i> running at different CRAC set-points using DVFS . . . . .	10
2.3	Our DVFS and load balancing scheme successfully keeps all processors within the target temperature range of 47°–49° C, with a CRAC set-point of 24.4° C. . . . .	18
2.4	Execution timing penalty with and without Temperature Aware Load Balancing . . . . .	19
2.5	Execution timelines before and after Temperature Aware Load Balancing for <i>Wave2D</i> . . . . .	20
2.6	Minimum core frequencies produced by DVFS for different applications at 24.4° C . . . . .	21
2.7	Average core frequencies produced by DVFS for different applications at 24.4° C . . . . .	21
2.8	Average frequency of processors for Jacobi2D using <i>TempLDB</i> . . . . .	22
2.9	Utilization of processors for Jacobi2D using <i>TempLDB</i> . . . . .	22
2.10	Frequency sensitivity of the various applications . . . . .	23
2.11	Machine and cooling power consumption for no-DVFS runs at a 12.2°C set-point and various <i>TempLDB</i> runs . . . . .	25
2.12	Savings in cooling energy consumption with and without Temperature Aware Load Balancing (higher is better) . . . . .	27
2.13	Change in machine energy consumption with and without Temperature Aware Load Balancing (values less than 1 represent savings) . . . . .	28
2.14	Normalized machine energy consumption for different frequencies using 128 cores . . . . .	30

2.15	The time <i>Wave2D</i> spent in different frequency levels . . . . .	30
2.16	Total power draw for the cluster using <i>TempLDB</i> at CRAC set-point of 24.4°C . . . . .	31
2.17	Power consumption of two applications as their DVFS settings stabilize to a steady state . . . . .	31
2.18	Timing penalty and energy savings of <i>TempLDB</i> and <i>RefineLDB</i> com- pared to naive DVFS . . . . .	32
2.19	Normalized time against normalized total energy for a representative sub- set of applications . . . . .	33
3.1	Histogram of max temperature for each node of the cluster using <i>Wave2D</i> .	38
3.2	Effect of cooling down processors on MTBF of the system . . . . .	39
3.3	Dynamic power management and resilience framework. . . . .	47
3.4	Reduction in execution time for different temperature thresholds . . . . .	50
3.5	Execution time penalty for DVFS . . . . .	53
3.6	Gains/cost of increasing reliability for different temperature thresholds . . .	54
3.7	Reduction in machine energy consumption for all applications . . . . .	56
3.8	Execution time reduction for all applications at large scale . . . . .	57
3.9	Projected efficiency for <i>Wave2D</i> . . . . .	58
3.10	Reduction in execution time for different memory sizes of an exascale machine . . . . .	59
4.1	Average time per step of <i>Lulesh</i> for configurations selected in Step 1 . . . . .	66
4.2	Average time per step of <i>Lulesh</i> after interpolation (Step 2) . . . . .	68
4.3	Speedups obtained using CPU and memory power capping in an over- provisioned system . . . . .	69
4.4	Observed speedups using different number of profile configurations (points) as input to our interpolation scheme . . . . .	72
4.5	Optimized CPU and memory power caps under different power budgets compared to the maximum CPU and memory power drawn in the baseline experiments . . . . .	73
4.6	Optimal number of nodes under different total power budgets . . . . .	74
4.7	Speedups over the case of $p_c = 25W$ for different number of nodes ( $n$ ) . . . .	74
4.8	Measured CPU and memory power for two different configurations with significantly different power allocations but similar execution time . . . . .	76
4.9	Speedups for power capping both CPU and memory (C&M) compared to CPU (C) only . . . . .	77
4.10	Estimated speedups for different base powers in case of $P=800W$ . . . . .	77
5.1	A high level overview of PARM . . . . .	83
5.2	Integer Linear Program formulation of PARM scheduler . . . . .	85
5.3	Model estimates (line) and actual measured (circles) execution times for all applications as a function of CPU power (a-e). Modeled power aware speedups for all applications (f). . . . .	92

5.4	Modeled (lines) and observed (markers) power aware speedups for four applications . . . . .	93
5.5	(a) Average completion times, and (b) average response times for SetL and SetH with SLURM and noSE, wSE versions of PARM. (c) Average number of nodes and average CPU power in the wSE and noSE versions of PARM. . . . .	96
5.6	Average completion times of baseline, <i>noSE</i> and <i>wSE</i> . Job arrival times in all the sets (Set1, Set2, Set3) were scaled down by factor $\gamma$ to get diversity in job arrival rate . . . . .	100
5.7	Reduction in job arrival times while maintaining the same QoS as the baseline scheduler . . . . .	103
5.8	Average completion times for Set 1 for different values of ( $\alpha$ ) . . . . .	104
5.9	Maximum (worst) completion times for Set 1 for different values of ( $\alpha$ ) . . . . .	104
5.10	CDF for completion times for baseline and wiSE for different $\alpha$ using SET1 . . . . .	105
5.11	Effect of increasing the number of power levels ( $ P_j $ ) on the average completion time of Set 1 ( $\gamma = 0.5$ ). . . . .	106
5.12	Effect of increasing the number of power levels ( $ P_j $ ) on the maximum completion time of Set 1 ( $\gamma = 0.5$ ). . . . .	106

# List of Tables

2.1	Description for variables used in Algorithm 1 . . . . .	13
2.2	Performance counters for Charm++ applications on one core . . . . .	21
3.1	Parameters of the performance model . . . . .	41
3.2	Description for variables used in Algorithm 2 and Algorithm 3 . . . . .	43
3.3	Application parameters for <i>NC</i> case . . . . .	49
3.4	MTBF (sec) for different temperature thresholds (42° C - 54° C) . . . . .	51
4.1	Terminology . . . . .	63
5.1	Integer Linear Program Terminology . . . . .	84
5.2	Obtained model parameters . . . . .	94
5.3	Comparison of the baseline, wSE and noSE scheduling policies for different data sets. . . . .	101
5.4	Comparison of <i>wSE</i> with the baseline scheduler running on an overprovisioned system (at different CPU power caps) using Set 2 ( $\gamma = 0.5$ ) . . . . .	102
A.1	Summary of features of clusters used in this thesis . . . . .	112

# List of Algorithms

1	Temperature Aware Refinement Load Balancing . . . . .	14
2	Temperature Control . . . . .	45
3	Communication Aware Load Balancing . . . . .	46

# Introduction

Computational scientists are among the leading users of high performance computing (HPC). These scientists usually run codes that simulate physical processes. Such simulation codes have an everlasting demand for computational power. In order to satisfy the demands for running these computational models, the HPC community will need to keep advancing their quest for larger machines. Soaring energy consumption, accompanied by declining reliability, together loom as the biggest hurdles for the next generation of supercomputers. As we approach the exascale era, both hardware and software designers will need to account for power, energy, and reliability of the machine while optimizing performance.

The combined energy consumption for data centers worldwide totaled 235 billion kWh in 2010 [1]. Most HPC researchers have been primarily focussing on energy minimization in the past decade [2,3]. The majority of this work is concentrated on reducing machine energy consumption. In this dissertation, we first attack the ‘other’ side of the problem i.e., cooling energy consumption, which can account for up to 50% of the total energy consumption of a data center [4–7]. Chip manufacturers have ceased to increase processor frequency and have resorted to adding more cores on a chip to keep up with the ever increasing demand for faster computers. This stagnation in processor frequency has been caused by a sharp increase in the heat density of chip. Earlier studies show a connection between the operating temperature of a processor and its reliability [8–10]. These studies mention the existence of an exponential relationship between a processor’s temperature and its Mean Time Between Failures (MTBF). Most HPC research focused on energy optimization and machine reliability does not consider the impact of processor temperature. Although thermal considerations have not been a primary concern for recent supercomputers, it can significantly improve MTBF and hence, performance of future supercomputers. An exascale machine is predicted to have more than 200,000 sockets [11]. Recent studies also show that supercomputers can

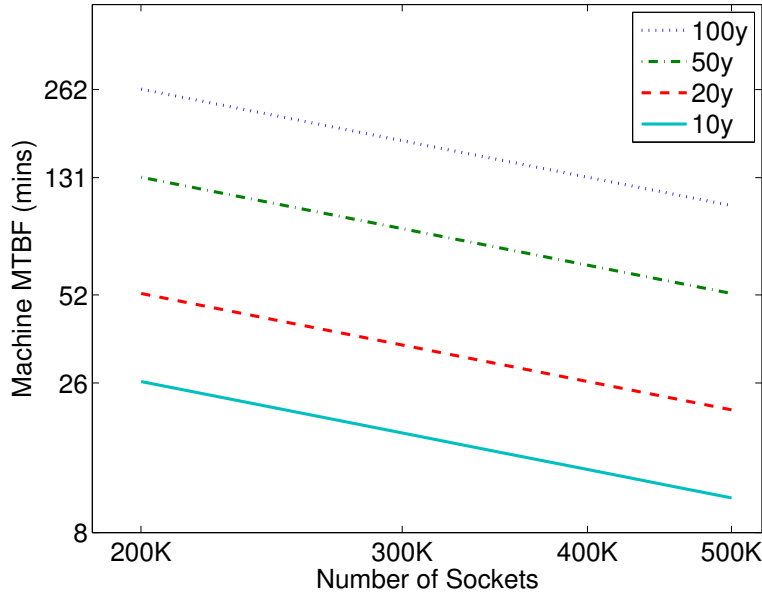


Figure 1.1: Mean Time Between Failures (MTBF) for different numbers of sockets using different MTBF per socket.

have a per socket MTBF as low as 5 years [12]. The implications of such large numbers of sockets coupled with the existing MTBF values per socket are depicted in Figure 1.1. This figure shows the MTBF of large supercomputers for different numbers of sockets and different MTBF per socket. Figure 1.1 shows that with a per socket MTBF of 5 years, a 200K socket machine is likely to fault every 26 mins. Such a high fault rate could have a dramatic effect on machine utilization. On the other hand, a per socket MTBF of 100 years can improve the machine reliability and increase the machine MTBF to 262 mins for a 200K socket machine. This thesis makes an attempt at improving the per socket MTBF of a large machine by using Dynamic Voltage and Frequency Scaling (DVFS) in conjunction with an adaptive runtime system.

Although energy minimization and thermal control are major challenges, in order to reach exascale computing within the 20MW power envelope proposed by the DOE, data centers would have to significantly improve their performance per watt. Figure 1.2 shows the power consumption and the theoretical peak performance of all the supercomputers from the Top500 [13] for which power consumption data is available (blue circles). It also plots the power consumption bound (20MW) set by the DOE for the exascale machine (red box). Given the trend of current supercomputers, it is unlikely that the HPC community will achieve exascale computing within the 20MW power budget. Looking at the data from Figure 1.2, 100MW seems to be a more realistic target to achieve an exaflop. Although



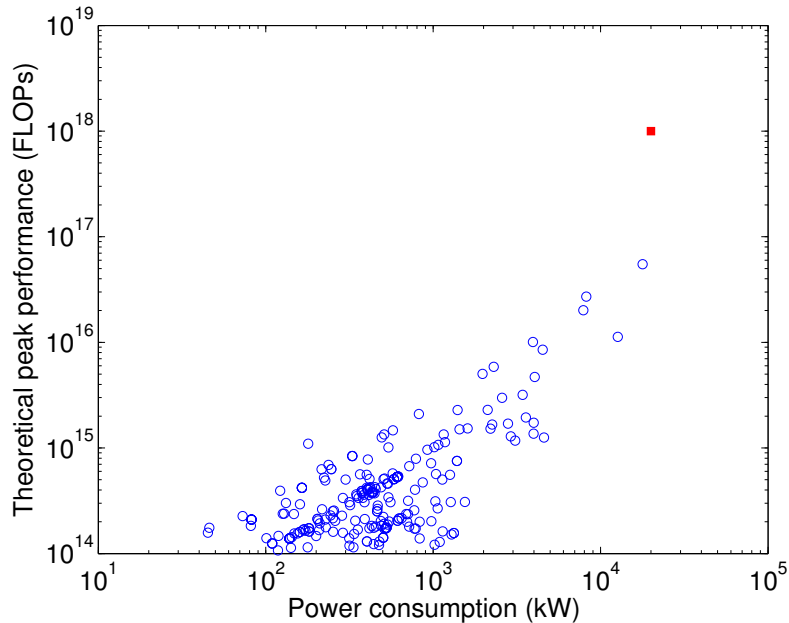


Figure 1.2: Power consumption and theoretical peak performance for supercomputers from the Top500 (blue circles). The proposed Exascale machine under a power budget of 20MW (red square).

hardware advances will be needed to build an exascale machine, efficient runtime techniques are necessary to make the best use of what the hardware will provide.

## 1.1 Thesis Organization

This thesis is organized in three major parts. Part one contains Chapter 2 and Chapter 3. This part demonstrates techniques for controlling core temperature and their impact on performance and reliability. Chapter 2 describes how Dynamic Voltage and Frequency Scaling (DVFS) can restrain processor temperatures and our scheme that uses object migration to minimize the timing penalty associated with DVFS. Chapter 2 further presents the experimental results for restraining processor temperatures using different applications, and demonstrates the reduction in timing penalty as well as energy consumption. It includes a comprehensive discussion about application reaction to thermal restraint. Chapter 3 introduces a novel technique that combines fault tolerance with thermal restraint to improve system reliability. It demonstrates how restraining core temperatures can eventually benefit application performance as a result of improved machine reliability. It also presents the estimated benefits in machine reliability and application performance of using temper-

ature restraint for massively parallel machines running different types of applications. We thank Esteban Meneses for his interest in the research on improving reliability using thermal restraint (Chapter 3). We had a lot of discussions which helped improve the quality of our work. In particular, Esteban’s incisive comments and his mathematical modeling background helped us a great deal.

Part two of the thesis tackles the imminent problem of data center operation under a strict power budget. It contains Chapters 4 and Chapters 5. Operating under a power constraint is a challenging problem as it poses a constraint rather than a restraint which is a less stricter limiting condition. While restraining, we *try* to apply a limit whereas in case of a constraint that limit is strictly enforced. In this part, we use Intel’s Running Average Power Library (RAPL) to cap processor and memory power for overprovisioned systems [14] to improve application performance. Chapter 4 uses RAPL to improve application performance for a single application executing in an overprovisioned system. Chapter 5 proposes a resource management strategy that maximizes job throughput by intelligently scheduling applications with different resource configurations. This chapter also proposes a detailed strong scaling power aware model that can estimate the execution time of an application based on its characteristics for any resource configuration. We thank Akhil Langer for his interest in the research on optimization under strict power budget (Chapter 4 and 5). We had numerous productive discussions during which we gave direction to this work. In particular, his insightful comments, his linear programming background, his work on the SLURM simulator, and clear presentation of the ideas (including writing of the papers) helped us a great deal.

Chapter 6 contains the last part of the thesis which summarizes the contributions of this thesis and possible directions for future work. We outline multiple directions in which we plan to extend our thesis work. The first idea relates to improving machine reliability by taking into account the effects of thermal throttling. The second idea explores the possibility of operating a data center under strict power *and* thermal constraints.

## Thermal Restraint Using Migratable Objects

Energy consumption has emerged as a significant issue in modern high-performance computing systems. Some of the largest supercomputers draw more than 10 megawatts, leading to millions of dollars per year in energy bills. What is perhaps less well known is the fact that 40% to 50% of the energy consumed by a data center is spent in cooling [4], [5], [6], to keep the computer room running at a lower temperature. How can we reduce this cooling energy?

Increasing the thermostat setting on the computer room air-conditioner (CRAC) reduces the cooling power. But the increase in the thermostat will also increase the ambient temperature in the computer room. The reason the ambient temperature is kept cool is to keep processor cores from overheating. If they run at a high temperature for a long time, the processor cores may be damaged. Additionally, cores consume more energy per unit of work when run at higher temperatures [15]. Further, due to variations in the air flow in the computer room, some chips may not be cooled as effectively as the rest. Semiconductor process variation will also likely contribute to variability in heating, especially in future processor chips. So, to handle such ‘hot spots’, the ambient air temperature is kept at a low temperature to ensure that no individual chip overheats.

Modern microprocessors contain on-chip temperature sensors that can be accessed by software with minimal overhead. Further, they also provide means to change the frequency and voltage at which the chip runs, known as *dynamic voltage and frequency scaling*, or DVFS. Running processor cores at a lower frequency (and correspondingly lower voltage) reduces the thermal energy that they dissipate, leading to a cool-down.

This suggests a method for keeping processors cool while increasing the CRAC set-point (i.e. the thermostat setting). A component of the application software can periodically check the temperature of the chip. When it exceeds a pre-set threshold, the software can

reduce the frequency and voltage of that particular chip. If the temperature is lower than a threshold, the software can correspondingly increase the frequency.

This technique will ensure that no processors overheat. However, in HPC computations, and specifically in tightly-coupled science and engineering simulations, DVFS creates a new problem. Generally, computations on one processor are dependent on the data produced by the other processors. As a result, if one processor slows down to half its original speed, the entire computation can slow substantially, in spite of the fact that the remaining processors are running at full speed. Thus, such an approach will reduce the cooling *power*, but increase the execution time of the application. Running the cooling system for a longer time can also *increase* the cooling energy.

We aim to reduce cooling power without substantially increasing execution time, and thus reduce cooling energy. We first describe the temperature sensor and frequency control mechanisms, and quantify their impact on execution time mentioned above (Section 2.2). Our solution leverages the adaptive runtime system underlying the Charm++ parallel programming system (Section 2.3). In order to minimize *total* system energy consumption, we study an approach of limiting CPU temperatures via DVFS and mitigating the resultant timing penalties with a load balancing strategy that is conscious of these effects (Section 2.4). We show the impact of this combined technique on application performance (Section 2.6) and *total* energy consumption (Section 2.7).

## 2.1 Related Work

Cooling energy optimization and hot spot avoidance have been addressed extensively in the literature of non-HPC data centers [16–19], which shows the importance of the topic. As an example, job placement and server shut down have shown savings of up to 33% in cooling costs [16]. Many of these techniques rely on placing jobs that are expected to generate more heat in the cooler areas of the data center. Such job placement schemes can not be directly applied to HPC applications because different nodes are running parts of the same application with similar power consumption. As an example, Rajan et al [20] use system throttling for temperature-aware scheduling in the context of operating systems. Given their assumptions, they show that keeping temperature constant is beneficial with their theoretical models. However, their assumption of non-migratability of tasks is not true in HPC applications, especially with an adaptive runtime system. Le et al. [21] constrain core temperatures by turning the machines on and off and consequently reduce total energy consumption by 18%. However, most of these techniques, cannot be applied to HPC applications as they are

not practical for tightly-coupled applications.

Minimizing energy consumption has also been an important topic for HPC researchers. However, most of the work has focused on machine energy consumption rather than cooling energy. Freeh et al. [2] show machine energy savings of up to 15% by exploiting the communication slack present in the computational graph of a parallel application. Lim et al [22] demonstrate a median energy savings of 15% by dynamically adjusting the CPU frequency/voltage pair during the communication phases in MPI applications. Springer et al. [3] generate a frequency schedule for a DVFS-enabled cluster that runs the target application. This schedule tries to minimize the execution time while staying within the power constraints. The major difference of our approach to the ones mentioned is that our DVFS decisions are based on saving cooling energy consumption by constraining core temperatures. The *total* energy consumption savings that we report represent both machine and cooling energy consumption.

Huang and Feng describe a kernel-level DVFS governor that tries to determine the power-optimal frequency for the expected workload over a short time interval that reduces machine energy consumption up to 11% [23]. Hanson et al. [24] devise a runtime system named PET for performance, power, energy and thermal management. They consider a more general case of multiple and dynamic constraints. However, they just consider a serial setting without the difficulties of parallel machines and HPC applications. Extending our approach for constraints other than temperature is an interesting future work.

Banerjee et al. [25] try to improve the cooling cost in HPC data centers by an intelligent job placement algorithm yielding up to 15% energy savings. However, they do not consider the temperature variations inside a job. Thus, their approach can be less effective for data centers with a few large-scale jobs rather than many small jobs. They also depend on job pre-runs to get information about the jobs. In addition, their results are based on simulations and not experiments on a real testbed. Tang et al. [26] reduce 30% of cooling energy consumption by scheduling tasks in a data center. However, the benefits of their scheme for large-scale jobs are questionable.

Merkel et al. [27] discuss the scheduling of tasks in a multiprocessor to avoid hot cores. However, they do not deal with complications of parallel applications and large-scale data centers. Freeh et al. [28] exploit the varying sensitivity of different phases in the application to core frequency in order to reduce machine energy consumption for load balanced applications. This work is similar to ours, as it deals with load balanced applications. They reduce machine energy consumption by a maximum of 16%. However, our work is different as we achieve much higher savings in *total* energy consumption primarily by reducing cooling energy consumption.

## 2.2 Limiting Temperatures

The design of a machine room or data center must ensure that all equipment stays within its safe operating temperature range while keeping costs down. Commodity servers and switches draw cold air from their environment, pass it over processor heatsinks and other hot components, and then expel it at a higher temperature. To satisfy these systems' specifications and keep them operating reliably, cooling systems in the data center must supply a high enough volume of sufficiently cold air to every piece of equipment.

Traditional data center designs treated the air in the machine room as a single mass, to be kept at an acceptable aggregate temperature. If the air entering some device was too hot, the CRAC's thermostat should be adjusted to a lower set-point. That adjustment would cause the CRAC to run more frequently or intensely, increasing its energy consumption. More modern designs, such as alternating hot/cold aisles [4] or in-aisle coolers, provide greater separation between cold and hot air flows and more localized cooling, easing appropriate supply to computing equipment and increasing efficiency.

However, even with this tighter air management, variations in air flow, system design, manufacturing and assembly, and workload may still leave some devices significantly hotter than others. To illustrate this sensitivity, we run an intensive parallel (*Wave2D*) application on a cluster (Energy Cluster) with a dedicated CRAC unit. We changed the machine room's cooling by manipulating the CRAC set-point. The details of the application and our Energy Cluster are described in Appendix B and Appendix A respectively. Figure 2.1 shows two runs of *Wave2D* with different CRAC set-point temperatures. For each run, we plot both the average core temperature across the entire cluster, and the maximum deviation of any core from that average.

Unsurprisingly, observed core temperatures correlate with the temperature of the air provided to cool them. With a set-point increase of  $2.3^{\circ}\text{C}$ , the average temperature across the system increases by  $6^{\circ}\text{C}$ . More noteworthy is that this small shift creates a substantial hot spot, that worsens progressively over the course of the run. At the higher  $25.6^{\circ}\text{C}$  set-point, the temperature difference from the average to the maximum rises from  $9^{\circ}\text{C}$  to  $20^{\circ}\text{C}$ . In normal operations, this difference of  $11^{\circ}\text{C}$  would be an unacceptable result, and the CRAC set-point must be kept low enough to avoid it.

An alternative approach, based on DVFS, shows promise in addressing the issue of over-cooling and hot spots. DVFS is already widely used in laptops, desktops, and servers in non-HPC data centers as a means to limit CPU power consumption. However applying DVFS naively to HPC workloads entails an unacceptable performance degradation. Many HPC applications are tightly-coupled, such that one or a few slow cores would effectively

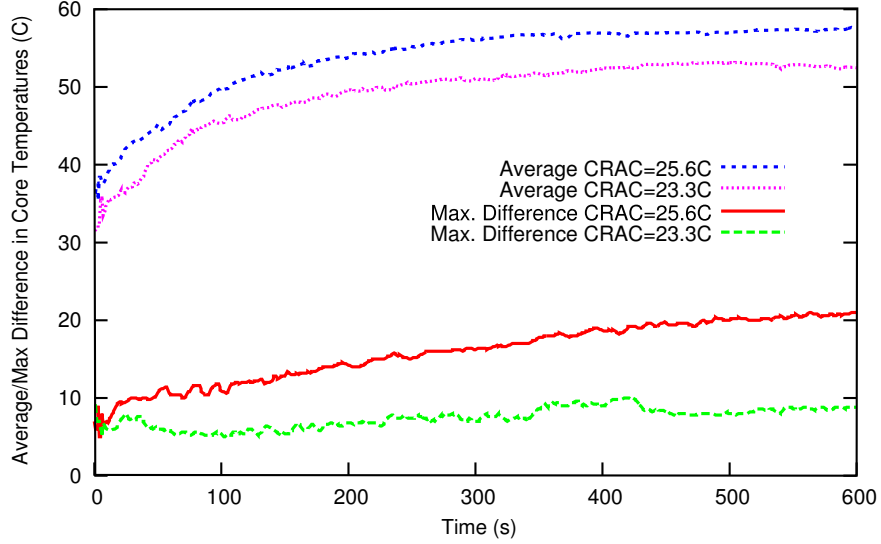


Figure 2.1: Average core temperatures and maximum difference of any core from the average for *Wave2D*

slow down an entire job. This *timing penalty* implies decreased throughput and increased time-to-solution.

To demonstrate the impact of DVFS, we repeat the earlier experiment with a temperature constraint. We fix a threshold temperature of  $44^{\circ}$  C that we wish to keep all CPUs below. We sample temperatures periodically, and when a CPU’s average temperature is over this threshold, its frequency is lowered by one step, i.e., increase the P-state by a level. If it is more than a degree below the threshold, its frequency is increased by one step i.e. decrease its P-state by a level. We repeat this experiment over a range of CRAC settings, and compute their performance in time and energy consumption relative to a run with all cores working at their maximum frequency and the CRAC set to  $12.2^{\circ}$  C. As shown in Figure 2.2, DVFS alone in this setting hurts performance and provides minimal savings in *total* energy consumption. Most of the savings from cooling energy consumption are offset by an increase in machine energy consumption. This effect arises because the decreased energy consumption of the slower cores is more than offset by the additional machine energy consumed by all the cores, including some at higher frequencies, running for the extended time. Not only that, the slower cores can sometimes add such a large timing penalty that even they start consuming more energy ( $24.4^{\circ}$  C CRAC set-point case) due to the extra time they have to run while parts outside the CPUs keep consuming the same power. Nevertheless, our results in Figure 2.3 (described in detail in Section 2.6) show that DVFS effectively limits both overall temperatures and hot spots.

More radical liquid-cooling designs mitigate some of the hot spot concerns, but they are

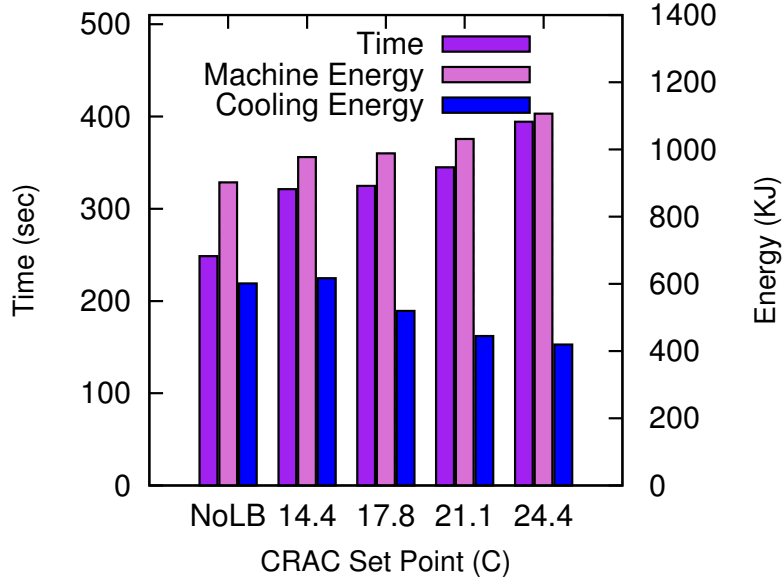


Figure 2.2: Execution time and energy consumption for *Wave2D* running at different CRAC set-points using DVFS

not a panacea. Equipment must be specifically designed to be liquid-cooled, and data centers must be built or retrofit to supply the coolant throughout the machine room. The present lack of commodity liquid-cooled systems and data centers means that techniques to address the challenges of air-cooled computers will continue to be relevant for the foreseeable future. Moreover, our techniques for limiting core temperatures can actually reduce the overall thermal load of an HPC system, leading to energy savings even for installations using liquid cooling.

## 2.3 Charm++ and Load Balancing

Charm++ is a general-purpose C++-based parallel programming system designed for productive HPC programming [29]. It is supported by an adaptive runtime system that automates resource management. It relies on techniques such as processor virtualization and over-decomposition (having more work units than the number of cores) to improve performance via adaptive overlap of computation and communication and data-driven execution. The automated resource management implies that the developer does not need to program in terms of the physical cores, but instead divides the work into pieces with a suitable grain size to let the system manage them easily.

A key feature of Charm++ is that the units of work decomposition are *migratable objects*.



The adaptive runtime system can assign these objects to any processor and move them around during program execution, for purposes including load balancing, communication optimization, and fault tolerance. To enable effective load balancing, it tracks statistics of each object’s execution, including its computation time and communication volume [30].

The runtime system provides a variety of plug-in *load balancing strategies* that can account for different application characteristics. Through a simple API, these strategies take the execution statistics from the runtime and generate a set of migration instructions, describing which objects to move between which processors. Application developers and users can provide their own strategy implementations as desired. Load balancing strategies can be chosen at compilation or run-time. The majority of these strategies are based on the heuristic ‘principle of persistence’, which states that each object’s computation and communication loads tend to persist over time. The principle of persistence holds for a large class of iterative HPC applications. In this study, we have developed a new load balancing strategy that accounts for the performance effects of DVFS-induced heterogeneity. The new strategy is described in detail in Section 2.4.

At small scales, the cost of the entire load balancing process, from instrumentation through migration, is generally a small portion of the total execution time, and less than the improvement that it provides. For cases where load balancing costs can be significant, a strategy must be chosen or adapted to match the application’s needs [31]. Our approach can be easily adapted to available hierarchical schemes, which have been shown to scale to the largest machines available [32]. By limiting the cost of decision-making and scope of migration, we expect these schemes to offer similar energy benefits.

### 2.3.1 AMPI

The Message Passing Interface (MPI) is a standardized communication library for distributed-memory parallel programming. MPI has become the dominant paradigm for large-scale parallel computing. Thus, techniques for addressing the energy consumption of large parallel systems must be applicable to MPI applications.

Charm++ provides an implementation of MPI known as Adaptive MPI (AMPI). AMPI makes the features of the Charm++ runtime system available to MPI programs. Common MPI implementations implement each unit of parallel execution, or *rank*, as a separate process. Pure MPI applications run one rank per CPU core, while others use fewer ranks and gain additional shared-memory parallelism via threading.

In contrast, AMPI encourages running applications with several ranks per core. AMPI

implements these ranks as light weight user-level threads, many of which can run in each process. The runtime schedules these threads non-preemptively, and switches them when they make blocking communication calls. Internally, these threads are implemented as migratable objects, enabling the same benefits for MPI programs as for native Charm++. In particular, AMPI allows us to apply the Charm++ load balancing strategies without intrusive modifications to application logic.

## 2.4 ‘Cool’ Load Balancer

In this section, we introduce a novel approach that reduces energy consumption of the system with minimal timing penalty. It is based on limiting core temperatures using DVFS and task migration. Because our scheme is tightly coupled to task migration, we chose Charm++ and AMPI as our parallel programming frameworks as they allow easy task (object) migration with low overhead. All implementations and experiments were done using Charm++ and AMPI. However, our techniques can be applied to any parallel programming system that provides efficient task migration.

The steps of our temperature-control scheme can be summarized as applying the following process periodically:

1. Check the temperatures of all cores
2. Apply DVFS to cores that are hotter or colder than desired
3. Address the load imbalance caused by DVFS using our load balancer, *TempLDB*:
  - (a) Normalize task and core load statistics to reflect old and new frequencies
  - (b) Identify overloaded or underloaded cores
  - (c) Move work from overloaded cores to underloaded cores

The remainder of this section describes this process in detail.

Our temperature control scheme is periodically triggered after equally spaced intervals in time, referred to as *steps*. Other DVFS schemes [23] try to react directly to the demands of the application workload, and thus must sample conditions and make adjustments at intervals on the order of milliseconds. In contrast, our strategy only needs to react to much slower shifts in chip temperature, which occur over intervals of seconds. At present, DVFS is triggered as part of the runtime’s load balancing infrastructure at a user-specified period.

Variable	Description
$\mathbf{n}$	number of tasks in application
$\mathbf{p}$	number of cores
$T_{max}$	maximum temperature allowed
$k$	current load balancing step
$C_i$	set of cores on same chip as core $i$
$taskTime_i^k$	execution time of task $i$ during step $k$ (in ms)
$coreTime_i^k$	time spent by core $i$ executing tasks during step $k$
$f_i^k$	frequency of core $i$ during step $k$ (in Hz)
$m_i^k$	core number assigned to task $i$ during step $k$
$\{task, core\}Ticks_i^k$	num. of clock ticks taken by $i^{th}$ task/core during step $k$
$t_i^k$	average temperature of chip $i$ at start of step $k$ (in °C)
$overHeap$	heap of overloaded cores
$underSet$	set of underloaded cores

Table 2.1: Description for variables used in Algorithm 1

Our control strategy for DVFS is to let the cores work at their maximum frequency as long as their temperature is below a threshold parameter. If a core’s temperature crosses above the threshold, it is controlled by decreasing the voltage and frequency using DVFS. When the voltage and frequency are reduced, power consumption will drop and hence the core’s temperature will fall. Our earlier approach [33] raised the voltage and frequency as soon as temperatures fell below the threshold, causing frequent changes and requiring effort to load balance in every interval. To reduce overhead, our strategy now waits until a chip’s temperature is a few degrees below the threshold before increasing its frequency.

The hardware in today’s cluster computers does not allow reducing the frequency of each core individually and so we must apply DVFS to the whole chip. This raises the question: what heuristic should we use to trigger DVFS and modulate frequency? In our earlier work [15], we conducted DVFS when *any* of the cores on a chip were considered too hot. However, our more recent results [33] show that basing the decision on *average* temperature of the cores in a chip results in better temperature control.

Another important decision is how much a chip’s frequency should be reduced (respectively, raised) when it gets too hot (is safe to warm up). Present hardware only offers discrete frequency and voltage levels built into the hardware, the ‘P-states’. Using this hardware, we observed that reducing the chip’s frequency by one level at a time is a reasonable heuristic because it effectively constrains the core temperatures in the desired range (Figure 2.3). Lines 1–6 of Algorithm 1 apply DVFS as we have just described. The description of the

variables and functions used in the algorithm is given in Table 2.1.

When DVFS adjusts frequencies differently across the cores in a cluster, the workloads on those cores change relative to one another. Because this potential for load imbalance occurs all at once, it makes sense to react to this load balance immediately. The system responds by rebalancing the assignment of work to cores according to the strategy described by lines 7–32 of Algorithm 1.

---

Algorithm 1: Temperature Aware Refinement Load Balancing

---

```

1: On every node  $i$  at start of step  $k$ 
2: if  $t_i^k > T_{max}$  then
3:   decreaseOneLevel( $C_i$ ) ▷ increase P-state
4: else if  $t_i^k < T_{max} - 2$  then
5:   increaseOneLevel( $C_i$ ) ▷ decrease P-state
6: end if
7: On Master core
8: for  $i \in [1, n]$  do
9:    $taskTicks_i^{k-1} = taskTime_i^{k-1} \times f_{m_i^{k-1}}^{k-1}$ 
10:   $totalTicks += taskTicks_i^{k-1}$ 
11: end for
12: for  $i \in [1, p]$  do
13:   $coreTicks_i^{k-1} = coreTime_i^{k-1} \times f_i^{k-1}$ 
14:   $freqSum += f_i^k$ 
15: end for
16: createOverHeapAndUnderSet()
17: while  $overHeap$  NOT NULL do
18:   $donor = deleteMaxHeap(overHeap)$ 
19:   $(bestTask, bestCore) =$ 
20:   $getBestCoreAndTask(donor, underSet)$ 
21:   $m_{bestTask}^k = bestCore$ 
22:   $coreTicks_{donor}^{k-1} -= taskTicks_{bestTask}^{k-1}$ 
23:   $coreTicks_{bestCore}^{k-1} += taskTicks_{bestTask}^{k-1}$ 
24:  updateHeapAndSet()
25: end while
26:
27: procedure isHeavy(i)
28: return  $coreTicks_i^{k-1} > (1 + tolerance) * totalTicks$ 
29:         $*(f_i^k / freqSum)$ 
30:
31: procedure isLight(i)
32: return  $coreTicks_i^{k-1} < totalTicks * f_i^k / freqSum$ 

```

---

The key principle in how a load balancer must respond to DVFS actuation is that the

load statistics must be adjusted to reflect the various different frequencies at which load measurements were recorded and future work will run. At the start of step  $k$ , our load balancer retrieves load information for step  $k-1$  from Charm++’s database. This data gives the total duration of work executed for each task in the previous interval ( $taskTime_i^{k-1}$ ) and the core that executed it ( $m_i^{k-1}$ ). Here  $i$  refers to task  $id$  and  $k-1$  represents last step. We normalize the task workloads by multiplying their execution times by the old frequency values of the core that hosted them. We then sum these normalized task workloads to compute the total load, as seen in lines 8–11. This normalization is an approximation to the performance impact of different frequencies. However, different applications might have different characteristics (e.g., cache hit rates at various levels, instructions per cycle) that determine the sensitivity of their execution time to core frequency. We plan to incorporate more detailed load estimators in our future work. The scheme also calculates the work assigned to each core and sum of frequencies for all the cores to be used later (lines 12-15).

Once the load normalization is done, we create a *max heap* for overloaded cores (*overHeap*) and a *set* for the underloaded cores (*underSet*) on line 16. The cores are classified as overloaded and underloaded by procedures *isHeavy()* and *isLight()* (lines 26–30), based on how their normalized loads from the previous step,  $k-1$ , compare to the frequency-weighted average load for the coming step  $k$ . We use a tolerance in identifying overloaded cores to focus our efforts on the worst instances of overload and minimize migration costs. In our experiments, we set the tolerance to 0.07, empirically chosen for the slight improvement that it provided over the lower values used in our previous work.

Using these data structures, the load balancer iteratively moves work away from the most overloaded core (*donor*, line 18) until none are left (line 17). The moved task and recipient are chosen as the heaviest task that the *donor* could transfer to any underloaded core such that the underloaded core does not become overloaded (line 19, implementation not shown). Once the chosen task is reassigned (line 20), the load statistics are updated and the data structures are updated accordingly (lines 21–23).

## 2.5 Experimental Setup

To evaluate our approach to reducing energy consumption, we must be able to measure and control core frequencies and temperatures, air temperature, and energy consumed by computer and cooling hardware. All experiments were run on real hardware and this chapter does not include any simulation results.

We tested our scheme on the Energy Cluster hosted by the Computer Science department

at University of Illinois Urbana Champaign (see Appendix A). Its cooling design is similar to the cooling systems of most large data centers. We were able to vary the CRAC set-point across a broad range as shown in our results (following sections).

Because the CRAC unit exchanges machine room heat with chilled water supplied by a campus-wide plant, measuring its direct energy consumption (i.e., with an electrical meter) would only include the mechanical components driving air and water flow, and would miss the much larger energy expenditure used to cool the water. To capture the machine room’s cooling energy, we use a model [21] based on measurements of how much heat the CRAC actually expels. The instantaneous power consumed by the CRAC to cool the temperature of the exhaust air from  $T_{hot}$  down to the cool inlet air temperature  $T_{ac}$  can be approximated by:

$$P_{ac} = c_{air} * f_{ac} * (T_{hot} - T_{ac}) \quad (2.1)$$

In this equation,  $c_{air}$  is the heat capacity constant and  $f_{ac}$  is the constant rate of air flow through the cooling system. We use temperature sensors on the CRAC’s vents to measure  $T_{hot}$  and  $T_{ac}$ . During our experiments, we recorded a series of measurements from each of these sensors, and then integrated the calculated power to produce total energy figures.

By working in a dedicated space, the present work removes a potential source of error from previous data center cooling results. Most data centers have many different jobs running at any given time. Those jobs dissipate heat, interfering with cooling energy measurements and increasing the ambient temperature in which the experimental nodes run. In contrast, our cluster is the only heat source in the space, and the CRAC is the primary sink for that heat.

We investigate the effectiveness of our scheme, using five different applications, of which three are Charm++ applications and two are written in MPI. These applications have a range of power profiles and are described in Appendix B.

Most of our experiments were run for 300 seconds as it provided ample time for all applications to settle to their steady state frequencies. All results that we show are averaged over three identically configured runs, with a cool-down period before each. All normalized results are reported with respect to a run where all 128 cores were running at the maximum possible frequency with Intel Turbo Boost in operation and the CRAC set to 12.2° C. To validate the ability of our scheme to reduce energy consumption for longer execution times, we ran *Wave2D* (the most power-hungry of the five applications we consider) for 2.5 hours. The longer run was consistent with our findings, with the temperature being constrained well within the specified range and we were able to reduce cooling energy consumption for the entire 2.5 hour period.

## 2.6 Constraining Core Temperatures and Timing Penalty

The approach that we have described in Section 2.4 constrains processor temperatures with DVFS while attempting to minimize the resulting timing penalty. Figure 2.3 shows that all of our applications when using DVFS and *TempLDB*, settle to an average temperature that lies in the desired range (the two horizontal lines at 47°C and 49°C on Figure 2.3). As the average temperature increases to its steady-state value, the hottest single core ends up no more than 6° C above the average (lower part of Figure 2.3) as compared to 20° C above average for the run where we are not using temperature control (Figure 2.1).

Figure 2.4 shows the timing penalty incurred by each application under DVFS, contrasting its effect with and without load balancing. The effects of DVFS on the various applications are quite varied. The worst affected, Wave2D and NAS MG, see penalties of over 50%, which load balancing reduces to below 25%. Jacobi2D was the least affected, with a maximum penalty of 12%, brought down to 3% by load balancing. In all cases, the timing penalty sharply decreases when load balancing is activated, generally by greater than 50%. Before analyzing the timing penalty for individual applications we first see how load balancing helps in reducing timing penalty compared to naive DVFS.

To illustrate the benefits of load balancing, we use Projections [34], which is a multipurpose performance visualization tool for Charm++ applications. Here, we use processor timelines to see the utilization of the processors in different time intervals. For ease of comprehension, we show a representative 16-core subset of the 128-core cluster. The top part of Figure 2.5 shows the timelines for execution of *Wave2D* with the naive DVFS scheme. Each timeline (horizontal line) corresponds to the course of execution of one core visualizing its utilization. The green and pink colored pieces show different computation but white ones represent idle time. The boxed area in Figure 2.5 shows some of the cores have significant idle time. The top 4 cores in the boxed area take much longer to execute their computation than the bottom 12 cores which is why the pink and green parts are longer for the top 4 cores. However, the other 12 cores execute their computation quickly and stay idle waiting for the rest of cores. The idle time is caused because DVFS decreased the frequency of the first four cores and so they are slower in their computation. It means that the timing penalty of naive DVFS is dictated by the slowest cores. The bottom part of Figure 2.5 shows the same temperature control but using our *TempLDB*. In this case, there is no significant idle time because the scheme balances the load between slow and fast processors by taking their frequencies into account. Consequently, the latter approach results in much shorter total execution time, as reflected by shorter timelines (and figure width) in the bottom part of Figure 2.5. Now we try to understand the timing penalty differences amongst different

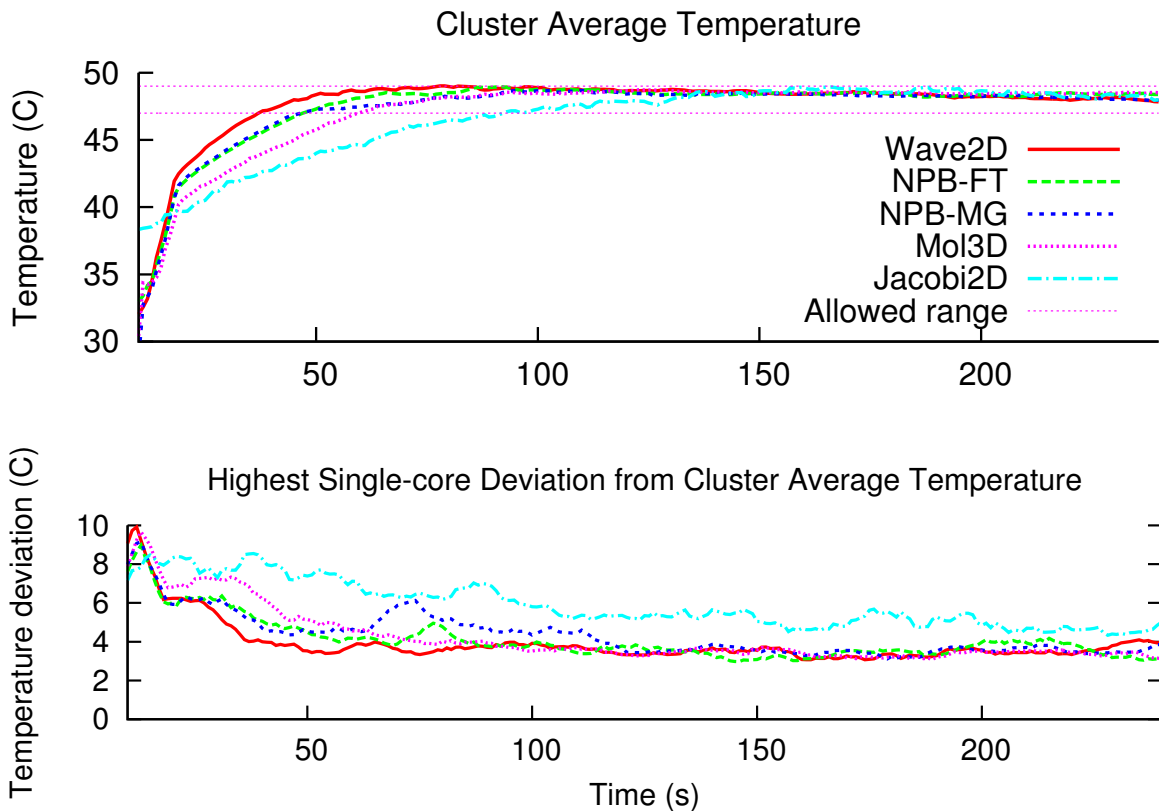


Figure 2.3: Our DVFS and load balancing scheme successfully keeps all processors within the target temperature range of 47°–49° C, with a CRAC set-point of 24.4° C.

applications by examining more detailed data. Jacobi2D experiences the lowest impact of DVFS, regardless of load balancing (Figure 2.4(a)). The small timing penalty for Jacobi2D occurs for several interconnected reasons. From the high level, Figure 2.3 shows that it takes the longest of any application to increase temperatures to the upper bound of the acceptable range, where DVFS activates. This slow ramp-up in temperature means that its frequency does not drop until later in the run, and then falls relatively slowly, as seen in Figure 2.6 which plots the minimum frequency at which any core was running (Figure 2.6(a)) and the average frequency (Figure 2.7(a)) for all 128 cores. Even when some processors reach their minimum frequency, Figure 2.7(a) shows that its average frequency decreases more slowly than any other application, and does not fall as far. The difference in the average frequency and the minimum frequency explains the difference between *TempLDB* and naive DVFS, as the execution time for *TempLDB* is dependent on average frequency whereas the execution time for naive DVFS depends on the minimum frequency at which any core is running. Another way to understand the relatively small timing penalty of Jacobi2D is to compare its utilization and frequency profiles. Figure 2.8(a) depicts each core’s average



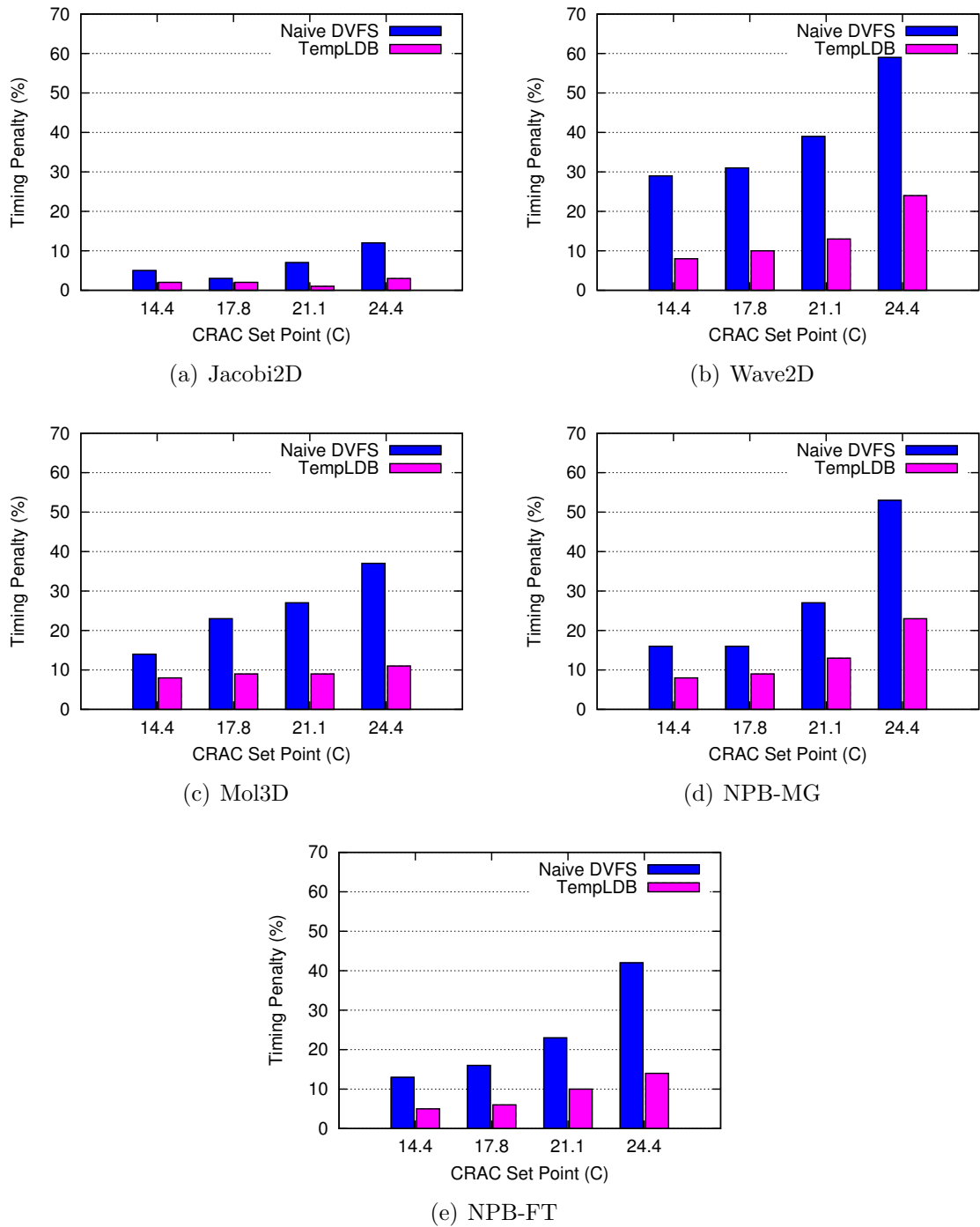


Figure 2.4: Execution timing penalty with and without Temperature Aware Load Balancing



Figure 2.5: Execution timelines before and after Temperature Aware Load Balancing for *Wave2D*

frequency over the course of the run. Figure 2.9(a) shows the utilization of each core while running Jacobi2D. In both figures, each bar represents the measurement of a single core. The green part of the utilization bars represents computation and the white part represents idle time. As can be seen, utilizations of the right half cores are roughly higher than the left half. Furthermore, the average frequency of the right half processors is roughly lower than the other half. Thus, lower frequency has resulted in higher utilization of those processors without much timing penalty. The reason this variation can occur is that the application naturally has some slack time in each iteration, which the slower processors dip into to keep pace with faster ones.

To examine the differences among applications at another level, Figure 2.10 shows the performance impact of running each application with the processor frequencies fixed at a particular value (the marking 2.4+ refers to the top frequency plus Turbo Boost). All applications slow down as CPU frequency decreases. However, Jacobi2D incurs the smallest timing penalty compared to other applications. This marked difference can be better understood in light of the performance counter-based measurements shown in Table 2.2. These

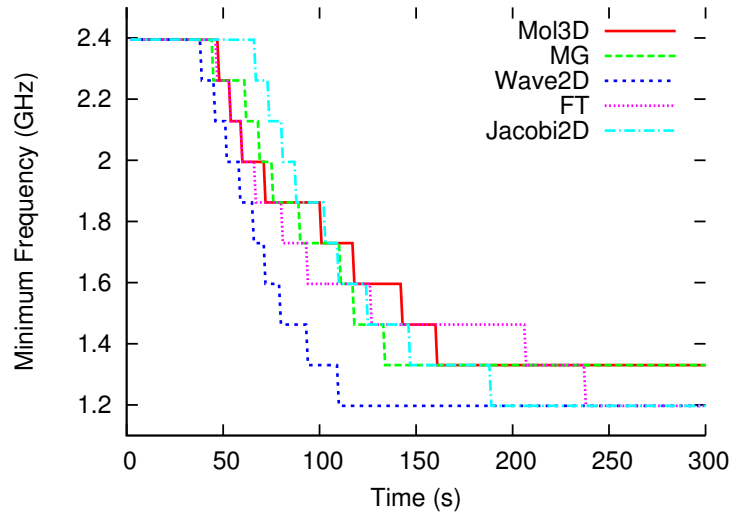


Figure 2.6: Minimum core frequencies produced by DVFS for different applications at 24.4°C

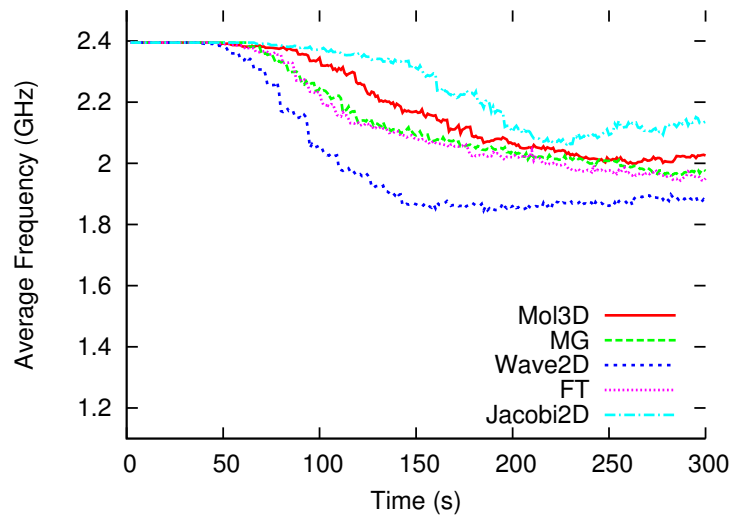


Figure 2.7: Average core frequencies produced by DVFS for different applications at 24.4°C

Counter Type	Jacobi2D	Mol3D	Wave2D
MFLOP/s	373	666	832
Traffic L1-L2 (MB/s)	762	1017	601
Cache misses to DRAM (millions)	663	75	402

Table 2.2: Performance counters for Charm++ applications on one core

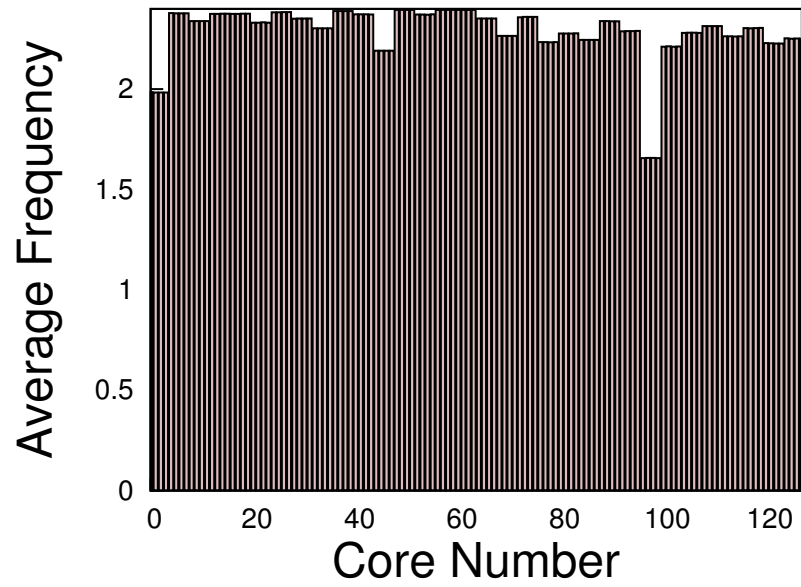


Figure 2.8: Average frequency of processors for Jacobi2D using *TempLDB*

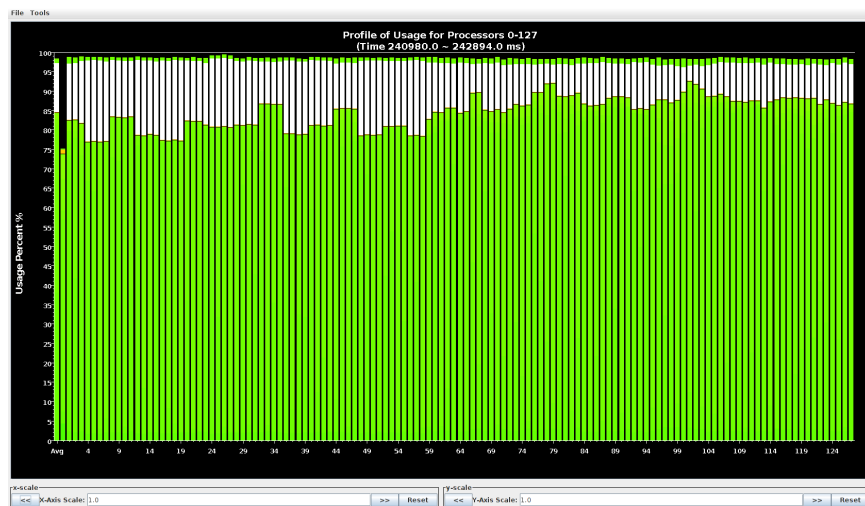


Figure 2.9: Utilization of processors for Jacobi2D using *TempLDB*

measurements were taken in equal-length runs of the three Charm++ applications using the PerfSuite toolkit [35]. Jacobi2D has a much lower computational intensity, in terms of FLOP/s, than the other applications. It also retrieves much more data from main memory, explaining its lower sensitivity to frequency shifts. Its lower intensity also means that it consumes less power and dissipates less heat in the CPU cores than the other applications, explaining its slower ramp-up in temperature, slower ramp-down in frequency, and higher steady-state average frequency. In contrast, the higher FLOP counts and cache access rates of Wave2D and Mol3D explain their high frequency sensitivity, rapid core heating, lower steady-state frequency, and hence the large impact DVFS has on their performance.

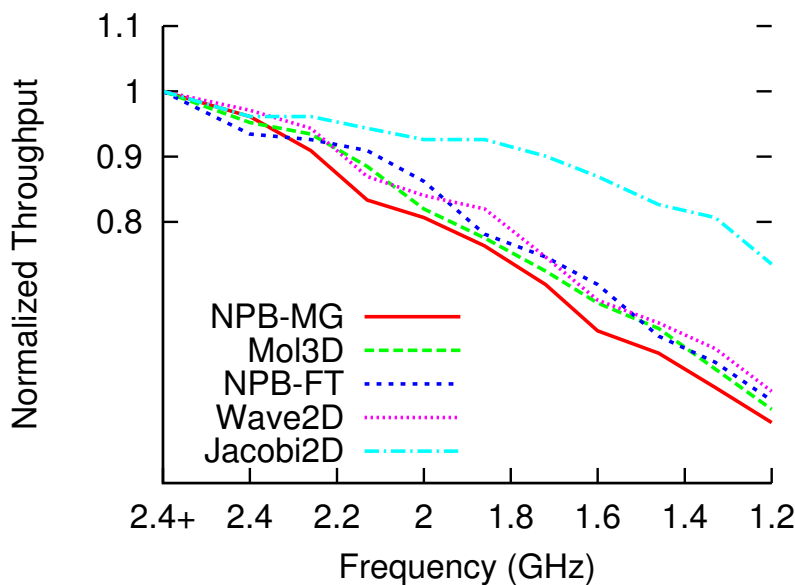


Figure 2.10: Frequency sensitivity of the various applications

## 2.7 Energy Savings

In this section, we evaluate the ability of our scheme to reduce *total* energy consumption. Our current load balancing scheme with the allowed temperature range strategy resulted in less than 1% time overhead for applying DVFS and load balancing (including the cost of object migration). Due to that change, we now get savings in both cooling energy consumption as well as machine energy consumption, although savings in cooling energy consumption constitute the main part of the reduction in total energy consumption. In order to understand the contribution for both cooling energy consumption and machine energy consumption, we look at them separately.

### 2.7.1 Cooling energy consumption

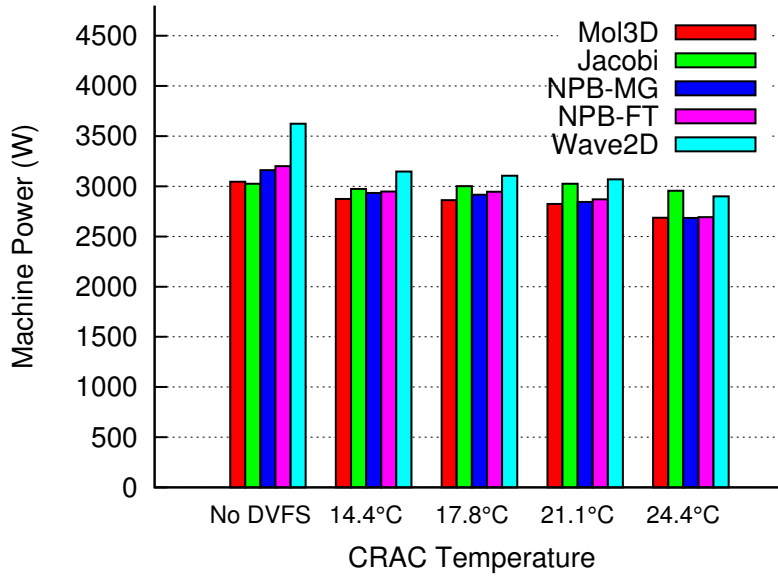
The essence of our work is to reduce cooling energy consumption by constraining core temperatures and avoiding hot spots. As outlined in Equation 2.1, the cooling power consumed by the air conditioning unit is proportional to the difference between the hot air and cold air temperatures going in and out of the CRAC respectively. As mentioned in earlier work [4–6], cooling cost can be as high as 50% of the total energy budget of the data center. However, in our calculation, we take it to be 40% of the total energy consumption of a baseline run with the CRAC at its lowest set-point, which is equivalent to 66.6% of the measured machine energy during that run. Hence, we use the following formula to estimate the cooling power by feeding in actual experimental results for hot and cold air temperatures:

$$P_{cool}^{LB} = \frac{2 * (T_{hot}^{LB} - T_{ac}^{LB}) * P_{machine}^{base}}{3 * (T_{hot}^{base} - T_{ac}^{base})} \quad (2.2)$$

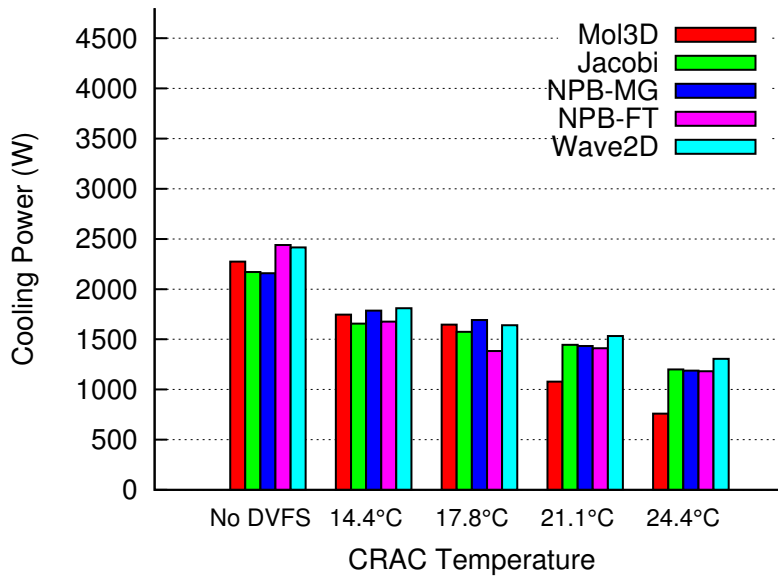
$T_{hot}^{LB}$  represents the temperature of hot air leaving the machine room (entering the CRAC) and  $T_{ac}^{LB}$  represents the temperature of the cold air entering the machine room.  $T_{hot}^{base}$  and  $T_{ac}^{base}$  represent the hot and cold air temperatures with the largest difference while running *Wave2D* at the coolest CRAC set-point (i.e., 12.2° C), and  $P_{machine}^{base}$  is the power consumption of the machine for the same experiment.

Figure 2.11 shows the machine power consumption and the cooling power consumption for each application using *TempLDB*. Figure 2.11(b) shows that the cooling power consumption falls as we increase the CRAC set-point for all applications. A higher CRAC set-point means the cores heat up more rapidly, leading DVFS to set lower frequencies. Thus, machine power consumption falls as a result of the CPUs drawing less power (Figure 2.11(a)). The machine’s decreased power draw and subsequent heat dissipation means that less energy is added to the machine room air. The lower heat flux to the ambient air means that the CRAC requires less power to expel that heat and to maintain the set-point temperature, as seen in Figure 2.11(b).

*Wave2D* consumes the highest cooling power for three out of the four CRAC set-points that we used, which is consistent with its high machine power consumption. Figure 2.12 shows the savings in cooling energy in comparison to the baseline run where all cores are working at the maximum frequency without any temperature control. These figures include the extra time that the cooling needs to run corresponding to the timing penalty introduced because of applying DVFS. Due to the large reduction in cooling power (Figure 2.11(b)) our scheme was able to save as much as 63% of the cooling energy in the case of *Mol3D* running at a CRAC set-point of 24.4° C. We can see that the savings in cooling energy



(a) Machine power consumption



(b) Cooling power consumption

Figure 2.11: Machine and cooling power consumption for no-DVFS runs at a 12.2°C set-point and various *TempLDB* runs

consumption are better with our technique than naive DVFS for most of the applications and the corresponding set-points. This improvement in energy consumption is mainly due to the higher timing penalty for naive DVFS runs, which causes the CRAC to work for much longer than the corresponding *TempLDB* run.

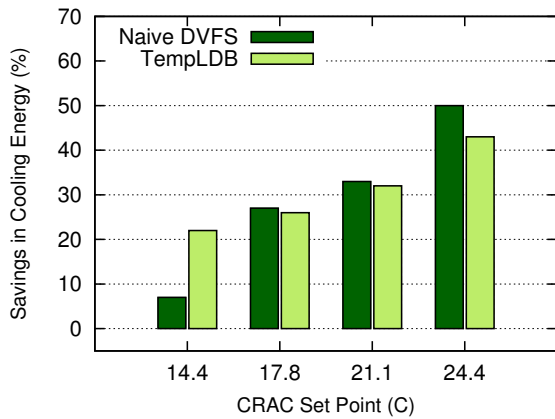
## 2.7.2 Machine energy consumption

Although *TempLDB* does not optimize for reduced machine energy consumption, we still end up showing savings for some applications. Figure 2.13 shows the change in machine energy consumption. A number less than 1 represents a saving in machine energy consumption whereas a value greater than 1 points to an increase.

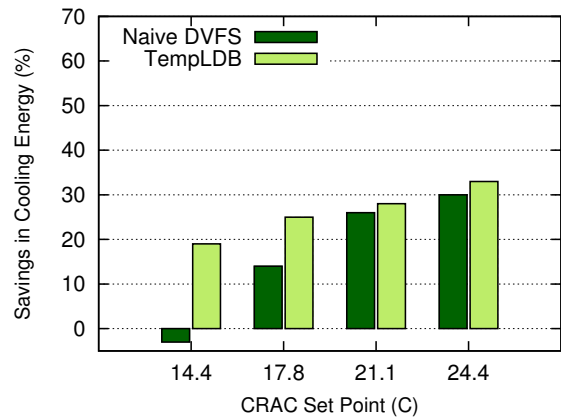
It is interesting to see that *NPB-FT* and *Wave2D* end up saving machine energy consumption when using *TempLDB*. For *Wave2D*, we end up saving 6% of machine energy consumption when the CRAC is set to 14.4°C whereas the maximum machine energy savings of *NPB-FT*, 4%, occurs when the CRAC is set to 14.4°C or 24.4°C. To find the reasons for these savings in machine energy consumption, we performed a set of experiments where we ran the applications with the 128 cores of our cluster fixed at each of the available frequencies. Figure 2.14 plots the normalized machine energy for each application against the frequency at which it was run. Power consumption models dictate that CPU power consumption can be regarded as being proportional to the cube of the frequency, which would imply that we should expect the power to fall as a cubic of frequency whereas the execution time increases only linearly in the worst case. This cubic relationship would imply that we should always reduce energy consumption by moving to a lower frequency. This proposition does not hold because of the high base power drawn by everything other than the CPU and memory subsystem, which is 40W per node for our cluster. We can say that while moving to each successive lower frequency we reach a point where the savings in the CPU energy consumption are offset by an increase in base energy consumption due to the timing penalty incurred, leading to the U-shaped energy curves. When our scheme lowers frequency as a result of core temperature crossing the maximum temperature value, we move into the more desirable range of machine energy consumption, i.e., closer to the minimum of the U-shape energy curves.

To see a breakdown of execution time, Figure 2.15 shows the cumulative time spent by all 128 cores at different frequency levels for *Wave2D* using *TempLDB* at a CRAC set-point of 24.4°C. We can see that most of the time is spent at frequency levels between 1.73GHz–2.0GHz, which corresponds to the lowest point for normalized energy for *Wave2D*

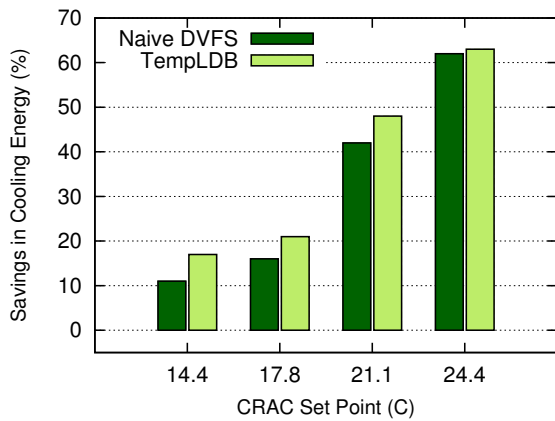




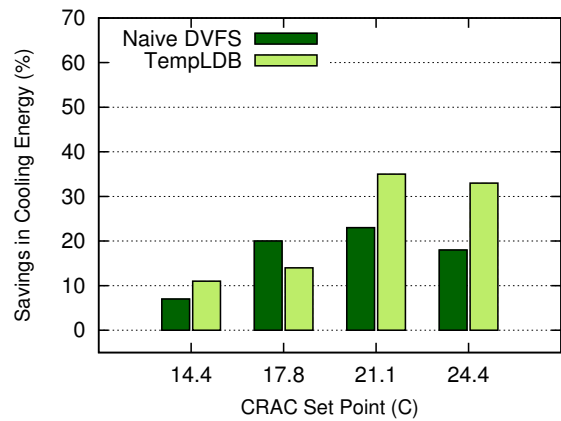
(a) Jacobi2D



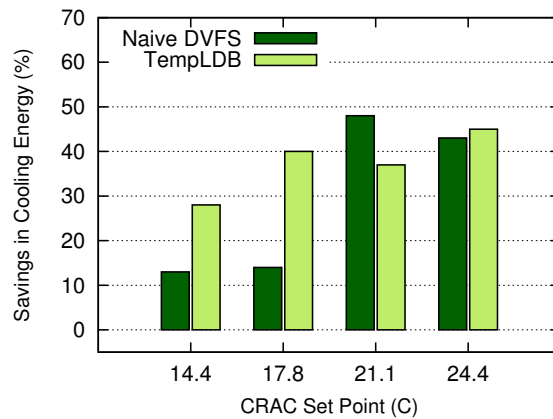
(b) Wave2D



(c) Mol3D

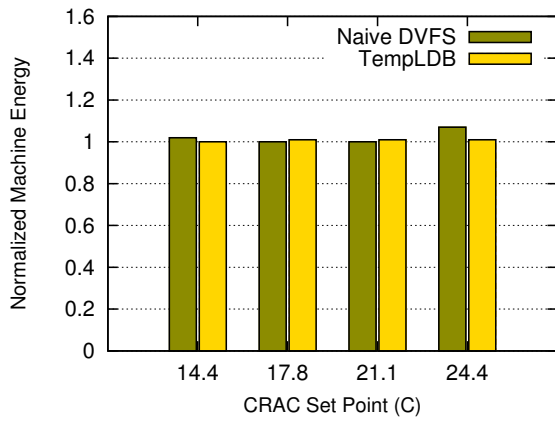


(d) NPB-MG

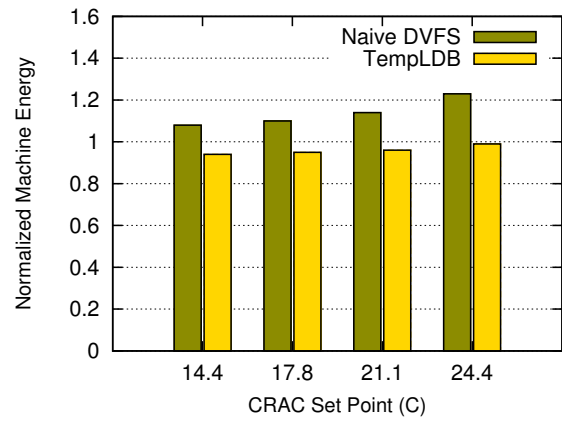


(e) NPB-FT

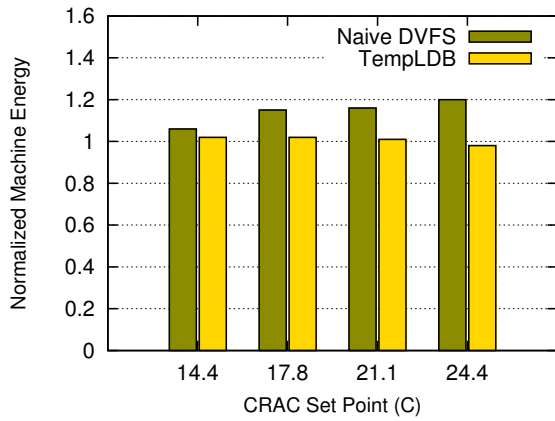
Figure 2.12: Savings in cooling energy consumption with and without Temperature Aware Load Balancing (higher is better)



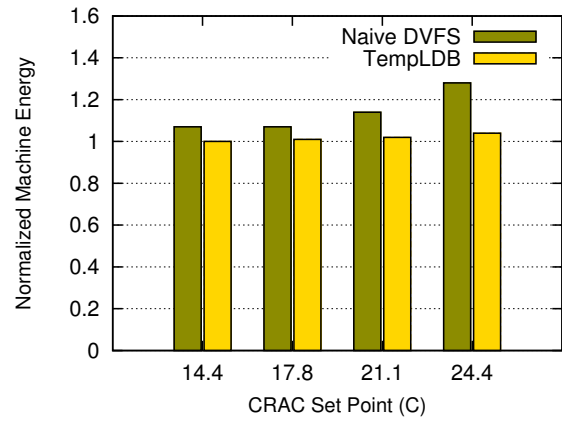
(a) Jacobi2D



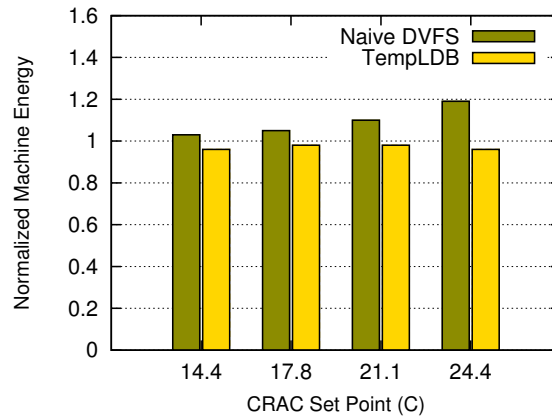
(b) Wave2D



(c) Mol3D



(d) NPB-MG



(e) NPB-FT

Figure 2.13: Change in machine energy consumption with and without Temperature Aware Load Balancing (values less than 1 represent savings)

in Figure 2.14.

In order to study the relationship between machine power consumption and average frequency we plotted the power consumption for each application over the course of a run using *TempLDB* in Figure 2.16. It was counter intuitive to see that despite starting at the same level of machine power consumption as *NPB-FT* and *NPB-MG*, *Jacobi2D* ended up having a much higher average frequency (Figure 2.7(a)). The other interesting observation that we can make from this graph is the wide variation in steady state power consumption among the applications.

Since all the applications are settling to the same average core temperature, the laws of thermodynamics dictate that a CPU running at a fixed temperature will transfer a particular amount of heat energy per unit of time to the environment through its heatsink and fan assembly. Thus, each application should end up having the same CPU power consumption. Similar CPU power consumption would mean that the difference in power draw among the applications in Figure 2.16 is caused by something other than CPU power consumption. Table 2.2 shows that *Jacobi2D* and *Wave2D* have many more cache misses than *Mol3D* and thus end up with a higher power consumption in the memory controller and DRAM, which do not contribute to increased core temperatures but do increase the total power draw for the machine.

In order to verify our hypothesis, we ran two of our applications, *Jacobi2D* and *Wave2D*, on a single node containing a 4-core Intel Core i7-2600K, with a temperature threshold of 50°C. Using our load balancing infrastructure and the newly added hardware energy counters in Intel’s recent Sandy Bridge technology present in this chip, we can measure the chip’s power consumption directly from machine specific registers using Running Average Power Limit (RAPL) library [36]. Both applications begin execution with the CPU at its maximum frequency, which our system decreases as temperatures rise.

The CPU power consumption results from these runs are graphed in figure 2.17. As expected, both applications settled near a common steady state of power consumption for the CPU package (cores and caches combined).

Before highlighting the key findings of our study, we compare our load balancer, i.e., *TempLDB*, with a generic Charm++ load balancer, i.e., *RefineLDB*. *RefineLDB*’s load balancing strategy relies on execution time data for each task without taking into account the frequency at which each core is working. Similar to *TempLDB*, *RefineLDB* also migrates extra tasks from the overloaded cores to the underloaded cores. We implemented our temperature control scheme using DVFS into this load balancer but kept the load balancing part the same. Because *RefineLDB* relies only on task execution time data to predict future load without taking into account the transitions in core frequencies, it ends up taking longer

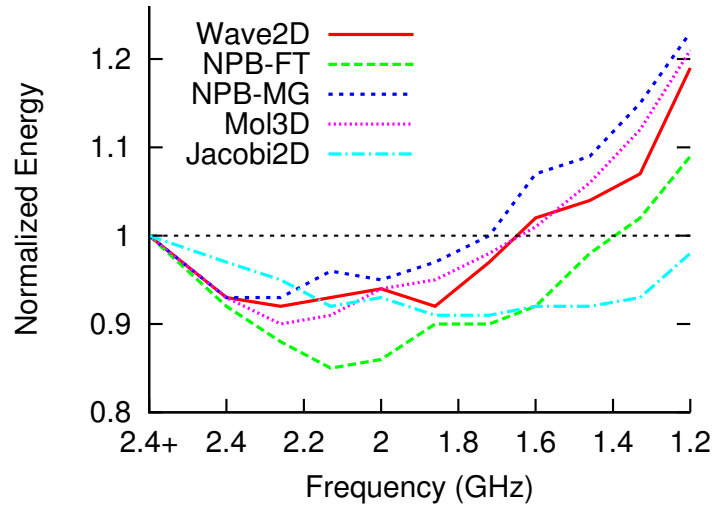


Figure 2.14: Normalized machine energy consumption for different frequencies using 128 cores

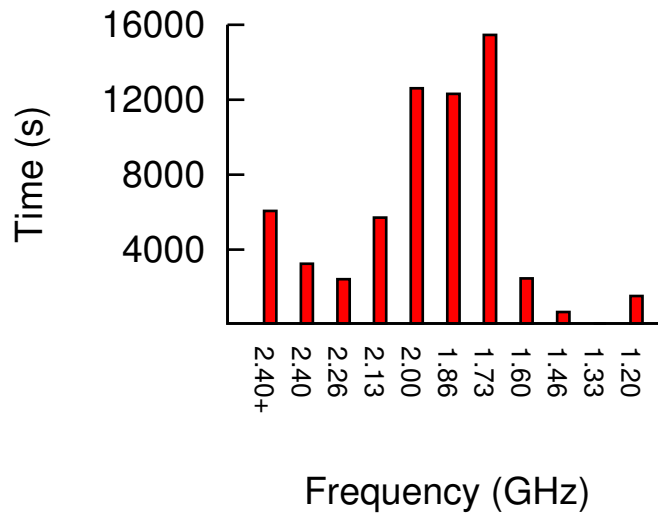


Figure 2.15: The time *Wave2D* spent in different frequency levels

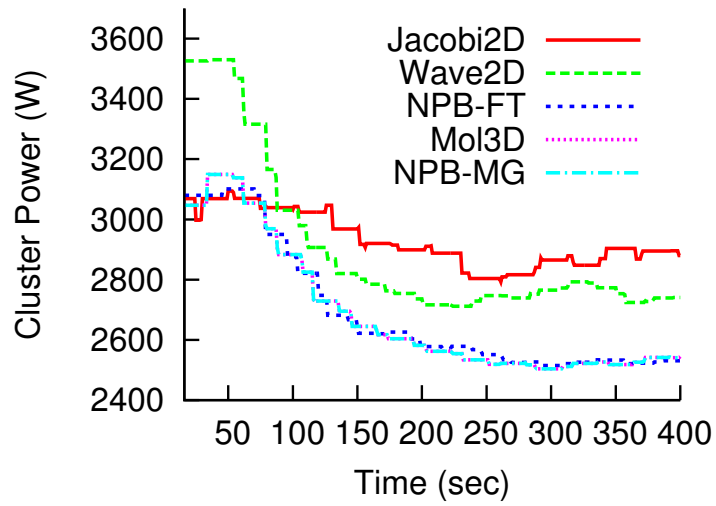


Figure 2.16: Total power draw for the cluster using *TempLDB* at CRAC set-point of 24.4 °C

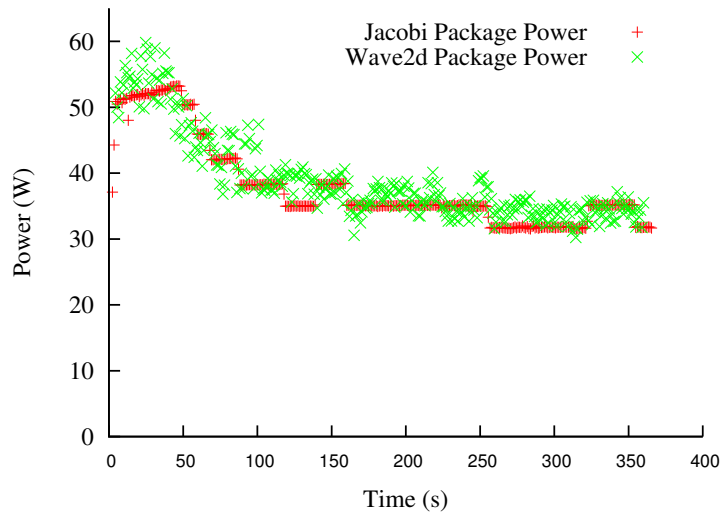


Figure 2.17: Power consumption of two applications as their DVFS settings stabilize to a steady state

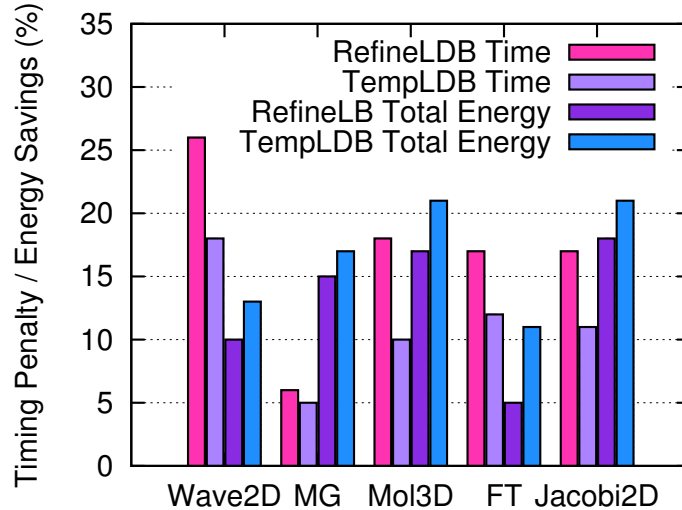


Figure 2.18: Timing penalty and energy savings of *TempLDB* and *RefineLDB* compared to naive DVFS

and consumes more energy to restore load balance. The improvement that *TempLDB* makes can be seen from Figure 2.18 which shows a comparison between both load balancers for all applications with the CRAC set-point at 22.2°C.

## 2.8 Tradeoff in Execution Time and Energy Consumption

The essence of our results can be seen in Figure 2.19, which summarizes the tradeoffs between execution time and *total* energy consumption for all five applications. Each application has two curves, one for each of the *Naive DVFS* and *TempLDB* runs. These curves give important information: the slope of each curve represents the execution time penalty one must pay in order to save each joule of energy. A movement to the left (reducing the energy consumption) or down (reducing the timing penalty) is desirable. For all CRAC set-points across all applications, *TempLDB* takes its corresponding point from the *Naive DVFS* scheme at the same CRAC set-point down (saving timing penalty) and to the left (saving energy consumption).

From Figure 2.19(b), we can see that *Wave2D* is only conducive to saving energy with the CRAC set below 21.1°C, as the curve becomes vertical with higher set-points. However we should note that the temperature range of 47°C–49°C was much lower than the average temperature *Wave2D* reached with the CRAC set at the coolest set-point of 12.2°C without any temperature control. Thus, a higher CRAC set-point imposes too much timing penalty to provide any total energy savings beyond the 21.1°C set-point. Even at 14.4°C we

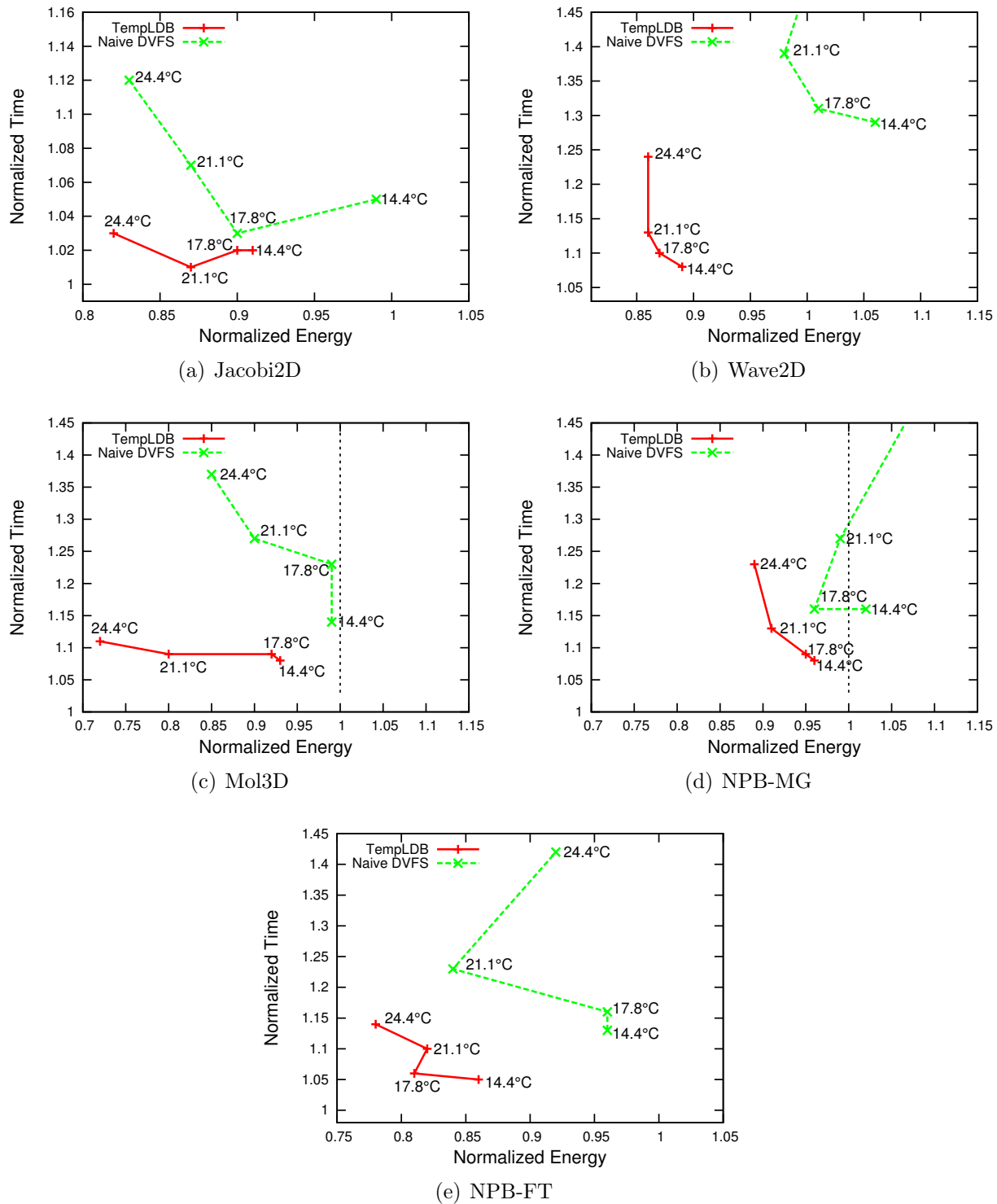


Figure 2.19: Normalized time against normalized total energy for a representative subset of applications

are able to reduce its total energy consumption by 12%. The benefits of using *TempLDB* will eventually end for any application, i.e., the curve will become vertical, as we keep on increasing the CRAC set-point. However, the set-point at which the benefits end would differ amongst different applications.

For *Mol3D*, the nearly flat curve shows that our scheme does well at saving energy, since we do not have to pay a large execution time penalty in order to reduce energy consumption. The same effect holds true for *Jacobi2D*. *NPB-MG*'s sloped curve places it in between these two extremes. It and *NPB-FT* truly present a tradeoff, and users can optimize according to their preferences.



## Thermal Restraint and Reliability

HPC research and its endeavor to build larger machines face several major challenges today including, power, energy, and reliability. Petascale systems spend significant time dumping checkpoint data to remote storage while executing large scientific applications. Although these systems are built from highly reliable individual components, the overall failure rate for them is high due to the sheer number of components involved in building such large machines. Current petascale machines have Mean Time Between Failures (MTBF) that can be anywhere from a few hours to days [37]. These MTBF numbers could be significantly smaller for an exascale machine as pointed out in Figure 1.1. Given the current per socket MTBF values, the proposed exascale machine can have an MTBF of less than an hour!

Past research has shown a relation between core temperatures and reliability. The failure rate of a compute node doubles with every  $10^\circ$  C increase in temperature [8,38–40]. This rule is commonly known as the *10-degree* rule. Most HPC researchers have focused on developing efficient fault tolerance protocols in the past [41–44]. The work presented in this chapter follows a different path. Instead of efficiently dealing with faults, we aim at *reducing* their occurrence. Hence, our scheme can be beneficial when combined with any fault tolerance protocol. In Chapter 2 we demonstrated the ability of thermal restraint to reduce total energy consumption of a data center. We now extend the scheme proposed in Chapter 2 and combine it with a checkpoint-restart protocol [41] to improve application performance in a faulty environment. In this chapter we show that by restraining processor temperatures, we can empower the user to *select* the reliability of the system from within a range. An increase in reliability can improve the performance of an application especially by using load balancing for overdecomposed systems [45]. We also show how different applications can affect the Mean Time Between Failures (MTBF) for a machine due to different thermal profiles. We present and analyze the tradeoffs of improving reliability and its associated cost,

i.e., the slowdown caused by DVFS-driven temperature control. In particular, this chapter makes the following contributions:

- We analyze how restraining temperature of individual processors improves the reliability of the entire machine (Section 3.2.1).
- We formulate a model that relates total execution time of an application to reliability and the associated slowdown for temperature restraint (Section 3.2.2).
- We propose, implement and evaluate a novel approach that extends our earlier work [33, 46] and combines temperature restraint, load balancing and checkpoint/restart to increase reliability while reducing total execution time for an application (Section 3.3). We do several experiments that span over an hour and have at least 40 faults. This work is, as far as we know, the first extensive experimental study that provides insights on the effects of temperature restraint on estimated *MTBF* for HPC machines.
- We first validate the accuracy of our model (Section 3.4) and then use it to show the scheme’s expected benefits for larger machines (Section 3.5). Our results show that for a 340K socket machine, we improve the machine efficiency from 0.01 to 0.22 as a result of improving the machine reliability by a factor of up to 2.29.

## 3.1 Related Work

The classical solution for coping with an ever increasing failure rate due to larger machine sizes and thermal variations is to increase the checkpoint frequency. Unfortunately, checkpoint/restart might not be usable indefinitely as the failure rate grows.

Some alternatives have been explored to keep up with a small *MTBF*. Using local storage to store the state of the tasks has been proposed in the double in-memory checkpoint/restart mechanism [41,47]. Checkpointing in the memory of the nodes is fast and checkpoint periods can become smaller to tolerate frequent failures. Although this mechanism may not tolerate the failure of more than one node, several studies have confirmed that in a high percentage of the failures, only one node is affected [47,48]. Another possibility is to improve recovery time through message-logging. In such protocols, a failure only requires the crashed node to roll back. The rest of the system will re-send the messages and wait for the crashed node to catch up with the rest of the system. A technique called parallel recovery [49] leverages message-logging by distributing the tasks on the failed node to be recovered in parallel on other nodes of the system. This mechanism has been demonstrated to tolerate a higher

failure rate [50]. More recently, replication of tasks has been proposed to deal with high failure rates [12]. However, replication decreases the utilization of the system to 50% at the best. An extremely high failure rate will make this sacrifice pay off, as the utilization of a system using checkpoint/restart drastically decreases if failures are very frequent.

In this dissertation, we take a different approach of dealing with faults. Instead of finding efficient schemes that deal with faults, we aim to *avoid* failures by controlling temperature in all nodes of a system using DVFS. The net result of this temperature capping is a smaller failure rate. We compensate for loss of performance due to DVFS with load balance and over-decomposition. A decreased failure rate is particularly more convenient for checkpoint/restart, but our scheme can be used in tandem with any fault-tolerance method. One of the key advantages of decreasing the failure rate is the reduction in maintenance cost of the supercomputing facility. Each failure may require at least a reboot, but in some situations manual intervention of experts is needed to diagnose the root cause of the crash.

## 3.2 Implications of Temperature Control

Processor temperature has a profound impact on the fault rate of a processor. For every 10° C increase in processor temperature the fault rate doubles [8, 38–40]. While restraining processor temperature improves reliability, it also causes an execution time slowdown due to DVFS. In this section, we use temperature control to estimate the improvement in reliability and its impact on the total execution time of an application.

### 3.2.1 Effects of Temperature Control on Reliability

MTBF for a processor ( $m$ ) is exponentially related to its temperature and can be expressed as: [8–10]

$$m = A * e^{-b*T} \tag{3.1}$$

where  $T$  is the processor temperature,  $A$  and  $b$  are constants. Assuming an  $m$  of 10 years at 40° C,  $m$  per processor based on the 10-degree rule can be expressed as:

$$m = 160 * e^{-0.069T} \tag{3.2}$$

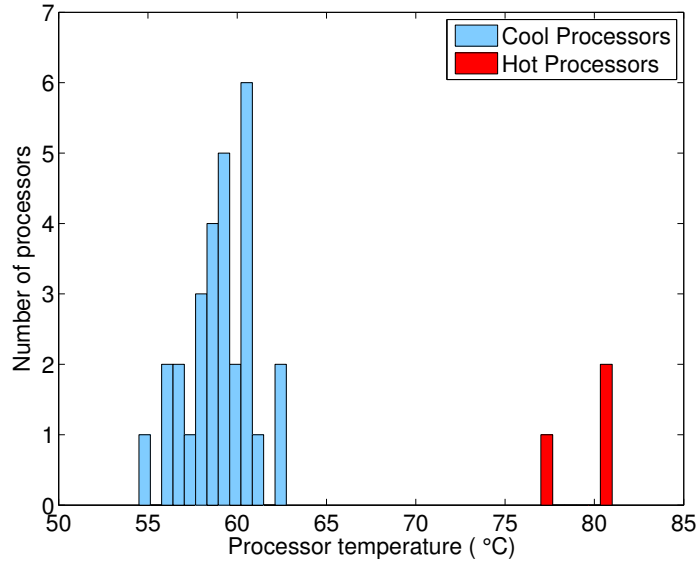


Figure 3.1: Histogram of max temperature for each node of the cluster using *Wave2D*

In a system where the failure of a single component can cause the entire application to fail, the MTBF of the system can be defined as ( $M$ ) [51]:

$$M = \frac{1}{\sum_{n=1}^N \frac{1}{m_n}} \quad (3.3)$$

where  $N$  is the number of nodes and  $m_n$  is the MTBF for socket  $n$ . Although the absolute value of core temperatures is important for each processor’s reliability (Equation 3.2), reliability of the entire cluster also depends on the variance of core temperatures for all processors present in the cluster (Equation 3.3). Presence of hot spots can degrade reliability of the system.

To analyze processor temperature behavior, we ran a 5-point stencil application, *Wave2D*, on a 32 node (128 cores) cluster for over 30 mins and recorded the maximum temperature reached by each processor. The results are pictured in Figure 3.1 where each bar shows the number of processors reaching a specific maximum temperature during the 30-min run. The red bars in Figure 3.1 indicate the presence of a hot spot composed of three processors (hot processors) that heated up to 78° C-80° C. The maximum temperature reached by the remaining 29 processors (cold processors) ranged from 55° C-63° C (shown in blue). The average temperature for the cool processors was  $T_c = 59^\circ \text{C}$ , with a standard deviation of  $\sigma = 2.17^\circ \text{C}$ . Feeding the temperature data from Figure 3.1 to Equations 3.2 and 3.3 estimates the MTBF to be 24 days for our cluster. As Equation 3.2 outlines, we can increase  $m$  for each processor by restraining its temperature to a lower value and hence increase overall  $M$

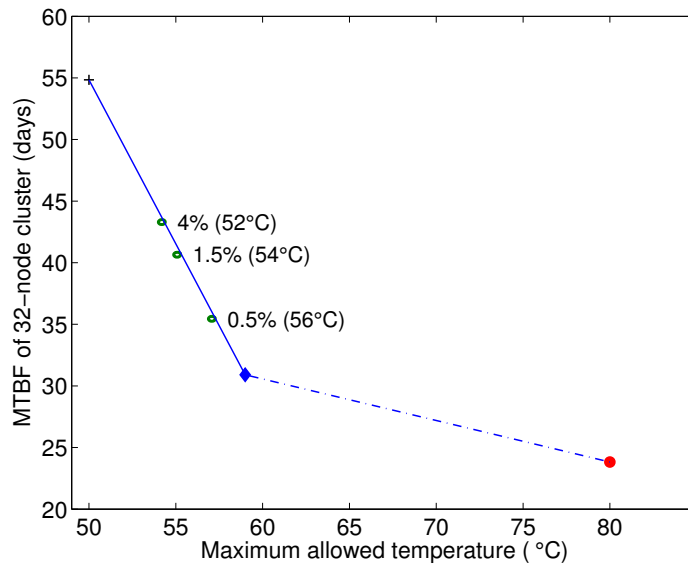


Figure 3.2: Effect of cooling down processors on MTBF of the system

for the cluster. To estimate the improvement in  $M$ , we do the following:

1. Remove the hot spot by bringing the *hot* processors' distribution back to that of *cool* processors
2. Shift the entire distribution towards the left so that all processors operate at an average temperature of  $50^\circ\text{C}$  instead of  $59^\circ\text{C}$

Suppose we remove the hot spot by restraining temperature for the three hot processors to  $T_c = 59^\circ\text{C}$ , i.e., the average temperature for cool processors. Using these new temperature values for the three processors in the hot spot, along with the actual temperature values we got for cool processors, we re-estimate  $M$  and notice an increase of 7 days (from 24 to 31 days). The estimated improvement in  $M$  after hot spot removal is shown by the dashed line in Figure 3.2 which joins the two points representing the value of  $M$  with (red circle) and without (blue diamond) hot spot. We can now predict  $M$  given a temperature restraint for a processor in the hot spot. For example, keeping the three processors in the hot spot to  $70^\circ\text{C}$  would result in an estimated 27.5 days for  $M$ .

So far we have argued that hot spot removal improves  $M$ . Next, we study the effect of restraining temperatures for all the processors to  $50^\circ\text{C}$ . For this, we generate 32 normally distributed random temperature values with a mean of  $50^\circ\text{C}$  and  $\sigma = 2.17^\circ\text{C}$  (same as cool processors) and re-estimate  $M$ . The improvement in  $M$  for any temperature restraint between  $50^\circ\text{C}$  to  $59^\circ\text{C}$  (black '+' and blue diamond in Figure 3.2 respectively) can be estimated from the solid line in Figure 3.2.

These improvements motivated us to use our temperature aware load balancer (Chapter 2) for restraining temperatures to study the slowdown associated with using DVFS for temperature control. For the purpose of this study, we assume that the reliability stays constant while the input voltage to the processor is decreased. Although processor reliability decreases if the processor is operating close to Near Threshold Voltage (NTV) values, the allowed range for DVFS is above the NTV numbers. Hence, our assumption of constant reliability for changing input voltage is reasonable for this study. To test how well DVFS restrains core temperature, we ran *Wave2D* using different temperature thresholds. The small green dots in Figure 3.2 represent experiments carried out on our Energy Cluster (see Appendix A). The percentage in the labels represents the slowdown in execution time compared to the experiment where temperatures are not restrained and all processors always work at maximum frequency. The number in brackets shows the temperature threshold used for that experiment. Decreasing temperature threshold causes the points to move towards the left indicating a decrease in average temperature for all processors. Since the processors are operating at lower temperatures, the estimated  $M$  (using actual temperature data) keeps increasing according to Equations 3.2 and 3.3. However, this improved reliability comes at the cost of DVFS induced slowdown which keeps increasing with reduction in temperature threshold.

### 3.2.2 Effects of Temperature Control on Total Execution Time

In this section, we focus on analyzing whether improvement in  $M$  is significant enough to overcome the slow down associated with temperature control. To this end, we combine the checkpointing technique for fault tolerance [41] with temperature control, to formulate the resulting execution time. This formulation will allow us to investigate the relative impact of different parameters of our framework and enable us to project the results to exascale.

Checkpoint-restart mechanism saves the current state of an application for later restart. Checkpoint time ( $\delta$ ), is the time to dump application state to local storage and checkpoint period ( $\tau$ ) is the frequency of checkpointing. In a fault-prone environment, if the system checkpoints too often, then time may be wasted unnecessarily in dumping the checkpoints. In contrast, a low checkpoint frequency will mean a high amount of work lost in a failure and hence large recovery time. Therefore, a balance must be found. Earlier work [52, 53] proposes well-known models to determine the optimum checkpoint period for a particular combination of system and application.

We leverage DVFS, to incorporate temperature control and its corresponding slowdown,

to extend a popular checkpoint/ restart model [52]. Our model assumes that failure arrival is exponentially distributed and failures are independent of each other. The exponential distribution was assumed to undertake experiments and our work is equally applicable to other fault distributions. We use a collection of parameters to represent different factors that affect performance of a resilient framework. Table 3.1 lists the parameters of our performance model along with a short description of each.

Parameter	Description
$W$	Time to completion in a fault-free scenario
$M$	MTBF of the system
$T$	Total execution time
$\delta$	Checkpoint time
$\tau$	Optimum checkpoint period
$R$	Restart time
$\mu$	Temperature control slowdown

Table 3.1: Parameters of the performance model

With the above parameters, we obtain the total execution time of an application as follows:

$$T = T_{Solve} + T_{Checkpoint} + T_{Recover} + T_{Restart} \quad (3.4)$$

where  $T_{Solve}$  is the time to complete program execution in a fault-free scenario,  $T_{Checkpoint}$  is the total checkpointing time during the entire program execution,  $T_{Recover}$  is the time to recover lost work for all faults occur during execution, and  $T_{Restart}$  is the time necessary to detect the failures and to have the entire system ready to resume execution.

The detailed formulation for total execution time ( $T$ ) of a program under temperature restraint becomes:

$$T = W\mu + \left(\frac{W\mu}{\tau} - 1\right)\delta + \frac{T}{M} \left(\frac{\tau + \delta}{2}\right) + \frac{T}{M}R \quad (3.5)$$

$\mu$  is the ratio between an application’s total execution time in a fault-free scenario with and without temperature restraint. In other words, the parameter  $\mu$  represents the cost of temperature restraint that includes load balancing decision time as well as object migration. In Equation 3.5,  $\left(\frac{W\mu}{\tau} - 1\right)$  represents the number of checkpoints,  $\frac{T}{M}$  is the number of faults expected to occur during execution, and  $\left(\frac{\tau+\delta}{2}\right)$  is the average recovery time per fault.

## 3.3 Approach

In this section, we propose a novel approach, based on task migration and temperature control, to *control* the estimated reliability of HPC machines (within a range). While doing so, our approach simultaneously minimizes total execution time including the overheads of fault tolerance, i.e., checkpointing, recovery and restart. Our scheme should work well with any parallel programming framework allowing task migration. We start by giving an overview of the system model, followed by details of how to use DVFS and task migration to restrain processor temperature efficiently. We then discuss the checkpoint/restart mechanism and conclude by giving an overview of how to combine temperature control, load balancing and checkpoint/restart.

### 3.3.1 System Model

We conceive the underlying machine as a set of *processors* connected through a network that does not guarantee in-order delivery. Each processor is able to run an arbitrary number of *tasks*. The collection of all tasks running on the processors compose the parallel application. Each task will hold a portion of the data and perform its part of computation. The only mechanism to exchange information in the task set is via message passing.

Tasks are *migratable*: each task can serialize its state and be moved to a different processor. A smart runtime system is responsible for monitoring the underlying machine and balancing the load of different processors to achieve better performance. The runtime system uses synchronization points in the application to trigger load balancing and checkpoint/restart frameworks. The runtime system also monitors the temperature in each processor and can change the frequency at which processors operate.

### 3.3.2 Temperature Control and Communication-Aware Load Balancer

We now describe our temperature control mechanism along with communication aware load balancing to mitigate the cost of temperature restraint. The idea is to let each processor work at the maximum possible frequency as long as it is below a user-defined maximum temperature threshold. Since machines of today do not allow DVFS on a per-core basis, we use the average temperature for all on-chip cores to decide whether or not to change the frequency. A key parameter for us is the lower temperature threshold after which we can increase the frequency of the chip. If this lower threshold is close to the maximum threshold,



Variable	Description
$\mathbf{n}$	number of tasks in the application
$\mathbf{p}$	number of processors
$T_{max}$	maximum temperature allowed
$T_{min}$	minimum temperature allowed
$k$	current load balancing step
$taskTime_i^k$	execution time of task $i$ during step $k$ (in ms)
$procTime_i^k$	time spent by processor $i$ executing tasks during step $k$ (in ms)
$f_i^k$	frequency of processor $i$ during step $k$ (in Hz)
$m_i^k$	processor number assigned to task $i$ during step $k$
$taskTicks_i^k$	number of clock ticks taken by $i^{th}$ task during step $k$
$procTicks_i^k$	number of clock ticks taken by $i^{th}$ processor during step $k$
$t_i^k$	average temperature of chip $i$ at start of step $k$ (in °C)
$overHeap$	heap of overloaded processors
$underSet$	set of underloaded processors

Table 3.2: Description for variables used in Algorithm 2 and Algorithm 3

it can cause *frequency thrashing* and lead to expensive object migrations done to achieve load balance.

The pseudocode for our temperature restraint strategy is given in Algorithm 2 with a description of variables in Table 3.2. We start with all processors checking their temperature against the user defined maximum threshold. If the temperature ( $t_i^k$ ) exceeds the maximum threshold, the frequency for that chip ( $C_i$ ) is decreased by one level (P-state). In contrast, if the temperature is less than  $T_{min}$ , the operating frequency for that chip is increased by one level.

Once the frequencies have been changed, the system might become load imbalanced where some processors (with lowered frequency) are now overloaded. We leverage task migratability to correct the load imbalance and transfer objects from the slower-hot processors to the faster-cool processors. This load balancing strategy is an extension of our previous work (Chapter 2) which did not account for communication costs in its load balancing decisions. Algorithm 3 shows the pseudocode for our *communication-aware load balancer*. We start by estimating the total *ticks* required for each task during the last load balancing period as a product of each task’s execution time and the frequency at which its *host* processor was operating (line 3). To fix load imbalance, we calculate the amount of work assigned to each processor (*procTicks*) during the recent load balancing period in terms of ticks

(line 7). While calculating *procTicks*, we also calculate the sum of frequencies (*sumFreqs* at line 8) at which all processors should operate in the *coming* load balance period. We use *sumFreqs* to categorize a processor as *heavy* or *light* for the upcoming load balance period in the function *createOverHeapAndUnderSet*. This function takes the *procTicks* for all processors and uses the *isHeavy* and *isLight* methods (line 26-line 31) to determine if a processor is overloaded or underloaded based on a *tolerance* number. It uses the *isHeavy* method to create a maximum heap for all overloaded processors whereas the underloaded processors are determined by using *isLight* method and are kept in a set.

After identifying overloaded and underloaded processors, we transfer tasks from the former to the latter until no overloaded processors are left in the maximum heap (line 11-line 24). For migration cost minimization, we assume that the initial task-to-processor mapping (*m* vector) is the best and strive to restore it when trying to transfer tasks. To track the initial mapping, we introduce the notion of a *foreign* task. A task is said to be *foreign* if it currently resides on a processor other than the one to which it was initially mapped. We then pop the most overloaded processor from the maximum heap (line 12) and check if it has any *foreign* tasks (line 13). If so, we randomly select one foreign task (line 14), otherwise we randomly select one regular task (line 16). Once the *bestTask* is determined, we look for the best possible processor to whom we could transfer the *bestTask*. The function *getBestProcList* (line 33-line 39) takes the *bestTask*, iterates over all underloaded processors and calculates the amount of communication that occurs between the *bestTask* and each of the underloaded processors *i*. The function *getCommForTask* on line 35 takes the *bestTask* along with an underloaded processor *i* and returns the amount of communication that occurs between them in kilobytes. Using the candidate processors from *sortedProcsList* (line 18), the method *getBestProc* selects the processor (*bestProc*) that communicates the most with *bestTask* and would not be overloaded after receiving *bestTask*. To trigger the actual transfer, the mapping ( $m_{bestTask}^k$ ) is updated along with the *procTicks* variables for both the *donor* and the *bestProc* (receiver) at line 20-22. Now that the *bestTask* has been decided for migration from *donor* to *bestProc*, we update the loads of *overHeap* and *underSet* to reflect this migration (line 23) and continue the loop from line 11.

---

Algorithm 2: Temperature Control

---

```
1: On every processor  $i$  at start of step  $k$ 
2: if  $t_i^k > T_{max}$  then
3:   decreaseOneLevel( $C_i$ ) ▷ increase P-state
4: else if  $t_i^k < T_{min}$  then
5:   increaseOneLevel( $C_i$ ) ▷ decrease P-state
6: end if
```

---

### 3.3.3 Checkpoint/Restart

Rollback-recovery techniques are highly popular in large-scale systems to provide fault tolerance. Among those techniques, checkpoint/restart is the preferred mechanism in HPC. The fundamental principle behind checkpoint/restart is to save the state of the system periodically and to rollback to the latest checkpoint in case of a failure. Several libraries implement one of the many variants of checkpoint/restart [41, 47, 54, 55].

Our fault tolerance scheme is called double local-storage checkpoint/restart [41]. Local-storage refers to any storage device local to the processor (main memory, solid-state drive, local hard disk). Additionally, every processor stores a checkpoint copy in two places. One checkpoint copy is saved in the local storage of the processor and another copy in the local storage of a checkpoint *buddy*. In case of a failure, all processors rollback to the previous checkpoint. The affected processor receives the checkpoint from its buddy. The rest of the processors pull the checkpoint from their own local storage.

Checkpointing is performed in coordination such that all participating processors store their checkpoint at a synchronization point determined by the programmer. Once the checkpoint call is made, every processor collects the state of all tasks residing on it and proceeds to store its two copies of the checkpoint. The runtime system provides a simple interface for each task to dump its state.

We assume the underlying system runs a failure detection mechanism with a processor being considered as the failure unit. Indeed, our checkpoint/restart is resilient to single-processor failures. Multiple-processor failures may be tolerated, without any guarantees for the general case. We follow the *fail-stop* model for processor failures. This means, after a processor crashes, it becomes unavailable and does not come back again. Such processor is replaced by a spare processor taken from a pool of available processors.

---

Algorithm 3: Communication Aware Load Balancing

---

```
1: On Master processor
2: for  $i \in [1, n]$  do
3:    $taskTicks_i^{k-1} = taskTime_i^{k-1} \times f_{m_i^{k-1}}^{k-1}$ 
4:    $totalTicks += taskTicks_i^{k-1}$ 
5: end for
6: for  $i \in [1, p]$  do
7:    $procTicks_i^{k-1} = procTime_i^{k-1} \times f_i^{k-1}$ 
8:    $freqSum += f_i^k$ 
9: end for
10: createOverHeapAndUnderSet()
11: while overHeap NOT NULL do
12:   donor = deleteMaxHeap(overHeap)
13:   if  $numForeignObjs(donor) > 0$  then
14:     bestTask = getForeignTask(donor)
15:   else
16:     bestTask = getRandomTask(donor)
17:   end if
18:   sortedProcsList = getBestProcsList(bestTask)
19:   bestProc = getBestProc(sortedProcsList)
20:    $m_{bestTask}^k = bestProc$ 
21:    $procTicks_{donor}^{k-1} - = taskTicks_{bestTask}^{k-1}$ 
22:    $procTicks_{bestProc}^{k-1} + = taskTicks_{bestTask}^{k-1}$ 
23:   updateHeapAndSet()
24: end while
25:
26: procedure isHeavy(i)
27: return  $procTicks_i^{k-1} > (1 + tolerance) * totalTicks$ 
28:        $*(f_i^k / freqSum)$ 
29:
30: procedure isLight(i)
31: return  $procTicks_i^{k-1} < totalTicks * f_i^k / freqSum$ 
32:
33: procedure getBestProcList(bestTask)
34: for  $i \in underSet$  do
35:    $bestProcs[i].comm = getCommForTask(i, bestTask)$ 
36:    $bestProcs[i].procId = i$ 
37: end for
38: return bestProcs
39:
```

---

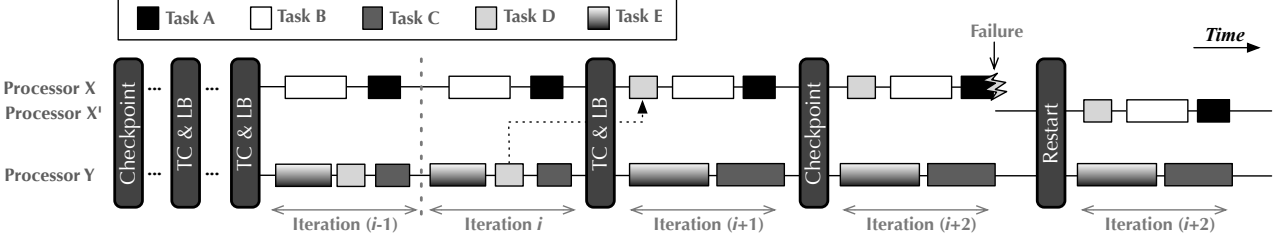


Figure 3.3: Dynamic power management and resilience framework.

### 3.3.4 Framework

In this section, we explain how we provide controllable resilience for HPC systems by bringing together all three modules of our approach, i.e., temperature control (*TC*), communication aware load balancing (*LB*) and checkpoint-restart. Figure 3.3 shows our framework with a system of two processors (*X* and *Y*) running a total of five tasks (from *A* to *E*) that are executed in each iteration of a parallel program. The initial distribution of tasks places tasks *A* and *B* on processor *X* while tasks *C*, *D*, and *E* are mapped to processor *Y*.

As Figure 3.3 shows, the program performs temperature control and load balancing (*TC & LB*) several times during a checkpointing period, i.e., between two adjacent checkpoints. The runtime system routinely adjusts the frequency of processors and solves the load imbalance that may appear. This temperature-capping process decreases the failure rate. However, if a failure occurs, the checkpoint/restart mechanism provides fault tolerance. The program performs several iterations until the *TC & LB* modules are called after iteration  $i$ . The *TC* module detects processor *Y* running at a temperature higher than the max threshold and reduces its frequency. Following this, the *LB* module takes control and removes the load imbalance by migrating task *D* from *Y* to *X* as outlined in Algorithm 3. The system checkpoints after iteration  $i + 1$  and continues execution. A failure takes down processor *X* during iteration  $i + 2$ , which gets replaced by a spare processor that we call processor  $X'$ . The checkpoint buddy of processor *X* provides checkpoint data for *X* to the replacement processor  $X'$  to resume execution until the program finishes.

## 3.4 Experiments

In this section, we provide a comprehensive experimental evaluation of our techniques using three different applications. The first one is *Jacobi2D*: a canonical benchmark that iteratively applies a five-point stencil over a 2D grid of points. The second application, *Wave2D*, uses a finite difference scheme over a 2D discretized grid to calculate the pressure resulting from

an initial set of perturbations. The third application, *Lulesh*, is a shock hydrodynamics application that was defined and implemented by Lawrence Livermore National Laboratory (LLNL) [56]. More details about these applications can be found in Appendix B.

The rest of this section describes our implementation, testbed and experimental results. All experimental results are based on real hardware, and this section does not present any simulation results.

### 3.4.1 Implementation Using Charm++

Charm++ is a parallel programming runtime system that leverages processor virtualization. It provides a methodology where the programmer divides the program into smaller chunks (objects or tasks) that are distributed among the  $p$  available processors by Charm++'s adaptive runtime system [45]. Each of these small chunks is a migratable C++ object that can reside on any processor. The runtime system tracks task execution time and maintains this log in a database to be used by a load balancer for quantifying the amount of work in each task [30].

Based on this information, if the load balancer in the runtime system detects load imbalance, it migrates objects from an overloaded processor to an underloaded one. At small scales, the cost of the entire load balancing process, from instrumentation through migration, is generally a small portion of the total execution time, and less than the improvement that it provides in execution time. When load balancing costs are significant, a strategy must be chosen or adapted to match the application's needs [31]. Our communication-aware load balancer can be adapted to existing hierarchical schemes, which have been shown to scale to the largest machines available [32]. More details about Charm++ load balancing can be found in Chapter 2.

Charm++ implements a coordinated checkpointing strategy in which all processors coordinate their checkpoints to form a consistent global state. Global state includes application-specific data representing all object data as well as the runtime system state that constitutes virtual processor data. Each physical processor keeps a copy of the runtime system state with an arbitrary number of objects and their states. The Charm++ runtime keeps an image of each object on two processors. The first copy resides on the processor which hosts the object whereas the other copy is kept on the *buddy* processor. During checkpointing each processor performs two concurrent steps: 1) packs its system state and sends it to its buddy, 2) packs the user data representing all objects it hosts and sends it to its buddy. In case of a crash, the recovery process is triggered in which all processors rollback to the most

Parameter	Lulesh	Jacobi2D	Wave2D
$\delta$ (s)	9.57	7.65	8.01
$T_{avg}$ ( $^{\circ}$ C)	55.31	53.42	55.56
$M$ (s)	40.31	44.40	39.02
$\tau$ (s)	18.2	18.4	17.0
$R$ (s)	2.2	1.52	1.60
<b>Recovery</b> (%)	33.31	29.05	31.19
<b>Checkpointing</b> (%)	21.40	20.11	20.89
<b>Restart</b> (%)	5.38	3.48	4.03

Table 3.3: Application parameters for *NC* case

recent checkpoint. The crashing processor is either replaced by a new processor or its objects are distributed among existing processors. The object data for the crashing processor is recovered from its buddy.

### 3.4.2 Testbed and Experimental Settings

We evaluated our scheme on the Energy Cluster described in Appendix A. This cluster uses a Liebert power distribution unit installed on the rack containing the cluster to measure the machine power at 1 second intervals on a per-node basis. We gather these readings for each experiment and integrate them over the execution time to obtain the total machine energy consumption.

In Section 3.2.1, we estimated the *MTBF* for our cluster ( $M$ ) to be in the range of 24 - 55 days. To carry out experiments representative of a much larger system, we scale our cluster  $M$  proportionally. We chose an  $m$  of 1 hour at  $40^{\circ}$  C per socket. For a system of 690K sockets, these settings emulate an  $m$  of 10 years per socket. After demonstrating the accuracy of our model by showing that it closely matches experimental results, we make predictions for larger machines. The three applications that we considered exhibited different temperature profiles. Therefore, to make our experiments realistic, we used actual temperature values to estimate  $M$  for each application for experiments without temperature restraint. More precisely, we estimate  $M$  using the maximum temperature that each of the 32 nodes reaches for each application. Table 3.3 shows the cluster-wide average max temperatures for each application in case of no temperature restraint. We refer to this baseline case as *NC* for the rest of the chapter. For experiments where we restrain temperatures, we use the maximum temperature threshold to estimate  $M$ . The values of  $M$  corresponding to each temperature threshold are shown in Table 3.4. After determining  $M$  for each temperature threshold, we generate sequences of exponential random numbers for each experiment, by taking each

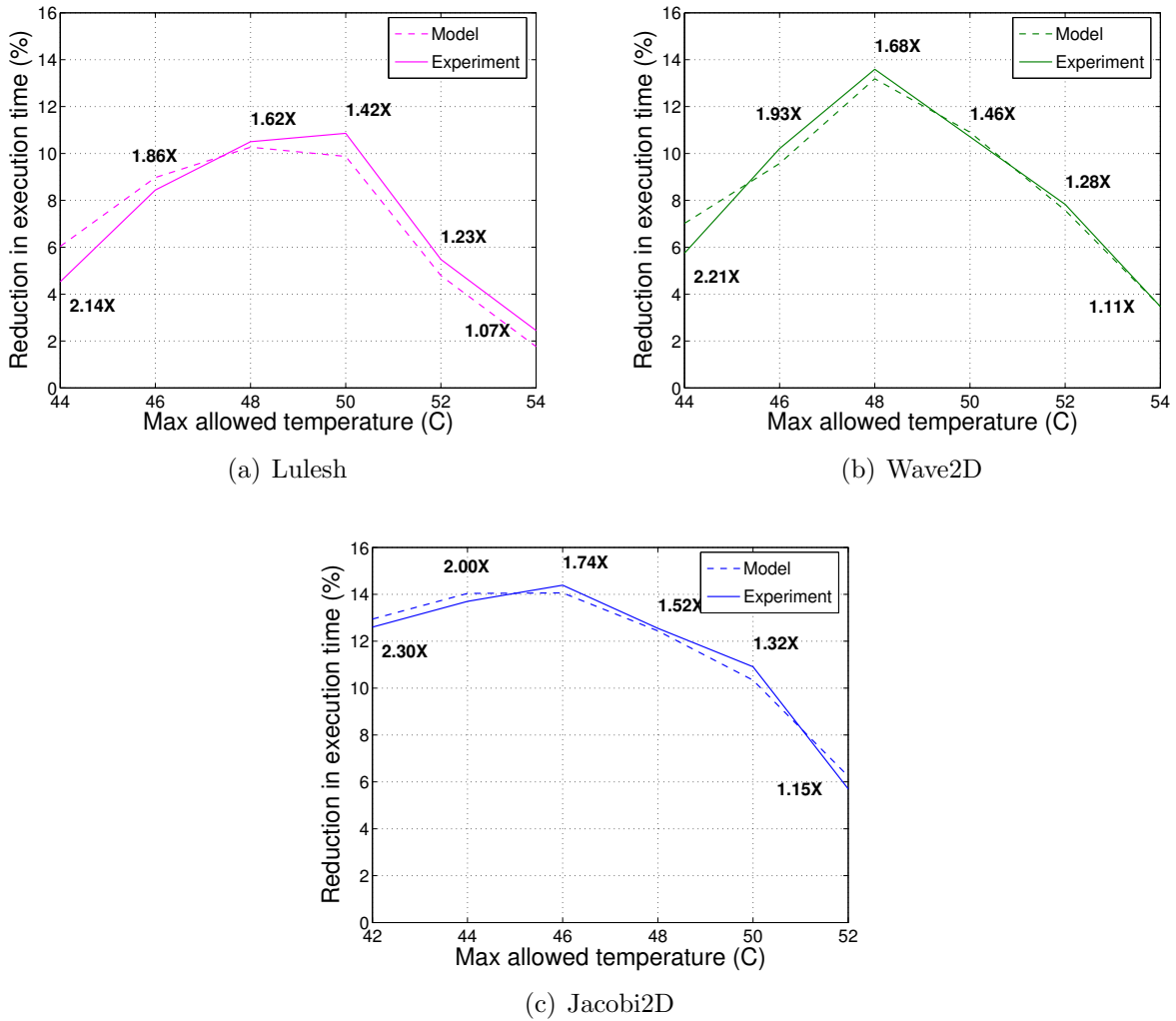


Figure 3.4: Reduction in execution time for different temperature thresholds

$M$  as the distribution mean. We manually insert faults according to these random number sequences for each experiment, by killing a process on any one of the nodes using the `kill -9` command to wipe off all data. To recover from the artificially inserted failures, we calculate the optimum checkpoint period ( $\tau$ ) for each experiment as follows [52]:

$$\tau = \sqrt{2\delta M} - \delta \quad (3.6)$$

Given that  $\tau$  depends on  $M$  and the checkpoint time ( $\delta$ ), we obtain a different optimum checkpoint period for each application when running at a given temperature threshold. The  $\delta$  for each application is listed in Table 3.3.



$T_{max}$	54	52	50	48	46	44	42
<b>M</b>	43.8	50.4	57.8	66.4	76.2	87.5	100.2

Table 3.4: MTBF (sec) for different temperature thresholds (42° C - 54° C)

### 3.4.3 Experimental Results

To establish and to quantify the benefits of our scheme and to validate the accuracy of our model (outlined in Section 5.4), we carried out a number of experiments. We demonstrate how we can improve reliability using temperature control and compare the execution time for experiments with and without temperature control. All experiments reported in this section are compared to the baseline experiments (represented by *NC*) where all processors always operate at the *max* frequency without any temperature control. Since the load balancing technique is not the main focus of this chapter, we would not be giving a detailed comparison of the improved load balancer proposed in Section 3.3 and the one proposed in Chapter 2. However, our proposed new strategy does improve execution time for all three applications. For  $T_{max} = 49^\circ$  C, the communication-aware load-balancer can reduce execution time by 14%, 18%, and 5% for *Wave2D*, *Lulesh* and *Jacobi2D*, respectively, compared to the load-balancer proposed in our earlier work [46]. Each data point (experiment) reported in this section represents a benchmark running for more than 1 hour and being subject to at least 40 faults.

Table 3.3 lists the average maximum temperature for each application. Both *Lulesh* and *Wave2D* have an average maximum temperature that is 2° C higher than that for *Jacobi2D*. Due to this difference in temperature profile, we ran *Jacobi2D* for a maximum temperature threshold range of 42° C-52° C as opposed to 44° C-54° C used for *Lulesh* and *Wave2D*. This difference in thermal profile is also responsible for making different applications operate at different average frequencies. For example, when running below a temperature threshold of 46° C, the average frequencies across the cluster for *Lulesh*, *Jacobi2D* and *Wave2D*, were 2.30 Ghz, 2.31GHz and 2.27 GHz, respectively. Although our testbed has a maximum Turbo Boost frequency of 2.8GHz, using DVFS to restrain temperatures resulted in lower average frequency for all applications. A detailed discussion about the interaction between temperature, frequency and performance can be found in Chapter 2.

Figure 3.4 shows percentage reduction in execution time using both temperature restraint and load balancing compared to the baseline experiments, i.e., *NC*. The two curves in each plot compare experimental results with model predictions. The model predictions for Figure 3.4 were gathered by feeding checkpoint time, slowdown, restart time and useful work time to Equation 3.5 and using golden section search and parabolic interpolation to

optimize  $\tau$  for minimum total execution time. The inverted U shape of all three curves strongly suggests a tradeoff between reliability ( $M$ ) and the DVFS induced slowdown ( $\mu$ ) due to temperature restraint. Figure 3.4 also shows the ratio of  $M$  for the machine using our scheme relative to the *NC* case. For example, by restraining temperatures to 42° C in case of *Jacobi2D*,  $M$  for the machine increased 2.3 times compared to the case of *NC*. Hence, restraining the temperature to a lower value may decrease the benefits of our scheme but it would always improve estimated reliability of the machine.

### 3.4.4 Interplay Between Temperature, MTBF and Checkpointing Overheads

*MTBF* for a machine ( $M$ ) is dependent on each processor’s temperature. Higher processor temperatures for *Lulesh* and *Wave2D* imply a lower  $M$  than *Jacobi2D* (Table 3.3). This forces *Wave2D* and *Lulesh* to spend a higher percentage of time in recovery as they encounter more failures compared to *Jacobi2D* (Table 3.3). Although  $M$  for *Wave2D* and *Lulesh* are close in the case of *NC*, they spend different percentages of time in recovery, i.e., 31.19% and 33.31% respectively. This observation can be explained by looking at their  $\tau$  values (Table 3.3). According to Equation 3.6, a larger checkpoint time ( $\delta$  in Table 3.3) for *Lulesh* results in a larger  $\tau$  which increases the *average* recovery time for *Lulesh* ( $\frac{\tau+\delta}{2}$  in Equation 3.5). On the other hand, *Lulesh*’s higher  $\tau$  causes it to spend almost an equal percentage of time in checkpointing as *Jacobi2D* and *Wave2D* , i.e., 21.40% (Table 3.3), despite *Lulesh*’s large  $\delta$ . Although the time per checkpoint ( $\delta$ ) for *Lulesh* is the highest, the product of the number of checkpoints and  $\delta$  is equal to other applications due to fewer checkpoints ( $\frac{W\mu}{\tau} - 1$ ) for *Lulesh*. *Lulesh* also spends 5.38% of its total time in restarts, which can be attributed to the higher restart cost of 2.2 seconds (Table 3.3).

### 3.4.5 Comparing the Benefits Across Applications

Although all three applications have a inverted U shaped curve, their maxima occur at different temperature thresholds. We define this optimum point for each application by the tuple  $(T_{max}, r_{max})$ , where  $T_{max}$  is the temperature threshold corresponding to the point that represents the maximum reduction in execution time for an application. Figure 3.4 shows that the optimum points for *Jacobi2D*, *Wave2D*, and *Lulesh* are (46° C,14.2%), (48° C,13.5%), and (50° C,11%) respectively. We notice that the applications differ in *both* members of the tuple. An application’s optimum point depends on the tradeoff between percentage reduc-

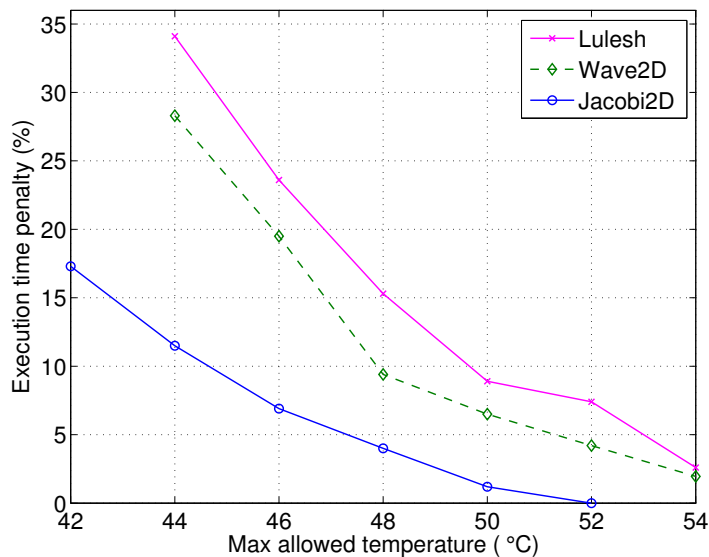


Figure 3.5: Execution time penalty for DVFS

tion in each category of total time (recovery, checkpoint and restarting times), which is a result of improvement in  $M$ , and its associated cost. This slowdown, including overhead of object migration during load balancing, is shown in Figure 3.5. The slowdown for each application increases as the temperature threshold decreases. As the temperature threshold decreases, the frequency at which a processor could operate also decreases. The reduced frequency in turn implies a higher slowdown. The slowdown is worse in case of CPU intensive applications. Figure 3.5 points to a similar trend. *Lulesh* is the most CPU intensive application whereas *Jacobi2D* has the highest memory footprint. Hence, the slowdown for *Lulesh* is higher than *Jacobi2D* for all temperature thresholds. In general, we should expect applications having high memory footprint to have smaller slowdown and hence, higher benefits for using our scheme. Figure 3.4 shows that *Jacobi2D* has the most gain, i.e., 14.2% using our scheme, whereas the gain for *Lulesh* is 11%. These gains validate our claim: lower the slowdown, higher the gain for using our scheme.

Another observation that we can make is that the temperature threshold and the cost of temperature control  $\mu$  are directly related. Figure 3.5 shows that *Lulesh* had the maximum slowdown leading to a larger optimum temperature threshold (50°C) and therefore it receives the least reduction in execution time (11%) among all three applications. On the other hand, *Jacobi2D*, experiences the least slowdown, which results in the highest reduction in execution time, i.e., 14.2%, and the lowest optimum temperature threshold. The slowdown for *Wave2D* lies in between *Lulesh* and *Jacobi2D*, which results in a reduction in execution time that is between 11%-14.2%, i.e., 13.5%.

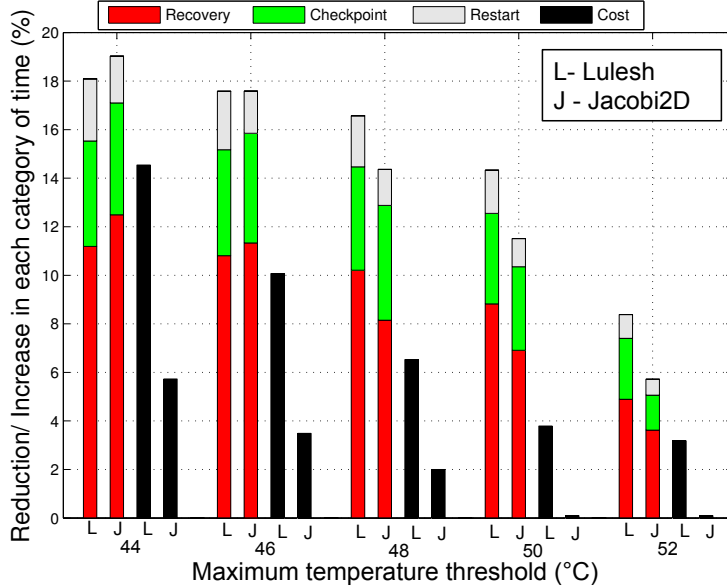


Figure 3.6: Gains/cost of increasing reliability for different temperature thresholds

### 3.4.6 Understanding Application Response to Temperature Restraint

All applications that we considered respond differently to temperature restraints which is why each one has a different optimum point. For more insights, we compare and contrast how *Jacobi2D* and *Lulesh* respond to temperature control in Figure 3.6. Here, we plot the percentage of time reduced for each category of execution time (including recovery, checkpoint, and restart times), as a percentage of total time taken in case of *NC*.

We used the following formula to determine the recovery percentage ( $p_i^{rec}$ ) corresponding to the maximum temperature threshold of  $i^\circ$  C for Figure 3.6:

$$p_i^{rec} = \frac{t_{NC}^{rec} - t_i^{rec}}{T_{NC}} * 100 \quad (3.7)$$

where  $T_{NC}$  is the total execution time in case of *NC*,  $t_{NC}^{rec}$  is the recovery time for *NC* and  $t_i^{rec}$  is the recovery time for the experiment where the maximum threshold was  $i^\circ$  C. Figure 3.6 also shows the cost of temperature control for *Lulesh* and *Jacobi2D* which represents DVFS-incurred slowdown in doing *useful work* ( $W\mu$  in Equation 3.5). This cost  $p_i^{cost}$  as well as the percentage reduction in checkpoint  $p_i^{ckpt}$  and restart times  $p_i^{res}$  are calculated similar to  $p_i^{rec}$  in Equation 3.7. We make two observations from Figure 3.6.

First, we look at the total gain (sum of recovery, checkpointing and restart gains). While the total gains are always greater for *Lulesh* compared to *Jacobi2D* (except for  $44^\circ$  C), its cost of temperature control is always significantly lesser than that for *Lulesh*. Hence, the

net gain (*total gains - cost*) for *Jacobi2D* makes it much more appropriate for our scheme compared to *Lulesh*.

Next, we observe that  $p_{48}^{rec}$ ,  $p_{50}^{rec}$  and  $p_{52}^{rec}$  are higher for *Lulesh* compared to *Jacobi2D* whereas for lower thresholds,  $p_{44}^{rec}$  and  $p_{46}^{rec}$  are lower for *Lulesh*. Recall from Figure 3.4 that *Lulesh* improves reliability of the system more than *Jacobi2D*, i.e., (1.86X, 2.14X) compared to (1.74X, 2.00X) for thresholds of 46° C and 44° C, respectively. Even then, the high timing penalty for *Lulesh* depicted in Figure 3.6 is limiting the gains from increased reliability. The timing penalty not only contributes directly as cost of improving reliability by prolonging useful work, it also indirectly affects the benefits of our scheme by limiting the gains that we obtain in recovery. So if a timing penalty of  $\mu$  gets added to the total execution time, then the faults, checkpoints and restart that happen during  $\mu$  essentially work to cancel out some of the gains achieved by temperature restraint during the earlier part of execution. The timing penalty is precisely what shrinks the gain bars in Figure 3.6. However, even with the higher timing penalty of *Lulesh*, its gains are sufficient to reduce execution time as compared to the case of *NC*.

### 3.4.7 Reduction in Energy Consumption

After highlighting how our scheme successfully reduces execution time and increases  $M$ , we now analyze the reduction in machine energy consumption that happens as a direct consequence of our scheme. Figure 3.7 shows the percentage reduction in machine energy consumption for each application compared to the baseline case (*NC*). These numbers represent actual machine energy consumption for experiments measured using power meters. The figure shows that we were able to reduce machine energy consumption by as much as 25% in case of *Jacobi2D* by restraining processor temperatures at 42° C. Although the reduction in execution time contributes to reduction in energy consumption, the major part of savings comes from temperature control which reduces the machine’s power consumption. In addition to the reported reduction in machine energy, our scheme should also reduce the cooling energy significantly (Chapter 2).

## 3.5 Projections

In Section 3.4, we thoroughly investigated our approach and validated our model by carefully comparing it against experimental results. Now, we use the validated model to project the benefits of our scheme for larger machines. We estimate improvement in machine efficiency

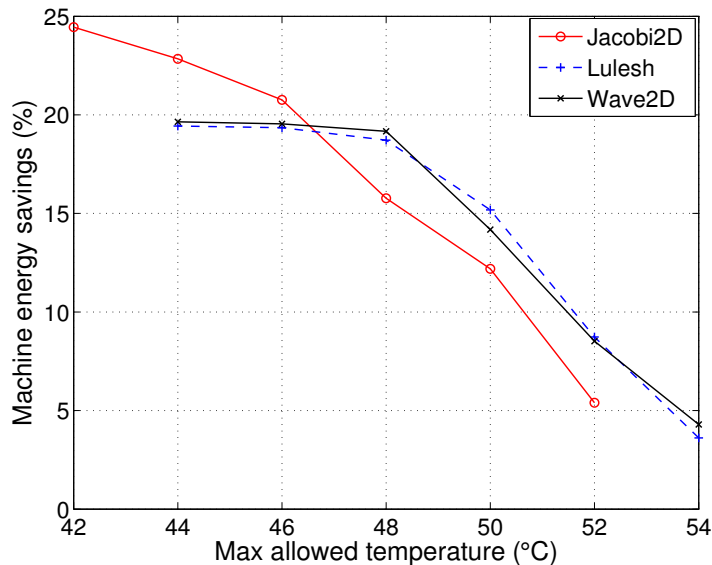


Figure 3.7: Reduction in machine energy consumption for all applications

for larger number of sockets and also analyze the benefits of our scheme while increasing memory size of an exascale machine.

### 3.5.1 Benefits for Increasing Number of Sockets

Figure 3.8 shows the reduction in execution time that we achieve for all three applications compared to the case of  $NC$ . For this plot, we use an  $m$  of 10 years per socket with a restart time of 30 secs. We show all three applications using their optimum temperature thresholds ( $T_{max}$ ) from Section 3.4.5. Moreover, to highlight how  $T_{max}$  influences the reduction in execution time, we plot *Jacobi2D* for  $T_{max}= 42^\circ$  C as well. We assume checkpoint time to be 240 secs [11]. The dashed black line in Figure 3.8 shows 0% reduction in execution time. The points below this signify an overhead of our scheme whereas the ones above this line represent reduction in total execution time using our scheme. The numbers in the legend of Figure 3.8 represent the *times* improvement in  $M$  for each application. Even though we can see an execution time penalty of 15% for 1K sockets in case of *Jacobi2D* with a  $T_{max}$  of  $42^\circ$  C, it increases the reliability of the machine by a factor of 2.29X. The same *Jacobi2D* runs with lesser penalty at  $T_{max}$  of  $46^\circ$  C for 1K sockets but its reliability decreases to 1.74X.

For a smaller number of sockets(less than 32K), running *Jacobi2D* with a  $T_{max}$  of  $42^\circ$  C incurs a cost that is much higher than the gain. However, beyond the crossover point (32K), the cost is justified as the gain becomes significantly higher. Hence, the optimum  $T_{max}$  can be different for different applications at various scales, e.g., at 230K sockets, *Jacobi2D* with

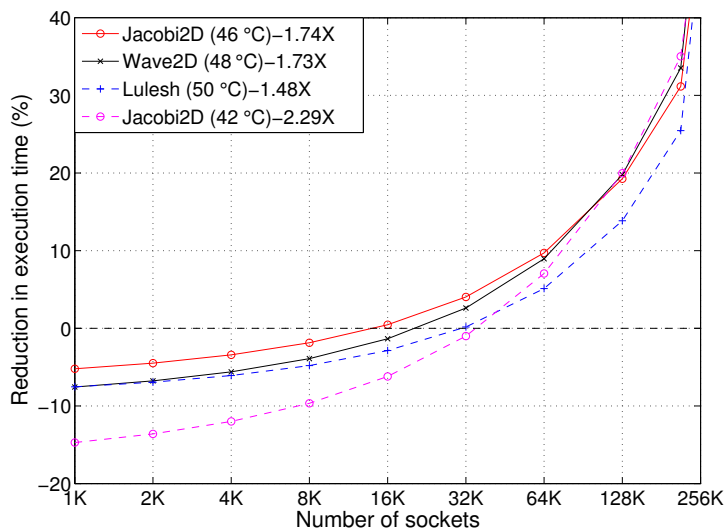


Figure 3.8: Execution time reduction for all applications at large scale

a  $T_{max}$  of 42° C reduces the execution time by 38% compared to 32% if run at  $T_{max}$  of 46° C.

Efficiency can be defined as the fraction of the total execution time, including the fault tolerance overheads, that is spent in doing useful work. A decrease in total execution time can be thought of as an improvement in machine efficiency. Figure 3.9 plots the machine efficiency for *Wave2D* at  $T_{max} = 48^\circ \text{C}$  using the same parameters as Figure 3.8. Even though we account for DVFS incurred slowdown in our efficiency calculation, our scheme still improves machine efficiency significantly for larger socket counts. The numbers shown in Figure 3.9 represent the ratio of efficiency for our scheme relative to the case of *NC*. For less than 32K sockets, we get a lower efficiency compared to the case of *NC* (efficiency  $< 1X$ ). However, after 32K sockets, our scheme starts outperforming the *NC* case ( $> 1$  efficiency values). For 340K sockets, our scheme is projected to operate the machine with an efficiency of 0.22 (95% reduction in execution time) compared to 0.01 for the *NC* case. Finally, for 350K sockets, the efficiency for *NC* case drops to 0.003 making the machine almost non-operational using only checkpoint/restart, whereas our scheme can still operate the machine at an efficiency of 0.20.

### 3.5.2 Sensitivity to Memory-per-socket and MTBF

The checkpoint time of 240 sec predicted in Kogge’s report [11] is made under the assumption that an exascale machine will have 224K sockets with 64GB of memory per socket. Adding more memory to the proposed machine increases the number of components that

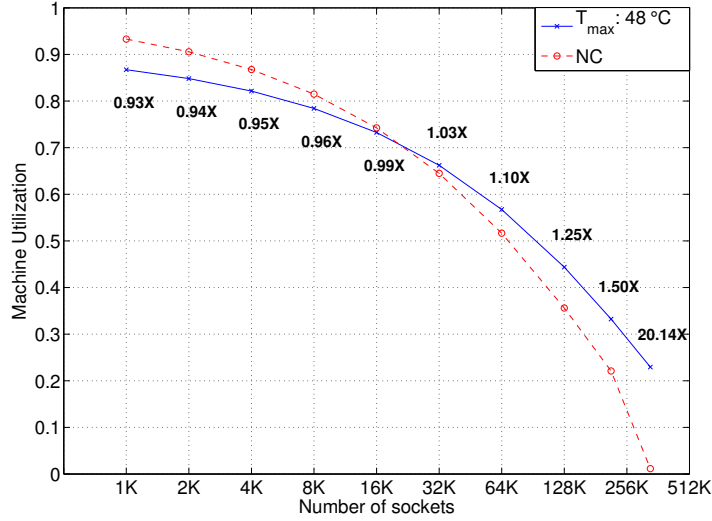


Figure 3.9: Projected efficiency for *Wave2D*

can significantly decrease the reliability. With the proposed memory size (13.6 PB), the machine will have a flop-memory ratio of 0.01 Petaflops/TB which is far smaller than 96 Petaflops/TB and 134 Petaflops/TB for Sequoia and the K computer [13] respectively. To evaluate if our scheme can enable an exascale system to have more memory, we predicted the improvement in  $M$  as well as the reduction in execution time that our scheme can achieve compared to the case of  $NC$  as we keep on increasing memory per socket. Adding memory implies more data to checkpoint. We use the same methodology used in Kogge’s report [11] to calculate the checkpoint time as we keep on increasing memory per socket. Figure 3.10 shows the results from our model for *Jacobi2D* projected on an exascale machine.  $MTBF$  per socket can have a significant effect on the total execution time of an application. The MTBF of LANL’s clusters is 10 years per socket [57] whereas Jaguar had a 50 years MTBF per socket [58]. Other studies show MTBF per socket to be between 20-30 years [59, 60]. For capturing the sensitivity of our scheme to MTBF, we plotted lines corresponding to 5 different MTBF per socket ranging from 10-50 years. Figure 3.10 shows that our scheme will decrease the execution time for any memory size per socket using any of the five MTBF values. Even the two memory sizes used in Kogge’s report [11], i.e., 16GB and 64GB, will end up benefitting from our scheme.



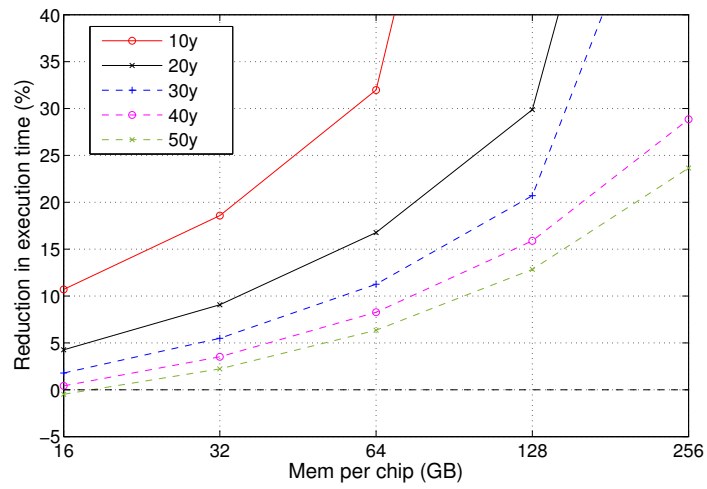


Figure 3.10: Reduction in execution time for different memory sizes of an exascale machine

# Optimizing Performance Under a Power Budget

The first part of the thesis emphasized the importance of thermal restraint for an HPC data center. Chapter 2 presented empirical results showing significant reductions in energy consumption of a 128-core cluster. Chapter 3 combined checkpointing and thermal restraint to improve application performance. In the next two chapters, we aim to deal with another important challenge that the HPC community faces: improving application performance under a strict power constraint.

Applications do not yield a proportional improvement in performance as the processor frequency is increased [61]. This insensitivity is mainly because memory accesses are much slower compared to processor frequency. Memory accesses therefore introduce stalls in processor cycles. The extent of improvement in application performance resulting from increased processor frequency depends on the application's computational and memory demands. As we approach the exascale era, the thrust is more on power consumption than on energy minimization. A strict power constraint poses a hard research challenge. DOE has currently set a bound of 20MW for an exascale system, therefore available power must be used efficiently to achieve the exascale goal. Scaling frequency via DVFS does not guarantee a strict limit on the power consumption of a processor. However, the recently released Intel's Sandy Bridge family of processors provide an enticing option of limiting the power consumption of a processor chip and memory (also available in IBM Power6 [62], Power7 [63] and AMD Bulldozer [64] architectures). The power consumption for package and memory subsystems can be user-controlled through the RAPL (Running Average Power Limit) library [65].

In this part of the thesis (Chapter 4 and Chapter 5), we use Intel's *power\_gov* [66] library that in turn uses RAPL to cap power of memory and package subsystems in order to optimize

application performance under a strict power budget for an *overprovisioned* system. An overprovisioned system [14] has more nodes than a conventional system operating under the same power budget. It cannot simultaneously power all nodes at peak power. However, capping package (CPU) and memory power below peak power can enable an overprovisioned system to operate all nodes simultaneously. Under a strict power budget, running the application on fewer nodes with a higher CPU/memory power per-node can sometimes be less efficient than running it on more nodes with relatively lower power per node. Capping the CPU and memory power to lower values enables us to utilize more nodes for executing an application. However, each additional node utilized has a fixed cost of powering up the motherboard, power supply, fans and disks referred to as the *base* power. The base power of a node determines the ease with which additional nodes can be utilized in an overprovisioned system. The opportunity cost of base power for these additional nodes is the performance benefit that can be achieved by increasing the CPU and memory power for the existing set of nodes. This opportunity cost can vary between applications.

The work presented in this chapter *optimizes* the number of nodes and the subsequent distribution of power between CPU and memory for an application under a strict power budget. The major contributions of this chapter are listed below:

- We propose an interpolation scheme that captures the effects of strong scaling an application under different CPU and memory power distributions with minimal profile information.
- We present experimental results showing speedups of up to 2.2X using an overprovisioned system compared to the case where CPU and memory powers are not capped.
- We show the optimized CPU and memory power distributions for different applications and examine the factors that influence them.
- We analyze the effect and importance of base power on achievable speedup for an overprovisioned system.

The rest of the chapter is organized as follows. Section 4.1 describes related work. In Section 4.2, we outline our interpolation scheme. Section 4.3 details our experimental setup. Section 4.4 presents a case study that demonstrates the working details of our scheme. In Section 4.5 we present our experimental results.

## 4.1 Related Work

To the best of our knowledge, this chapter provides the first study that estimates and analyzes the optimized *distribution* of power among the CPU and the memory subsystem, in the context of an overprovisioned system under a strict power budget. Rountree et al [65] have studied the variation in application performance under varying power bounds using RAPL. In continuation of this work, Patki et al [14] proposed the idea of overprovisioning the compute nodes in power-constrained high performance computing. Their work relies on selecting the best configuration out of a set of profiled configurations. Because of the sheer number of possible configurations, exhaustively profiling an application for all possible node counts, CPU power caps and memory power caps is practically infeasible. Our work introduces a novel interpolation scheme, that takes into account the effects of strong scaling an application under different CPU and memory power caps and estimates the missing configurations. Our work also differs from prior work [14] since we take into account the effect of memory capping that can significantly improve the speedups for most applications. Another novel aspect is that our scheme is based on *total* machine power which includes base power, i.e., power consumption of everything other than the CPU and the memory subsystem, that can significantly alter the observed speedups across applications.

The idea of overprovisioning has been studied and implemented in the architecture community in a similar context [67] e.g. Intel’s Nehalem has overprovisioned cores. The CPU can either run all of these cores at lower clock frequencies or a few of them at highest clock frequencies due to power and thermal bounds. Additionally, earlier work has mostly focussed on reducing energy consumption under a time bound for HPC applications. Rountree et al [2] have used linear programming to reduce energy consumption with negligible execution time penalty. In our earlier work, we have used DVFS to trade execution time for lower cooling and machine energy consumptions [33, 46].

## 4.2 Approach

Power consumption of different applications varies significantly. Moreover, the usefulness of increasing the power budget of an application also varies between applications [61]. We formulate our problem statement as follows:

*Optimize the numbers of nodes ( $n$ ), the CPU power level ( $p_c$ ) and memory power level ( $p_m$ ) that minimizes execution time ( $t$ ) of an application under a strict power budget ( $P$ ), on an overprovisioned high performance computation cluster with  $p_b$  as the base power per*

Variable	Description
W	Watts
$p_b$	node base power (W)
$p_c$	CPU/Package power cap (W)
$p_m$	memory power cap (W)
$P_c$	set of allowed CPU caps used
$P_m$	set of allowed memory caps used
N	set of number of nodes used
$\mathcal{P}_c$	set of CPU power caps used for profiling in <i>Step 1</i>
$\mathcal{P}_m$	set of memory power caps used for profiling in <i>Step 1</i>
$\mathcal{N}$	set of number of nodes used for profiling in <i>Step 1</i>
P	maximum allowed power budget (W)
t	execution time for an application (s)

Table 4.1: Terminology

*node.*

In this section, we outline our interpolation scheme that estimates execution time using application profiles for different scales, CPU power levels and memory power levels. The terminology used in the chapter is defined in Table 4.1. We denote an operating configuration by  $(n \times p_c, p_m)$  where  $n$  is the number of nodes and  $p_c, p_m$  are the CPU and memory power caps, respectively. To determine the optimized configuration for running an application, we need to profile the application for each configuration  $(n \times p_c, p_m)$  where  $n \in N, p_c \in P_c, p_m \in P_m$ . Such exhaustive profiling adds up to a total of  $|N| \times |P_c| \times |P_m|$  possible configurations, assuming  $P_c$  and  $P_m$  have integral values only. Such exhaustive profiling of an application is practically infeasible because of the sheer number of possible configurations. For example, in a cluster with only 20 nodes, 71 CPU power levels and 28 memory power levels, we would need to profile the application for 39,760 possible configurations, which is practically infeasible. Therefore, we break the application performance analysis into two steps: performance measurement by actual profiling (*Step 1*) followed by performance estimation using curve fitting/ interpolation (*Step 2*).

### Step 1: Performance measurement by actual profiling

We start application profiling by running it for a selected set of configurations that span the entire range of available configurations. In other words, we only profile the application for a subset of the total possible configurations, i.e.,  $(n \times p_c, p_m)$  where  $n \in \mathcal{N}, p_c \in \mathcal{P}_c, p_m \in \mathcal{P}_m$ .

## Step 2: Performance prediction by curve fitting or interpolation

In this step, we use curve fitting on the profiled data obtained in *Step 1* to estimate the execution time for *any* possible configuration  $(n \times p_c, p_m)$  where  $n \in N$ ,  $p_c \in P_c$  and  $p_m \in P_m$ . Behavior of execution time ( $t$ ) with  $n, p_c$ , and  $p_m$ , can be represented in a 4D plot. However, visualizing a 4D plot can be tedious. Hence, we present application profiles by plotting  $t$  against the total power  $p$  in 2D, where  $p$  takes  $p_c, p_m$ , and  $n$  into account, using the following equation:

$$p = n * (p_b + p_c + p_m) \quad (4.1)$$

Presenting the profile in a 2D plot facilitates its visualization and makes it easier to determine the optimized configuration. To estimate execution time for any configuration we need to find the relationship of execution time to power consumption across the three dimensions, i.e.,  $n, p_c$ , and  $p_m$ . Beginning with the  $|\mathcal{N}| \times |\mathcal{P}_c| \times |\mathcal{P}_m|$  actually profiled configurations in *Step 1*, interpolation is accomplished in the following three steps:

1. Interpolation across memory power: For each pair of  $(n, p_c)$  where  $n \in \mathcal{N}, p_c \in \mathcal{P}_c$ , we fit a curve  $\phi_{n,p_c}(x)$  across the profiled values of memory caps, i.e.,  $p_m \in \mathcal{P}_m$ , where  $x \in P_m$ . This process yields  $|\mathcal{N}| \times |\mathcal{P}_c|$  such curves. A given curve,  $\phi_{n,p_c}$ , can be used to obtain an estimate of  $t$  corresponding to any  $p_m \in P_m$  using  $n$  nodes capped at CPU power level of  $p_c$ . Using the  $\phi_{n,p_c}$  curves, we can estimate the execution times for all configurations  $(n \times p_c, p_m)$  where  $n \in \mathcal{N}, p_c \in \mathcal{P}_c$ , and  $p_m \in P_m$ .
2. Interpolation across node counts: To capture the behavior of strong scaling, we fit a curve  $\psi_{p_c,p_m}(x)$  across the profiled values of  $n$ , i.e.,  $n \in \mathcal{N}$ , where  $x \in N$ , for each pair of  $(p_c, p_m)$  where  $p_c \in \mathcal{P}_c$  and  $p_m \in P_m$ . This process results in  $|\mathcal{P}_c| \times |\mathcal{P}_m|$  strong scaling curves. A given strong scaling curve,  $\psi_{p_c,p_m}$ , can estimate  $t$  for any  $n \in N$  where each node is operating under CPU and memory power caps of  $p_c$  and  $p_m$  respectively. These strong scaling curves can be used to obtain values of  $t$  for all configurations  $(n \times p_c, p_m)$  where  $n \in N, p_c \in \mathcal{P}_c$ , and  $p_m \in P_m$ .
3. Interpolation across CPU power: Finally, we interpolate  $t$  across CPU power. We fit a curve  $\theta_{n,p_m}(x)$  across the profiled values of  $p_c$  ( $p_c \in \mathcal{P}_c$ ) where  $x \in P_c$ , for every pair of  $(n, p_m)$  such that  $n \in N$  and  $p_m \in P_m$ . We retrieve  $|N| \times |P_m|$  curves for interpolating across  $p_c$ . A given curve,  $\theta_{n,p_m}$ , estimates  $t$  for any  $p_c \in P_c$  using  $n$  nodes operating under a memory power cap of  $p_m$ . These  $\theta_{n,p_m}$  curves can be used to estimate

execution times for all possible configurations, i.e.,  $(n \times p_c, p_m)$ , where  $n \in N$ ,  $p_c \in P_c$  and  $p_m \in P_m$ .

### 4.3 Setup

We used the Power Cluster to carry out all experiments for this chapter (see Appendix A). The Intel Sandy Bridge processor family supports on board power measurement and capping through the Running Average Power Limit (RAPL) interface [36]. The Sandy Bridge architecture has four power planes: Package (PKG), Power Plane 0 (PP0), Power Plane 1 (PP1) and DRAM. RAPL is implemented using a series of Machine Specifics Registers (MSRs) that can be accessed to read power readings for each power plane. RAPL supports power capping PKG, PP0 and DRAM power planes by writing into the relevant MSRs. The average base power per node ( $p_b$ ) for our cluster was 38 watts. The base power was measured using the in-built power meters on the Power Distribution Unit (PDU) that powers our cluster. We experimented with *Lulesh*, *Wave2D* and *LeanMD* to demonstrate the use of our scheme (see Appendix B).

### 4.4 Case Study: Lulesh

In this section, we demonstrate the application of our scheme in estimating the optimized configuration for an iterative application under a strict power budget by considering the *Lulesh* application. The profiling experiments were conducted on the Power cluster outlined in Appendix A. The following CPU and memory power caps were selected for profiling (*Step 1*):

$$\begin{aligned} \mathcal{P}_c &= \{28, 32, 36, 44, 50, 55\} \\ \mathcal{P}_m &= \{8, 10, 14, 18\} \end{aligned}$$

Since determining the optimized number of nodes ( $n$ ) is part of our scheme, we profile the application for strong scaling as well:

$$\mathcal{N} = \{5, 8, 12, 16, 20\}$$

Figure 4.1 shows *Lulesh*'s execution profile for some of these configurations. The Y-axis corresponds to the average execution time per step, and the X-axis shows the *total* power

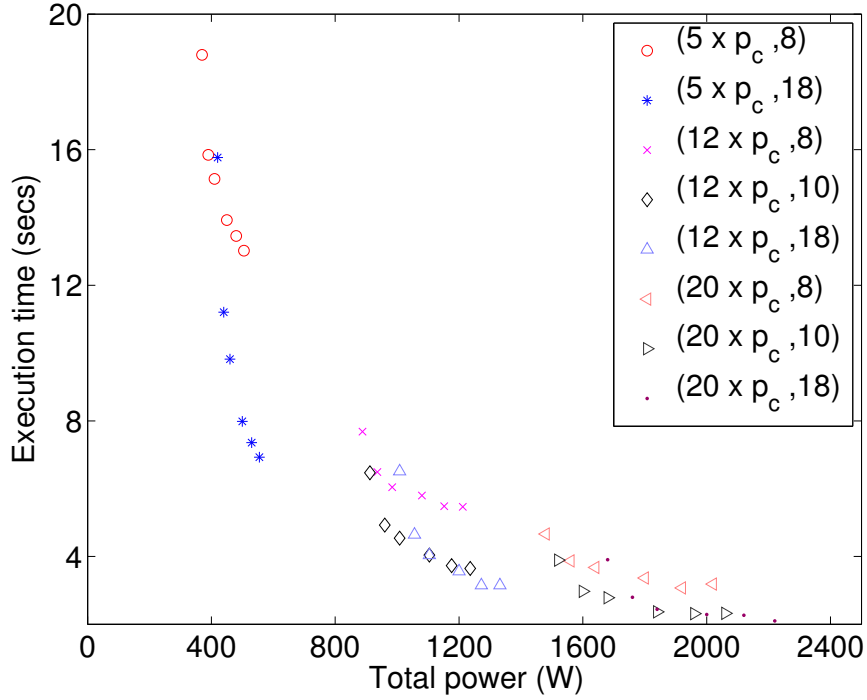


Figure 4.1: Average time per step of *Lulesh* for configurations selected in Step 1

( $p$ ) of the system (calculated using Equation 4.1). Each set of configurations in Figure 4.1 contains 6 points corresponding to varying CPU power, i.e.,  $p_c \in \{28, 32, 36, 44, 50, 55\}$ . The leftmost point for each set corresponds to  $p_c = 28W$ , whereas the rightmost point uses  $p_c=55W$ . Based on the profile data, we can pick an efficient configuration for a given power budget as follows: We draw a vertical line at the given power budget  $P$  and choose the lowest point on or to the left of that vertical line. Following are three examples of finding the optimized configurations for a given power budget ( $P$ ).

- $P = 1200W$ : the best profiled configuration is  $(12 \times 44, 18)$ .
- $P = 1600W$ : the best profiled configuration is  $(20 \times 32, 10)$ . In this case, using more nodes with each node capped at relatively lower CPU and memory power levels is better compared to the  $P = 1200W$  case, in which fewer nodes are used at a higher CPU and memory power levels.
- $P = 800W$ : Since we do not have profile data close to the power budget of 800W, we have to proceed leftwards to the  $(5 \times 55, 18)$  configuration. This configuration corresponds to a total power consumption of 555W. Hence, the available power is not completely used which makes it an inferior solution.



We now see how our interpolation scheme can improve the solution. We need to identify the three sets of functions  $\phi_{n,p_m}$ ,  $\psi_{p_c,p_m}$ , and  $\theta_{n,p_c}$  that interpolate across all three dimensions. Figure 4.1 shows that the behavior of  $t$  across all three dimensions is the same.  $t$  is more sensitive to each of  $n$ ,  $p_c$ , and  $p_m$  at lower values of  $p$  as compared to larger values of total power ( $p$ ). For example, for  $n = 12$  and  $p_m = 18$ ,  $t$  reduces faster for  $p_c$  in the range 28W to 36W compared to the case when  $p_c$  is in the range 44W to 55W. Similarly, for  $n = 12$  and  $p_c = 55$ ,  $t$  reduces faster when  $p_m$  is in the range 8W to 10W compared to when  $p_m$  is in the range 10W to 18W. This pattern can be modeled by the use of two exponential terms. We therefore express execution time ( $t$ ) for each of these curves,  $\phi_{n,p_c}$ ,  $\psi_{p_c,p_m}$  and  $\theta_{n,p_m}$  by:

$$t(p) = \frac{a}{e^{b*p}} + \frac{c}{e^{d*p}} \quad (4.2)$$

where  $a$ ,  $b$ ,  $c$ , and  $d$  are constants and  $p$  is total power budget. As mentioned in Section 4.2, while interpolating across each of the  $n$ ,  $p_c$  and  $p_m$  dimensions, the other two dimensions remain constant. Hence,  $p$  (Equation 4.1) only captures the change in power consumption for the dimension being interpolated since the other terms in Equation 4.1 are constant. We use `Matlab`'s curve fitting toolbox that uses linear and non linear regression to determine these constants for each of the curves. Based on the characteristic mentioned above, Equation 4.2 can be thought of as having two parts:  $f_l(p)$  and  $f_h(p)$ .

$$t(p) = f_l(p) + f_h(p) \quad (4.3)$$

For lower values of  $p$ ,  $f_l(p)$  dominates  $f_h(p)$ , whereas  $f_h(p)$  becomes dominating at higher values of  $p$ . This behavior is achieved by selecting appropriate constants. At lower values of  $p$ , values of  $t$  are large and decrease at a faster rate. Hence, the constants  $a$  and  $b$  in  $f_l(p)$  are large. When  $p$  is large,  $t$  is smaller and decreases slowly with  $p$ . This implies smaller values for the constants  $c$  and  $d$  in  $f_h(p)$ . For large values of  $p$ , a higher value of  $b$  also makes  $f_l(p)$  negligible.

Figure 4.2 plots a few of  $\phi_{n,p_c}$ ,  $\psi_{p_c,p_m}$  and  $\theta_{n,p_m}$  curves for interpolating across the three dimensions, i.e.,  $n$ ,  $p_c$ , and  $p_m$ . To simplify the discussion we omit a few profile points from Figure 4.2. We remove  $p_c = 28W$  from  $\mathcal{P}_c$  so that it now is  $\mathcal{P}_c = \{32, 36, 44, 50, 55\}$ . We now explain how these curves were obtained by applying *Step 2* described in Section 4.2.

- We demonstrate interpolation across memory using the following example.  $\phi_{12,55}$  from Figure 4.2 is obtained by fitting the curve from Equation 4.2 to configurations  $(12 \times 55, p_m)$  for  $p_m \in \{8, 10, 14, 18\}$  and evaluating the constants. We can now estimate  $t$  for configuration  $(12 \times 55, 9)$  using  $\phi_{12,55}$  and Equation 4.1. This configuration is

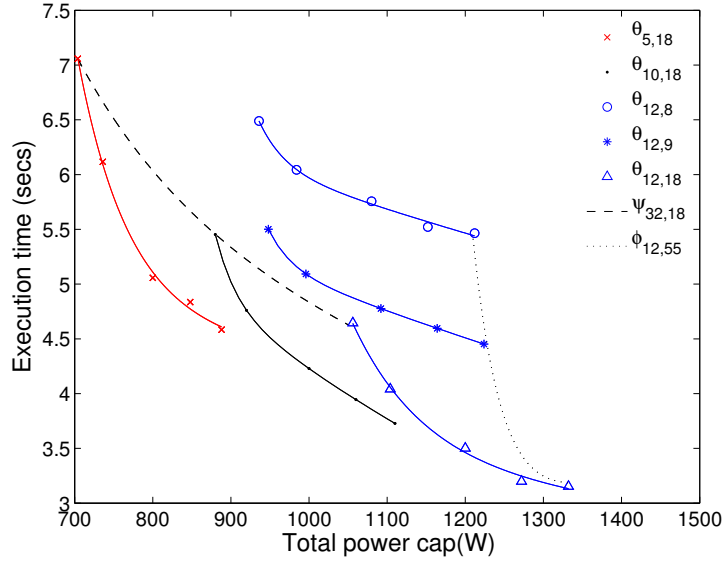


Figure 4.2: Average time per step of *Lulesh* after interpolation (Step 2)

represented by the rightmost '\*' (in blue) in Figure 4.2. Similarly, we can fit curves to profile data to obtain the curves  $\phi_{12,p_c}$  for  $p_c \in \{32, 36, 44, 50\}$ . Using these curves, we can estimate  $t$  for configurations  $(12 \times p_c, 9)$  for  $p_c \in \{32, 36, 44, 50, 55\}$ . These configurations are shown by '\*' in Figure 4.2.

- To estimate the strong scaling performance for different values of  $n$ , we use curve fitting for fixed values of  $p_c$  and  $p_m$ . For example,  $\psi_{32,18}$  is obtained by fitting the curve from Equation 4.2 to configurations  $(n \times 32, 18)$ , for  $n \in \{5, 8, 12, 16, 20\}$ . We later use this curve to estimate  $t$  for  $n = 10$ . This configuration is represented by the topmost solid black circle in Figure 4.2. We obtain the curves  $\psi_{p_c,18}$  for  $p_c \in \{32, 36, 44, 50\}$  in a similar manner and evaluate them at  $n = 10$  to estimate  $t$  for combinations  $(10 \times p_c, 18)$  for  $p_c \in \{32, 36, 44, 50\}$  (Figure 4.2).
- In the final step, we interpolate data from the previous step to estimate the execution times for all CPU power caps. All solid lines in Figure 4.2 correspond to interpolation across CPU power. For example,  $\theta_{5,18}$  is obtained by fitting Equation 4.2 to configurations  $(5 \times p_c, 18)$  for  $p_c \in \{32, 36, 44, 50, 55\}$ . Finally, we have  $|N| \times |P_m|$  curves for  $\theta$ .

As a result of interpolating across these three dimensions, we now have a *set* of curves,  $\theta_{n,p_m}$ , that represent *all* possible configurations that could be obtained using exhaustive profiling. To get the optimized configuration for a power budget  $P$ , we evaluate the  $\theta$  curves

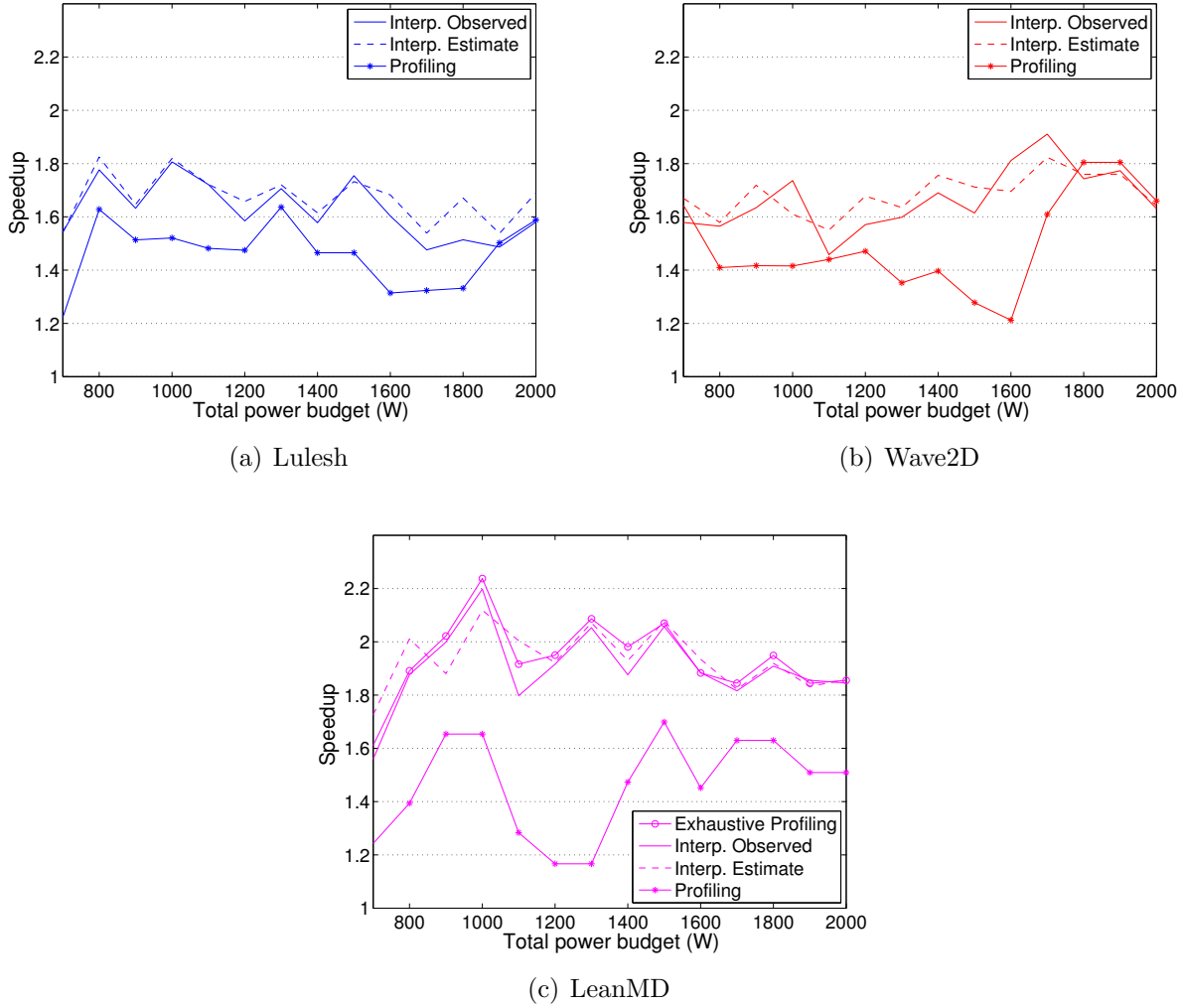


Figure 4.3: Speedups obtained using CPU and memory power capping in an over-provisioned system

for that  $P$  and chose the configuration that results in the minimum  $t$ . If the curve  $\theta_{n^0, p_m^0}(P)$  results in the minimum  $t = t^0$ , the optimized configuration is given by  $(n^0 \times \frac{P}{n^0} - p_b - p_m^0, p_m^0)$  after using Equation 4.1 and solving for  $p_c$ .

## 4.5 Results

In this section, we use our interpolation model to estimate optimized configurations for different power budgets for the three parallel applications mentioned in Section 4.3. Machine vendors specify the thermal design power (TDP) for CPU and memory subsystems. These

numbers represent the maximum power each of these subsystems can draw while operating within the thermal limits. Data centers do not take application characteristics into account and therefore calculate the total power assuming that each node can draw the TDP wattage specified by the manufacturer. We refer to this configuration as the *baseline* configuration. The *baseline* configuration for a power budget of  $P$  is given by:

$$(n_b \times TDP_c, TDP_m)$$

$$\text{where } n_b = \left\lfloor \frac{P}{p_b + TDP_c + TDP_m} \right\rfloor,$$

and  $TDP_c$  and  $TDP_m$  represent the CPU and memory TDP values respectively. For our testbed cluster,  $TDP_c = 95\text{W}$  and  $TDP_m = 35\text{W}$ . TDP of a node for our cluster totals to  $168\text{W}$  after adding the base power of  $38\text{W}$ . Hence, for the baseline case we employ the maximum number of nodes, without power capping, accounting for a maximum possible power draw of up to  $168\text{W}$  per node, i.e.,  $n_b = \frac{P}{168}$ . We compare the benefits resulting from power capping CPU and memory subsystems using our scheme against the baseline case for different power budgets. We use speedup over the baseline case as the metric for comparison. Speedup is defined as the ratio of the execution time for the baseline case and the execution time that results from the optimized configuration estimated by our scheme. We perform real experiments to corroborate the estimates made using our scheme. In particular, we present results to gauge the effectiveness of our approach to meet the following criterion:

- Speedup achieved: Comparing the best configurations from profiled data (Step 1) to the best configurations estimated using our scheme (Step 2).
- Quality of solution: Comparing model estimates to actual experimental results
- Cost of estimating the optimized configuration: Amount of profiling required to make accurate predictions.

#### 4.5.1 Benefits of Using our Interpolation Scheme

In Figure 4.3, we present the speedups achieved using power capping in an over-provisioned system for different power budgets. The ‘Profiling’ curve plots the actual speedups that are obtained by selecting the optimized configuration from the profiled data from Step 1 (without interpolation). The ‘Interp. Estimate’ plots the estimated speedups obtained from the interpolated curves from Step 2. We do actual experiments for the optimal configurations predicted in Step 2 and plot the observed speedups shown as the ‘Interp. Observed’ curve.

We can see from Figure 4.3 that the observed speedups ('Interp. Observed') match closely to the estimated speedups ('Interp. Estimate'). The difference in the estimated and observed speedups can be attributed to system/cluster noise and to the estimation accuracy of our interpolation scheme. Speedups of *Lulesh*, *Wave2D*, *LeanMD* fall in the range [1.55,1.80], [1.45,1.9], [1.57,2.2] respectively. Although each application ends up in a different speedup range, we get a minimum speedup of at least 1.45X for any power budget. Speedup that an application can achieve is attributed to two factors:

- The difference between the CPU/memory TDP and the *actual* (measured) power consumed by the CPU/memory.
- The sensitivity of execution time to the CPU/memory subsystems power consumption.

Performance can be improved by exploiting the first attribute through a single profiling run. We can profile the application and determine the maximum CPU and memory power consumed by the machine during the execution. However, speeding up the application by exploiting the second factor is only possible if the relationship between  $t$ ,  $p_c$ , and  $p_m$  is known. Figure 4.3 also compares the speedups for optimized configurations estimated by our model and profiling data. Although using only profiling data can speed up an application, the configurations estimated by our scheme are much superior in terms of speedup. The observed speedups resulting from our scheme for *LeanMD* are generally 0.40X greater than the configurations estimated by simple profiling (Step 1).

We could improve on the speedups from just profiling (Step 1) through more exhaustive profiling, which would require considerable machine time. We mentioned in Section 4.2 that  $|N| \times |P|_c \times |P|_m$  runs are required to profile an application exhaustively. Considering the permissible ranges of  $p_c$ ,  $p_m$ , and  $n$  for our testbed, we need to run each application for 39760 configurations, which is infeasible. However, for *leanMD* we did exhaustive profiling since memory power is always less than 8W. We only need to profile it for different values of  $n$  and  $p_c$ . The speedups from this exhaustive profiling for *LeanMD* are shown in Figure 4.3 by the curve labeled 'Exhaustive Profiling'. These speedups are close to the speedups estimated by our interpolation scheme, which indicates the high accuracy of our scheme in predicting the *optimized* configurations.

## 4.5.2 Profiling Requirements for Interpolation

To analyze the robustness of our scheme in estimating optimized configurations, we used different amounts of profile data as an input to our interpolation scheme. Since there are

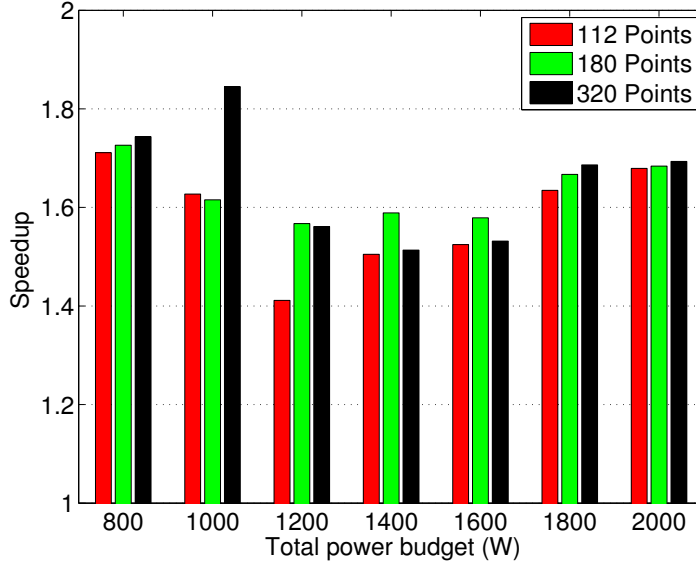


Figure 4.4: Observed speedups using different number of profile configurations (points) as input to our interpolation scheme

four unknowns ( $a$ ,  $b$ ,  $c$ , and  $d$ ) in Equation 4.2, we require at least 4 data points to fit across each dimension, i.e.,  $n$ ,  $p_c$  and  $p_m$ . Hence, we need at least 64 configurations (data points) for interpolation. We used our scheme to estimate optimized configurations for three different sets of profile data for *Lulesh*. Each profile data set had a different number of profiled configurations, i.e., 112, 180 and 320 configurations. We used each of these profile data sets as input to our interpolation scheme and evaluated the resulting speedups. Figure 4.4 shows the speedups achieved for various power budgets. These speedups are calculated by performing actual experiments corresponding to the optimized configuration for each case. Although the speedups resulting from optimized configurations generally improve as we increase the profile data points, we are able to achieve reasonable speedups with even 112 configurations.

### 4.5.3 Optimized Number of Nodes, CPU and Memory Power Distribution

We present the optimized  $p_c$  and  $p_m$  values that result from our scheme for different power budgets in Figure 4.5. We also plot the *actual (measured)* maximum values for CPU and memory power consumption in the baseline experiments for the same power budgets. Figure 4.5 shows that our scheme allocates higher CPU power ( $p_c$ ) for *Lulesh* and *LeanMD* as compared to *Wave2D*. These optimized values of  $p_c$  that result from our model lie in the range of [29,35] for *Wave2D*. The optimized values for  $p_c$  range from [41,46] and [40,47] for

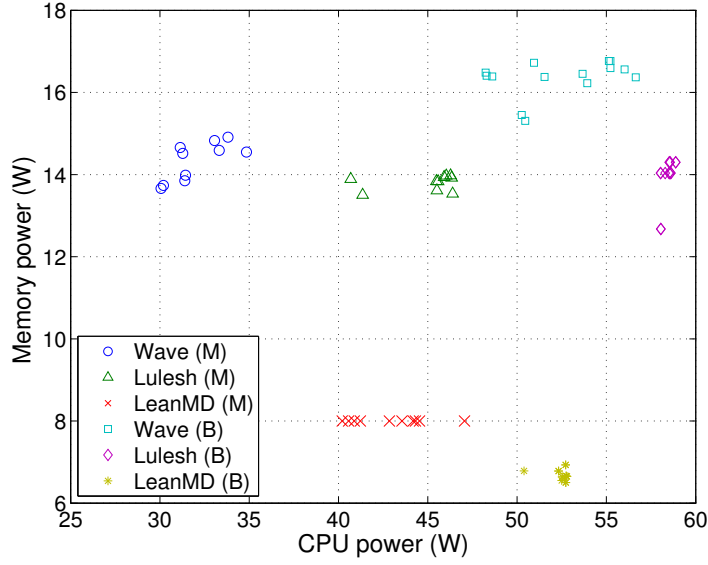


Figure 4.5: Optimized CPU and memory power caps under different power budgets compared to the maximum CPU and memory power drawn in the baseline experiments

*Lulesh* and *LeanMD*, respectively. Extra watts allocated to any of the applications outside the upper limit of its range can instead be used to power another node and strongly scale the application in an overprovisioned system. Figure 4.6 compares the optimized number of nodes for each application for different power budgets to the number of nodes used in the baseline case. The number of nodes in the baseline configuration are independent of the application. Our scheme caps the CPU and memory power to lower values, which enables it to use up to twice as many nodes as the baseline case. *Wave2D* generally requires the lowest combined CPU + memory power followed by *LeanMD* and *Lulesh* (Figure 4.5). Thus, *Wave2D* generally uses the highest number of nodes followed by *LeanMD* and *Lulesh*.

#### 4.5.4 Analyzing the Optimized Configurations

The difference in the maximum measured values of CPU power for the baseline case and the optimized value of  $p_c$  from our scheme is about 12W for *LeanMD* and *Lulesh* (Figure 4.5). This difference is as much as 20W in the case of *Wave2D*. To understand why the two cases are different, we plot speedups for different values of  $p_c$  and  $n$ . Speedups in Figure 4.7 are normalized with respect to the execution time at  $p_c = 25$ W. This normalization is done to measure the benefits of increasing the CPU power beyond the minimum CPU power cap allowed. *Lulesh* and *LeanMD* are more sensitive to  $p_c$  as compared to *Wave2D*. In fact, execution time for *Wave2D* ceases to improve beyond  $p_c=35$ W for any value of  $n$ . Our

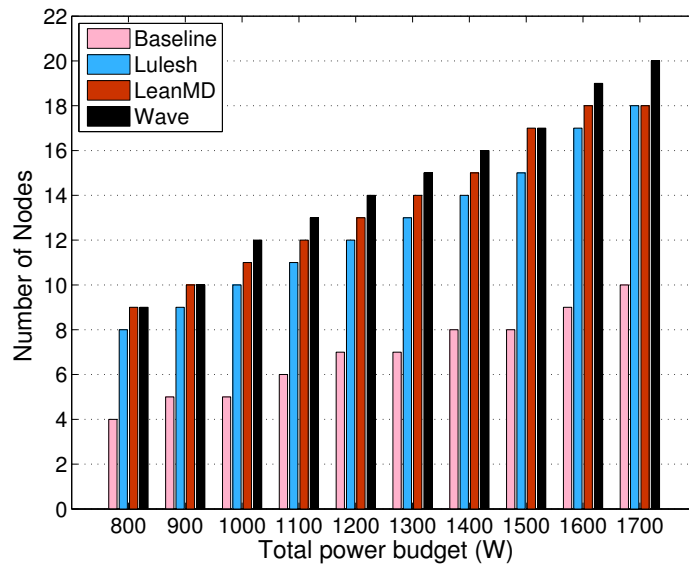


Figure 4.6: Optimal number of nodes under different total power budgets

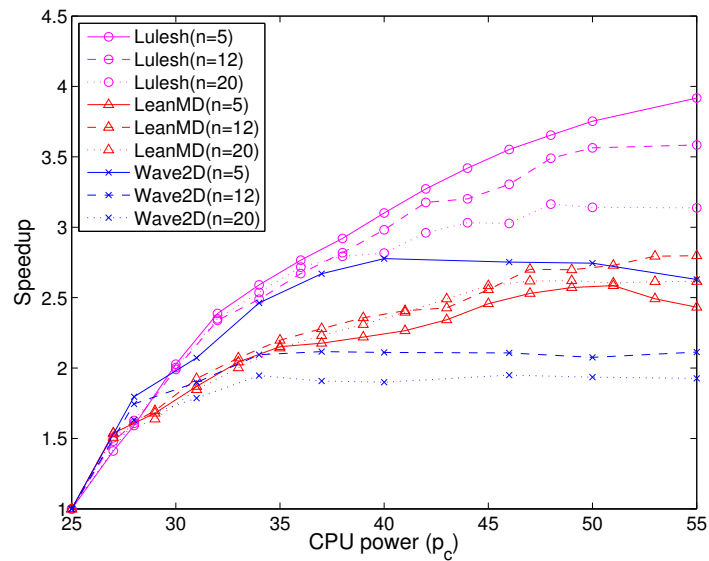


Figure 4.7: Speedups over the case of  $p_c = 25W$  for different number of nodes ( $n$ )



interpolation scheme detects this and keeps the optimized value of  $p_c$  in the range [29, 35]W. Similarly, the curves for *LeanMD* and *Lulesh* in Figure 4.7 flatten at about 46W and 48W, respectively. Thus, the optimized values of  $p_c$  are in the range of [41, 46]W and [40, 47]W for *LeanMD* and *Lulesh*, respectively. For most power budgets, the optimized CPU power cap ( $p_c$ ) for *Lulesh* lies in the range of [46, 47]W (barring the two that are close to 41W). This high value for CPU power cap is due to the high sensitivity of *Lulesh* on  $p_c$ . Due to this high sensitivity of execution time( $t$ ) on  $p_c$ , our scheme allocates the highest value for  $p_c$  to *Lulesh* as compared to the other two applications. In the other two applications, the scheme allocates relatively more nodes rather than increasing  $p_c$ , even though every additional node comes with an overhead - its base power.

The optimized memory power from our scheme and the maximum measured memory power in the baseline experiments are almost the same in *LeanMD* and *Lulesh* (Figure 4.5). For *LeanMD*, our model caps memory power at 8W which is the lowest memory power cap supported by the machine vendor. Since execution time is highly sensitive to  $p_m$  for *Lulesh*, reducing it results in a significant penalty in execution time. Our model captures this sensitivity and suggests a value of  $p_m$  that is close to the maximum memory power drawn in the baseline experiments (14W from Figure 4.5). However, for *Wave2D*, capping memory power at values less than the maximum power drawn in the baseline scenario, can give us higher speedups. Figure 4.5 shows a difference of 2W (on average) between the optimized values of  $p_m$  from our scheme and the max memory power drawn in the baseline experiments. To explore the reasons for the 20W/2W difference in *Wave2D* CPU/memory power values between our model and the baseline experiments observed in Figure 4.5, we study the behavior of CPU and memory power over the course of execution of an application. Figure 4.8 plots the measured CPU and memory power for the two configurations:  $c_1 = (5 \times 55, 18)$  and  $c_2 = (5 \times 34, 14)$ . The execution time for these configurations is almost the same (within 1% of each other), despite the significant difference in allocated power. Even though the max CPU power drawn reaches 53W for  $c_1$ , its average CPU power is just 2W higher than the average CPU power for  $c_2$ . Similarly, the max memory power drawn for  $c_1$  is 16W. Capping memory power to 14W in  $c_2$  does not affect execution time (Figure 4.8). Data centers operators have to account for the peak power drawn when deciding how many nodes to use. Due to the fluctuations in both CPU and memory power for  $c_1$ , the maximum power consumed by a node can reach up to 107W ( $53 + 16 + 38$ ). However, by using configuration  $c_2$ , the maximum power per node can be limited to 86W without any degradation in performance. Thus, our scheme can add more nodes while staying under the same power budget with an overprovisioned system.

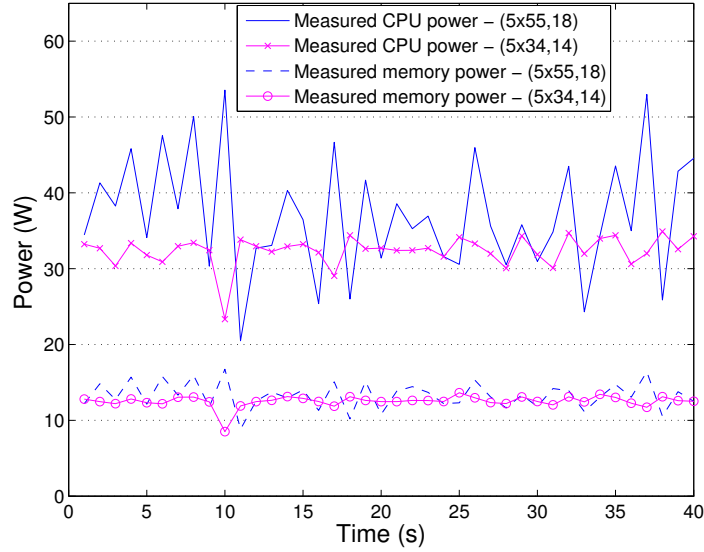


Figure 4.8: Measured CPU and memory power for two different configurations with significantly different power allocations but similar execution time

#### 4.5.5 Benefits of Capping Memory Power

To evaluate the impact of memory power capping, we compared the observed speedups from power capping both CPU and memory (C&M) with the observed speedups from just capping the CPU power (C). In the latter case, we determine the optimized configurations accounting for the maximum TDP wattage of memory, i.e., 35W per node. Figure 4.9 presents the speedup results for these two cases under three different power budgets. The speedups using CPU and memory power capping (C&M) are significantly higher than using only CPU power capping (M). With *LeanMD*, capping memory power increases the speedup from 1.43X to 1.94X for a power budget of 1400W. The ability to cap memory power in addition to CPU power can therefore significantly increase the speedups.

#### 4.5.6 Impact of Base Power on Speedups

The base power of the nodes plays an important role in determining the optimized configuration. It forms an important and essential part of our scheme. Figure 4.10 shows estimated speedups from our scheme for three different base powers ( $p_b$ ). These base powers of 10W, 38W, and 60W were measured on the Dell Optiplex 990, Dell PowerEdge R620, and Dell Precision T5500 machines, respectively, using a power meter. As mentioned in Section 5.6.2, the base power of a node in our testbed is 38W. Instead, if the base power was 10W, we

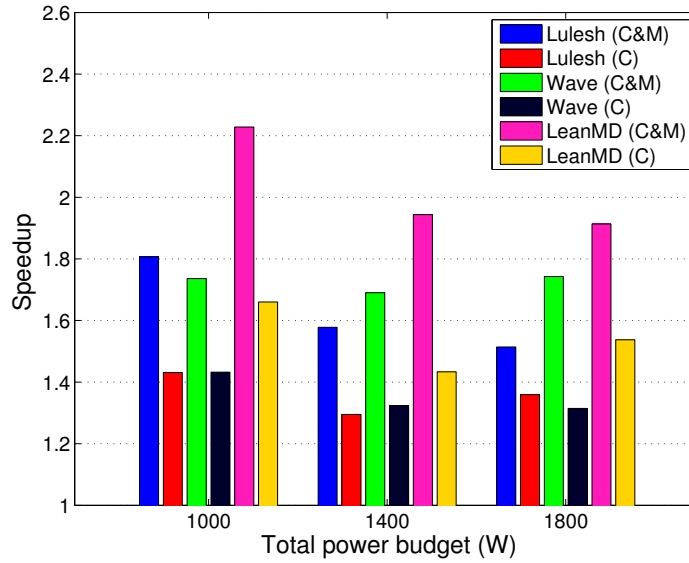


Figure 4.9: Speedups for power capping both CPU and memory (C&M) compared to CPU (C) only

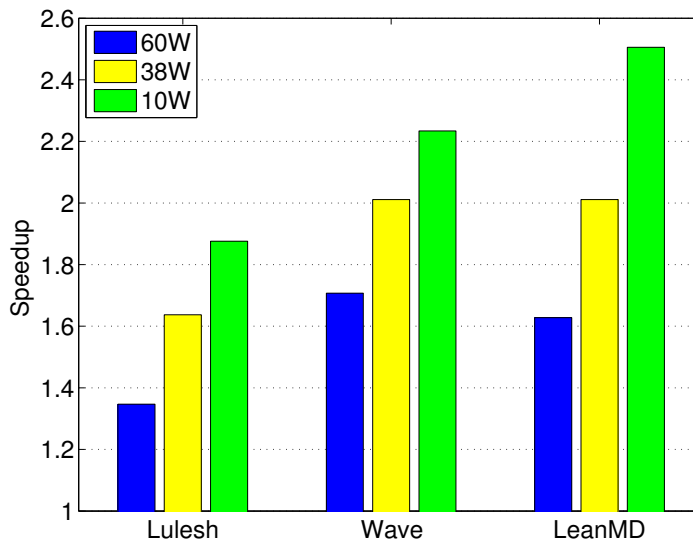


Figure 4.10: Estimated speedups for different base powers in case of  $P=800W$

can expect the speedup of *LeanMD* to increase from 2 to 2.5. Base power acts as the fixed cost for adding additional nodes in an over-provisioned system. For example, for  $P = 800\text{W}$ ,  $(15 \times 35, 8)$  and  $(7 \times 46, 8)$  are the optimized configurations for *LeanMD* using base powers of 10W and 60W respectively. For  $p_b = 10\text{W}$ , our model allocates less power to the CPU, i.e.,  $p_c=35$ , and uses 15 nodes. However, increasing  $p_b$  to 60W makes it expensive to add more nodes. For  $p_b=60\text{W}$ , our model allocates more power to the CPU, i.e.,  $p_c=46$ , while using only 7 nodes. Hence, the optimized configurations shown in Figure 4.5 would also change if the base power is changed. As the base power increases (decreases), we expect that the  $p_c$  and  $p_m$  from Figure 4.5 to increase (decrease). We have seen earlier that the optimized configurations depend on the relationship of execution time with  $p_m$  and  $p_c$ . After looking at Figure 4.10 we can now associate a correlation between optimum configuration and  $p_b$  as well. In general, we can conclude that decreasing the base power increases the speedup.

## Job Scheduling Under a Power Budget

In the last chapter we described our interpolation scheme that optimizes execution time for a single application under a power budget running on an overprovisioned system. In this chapter, we explore a global power monitoring strategy for high performance computing (HPC) that addresses optimum power allocation of resources at the data center level. This chapter builds on the last chapter by applying the lessons learned on a much larger scale, i.e., allocating resources optimally across a set of jobs.

Currently, some HPC data centers use a FIFO scheme with backfilling to schedule jobs. While such policies are fair, they do not guarantee throughput maximization of the data center. In addition, most HPC data centers are unaware of a job's power characteristics and hence allocate resources solely on the basis of required number of nodes. In this chapter, we present a *resource management* scheme, powered by a novel scheduling methodology that determines the optimal schedule and resource combination, i.e., number of nodes and CPU power cap, for the jobs submitted to an HPC data center that maximizes throughput under a strict power budget. In addition to the scheduling policy, this chapter also describes a detailed strong scaling power aware model that estimates application execution time for different resource combinations, i.e., number of nodes and the CPU power level for all of them. The major contributions of the chapter are:

- An online resource manager (PARM) that uses overprovisioning, power capping and job malleability along with power-response characteristics of each job for scheduling and resource allocation decisions that improves the job throughput of the data center significantly (Section 5.3).
- A performance model that accurately estimates an applications performance for a given number of nodes and CPU power cap (Section 5.4). We demonstrate the use of our

model by estimating characteristics of five applications having different power-response characteristics (Section 5.5.3).

- An evaluation of our online resource manager on a 38 node cluster with two different job data sets. A speedup of 1.7 was obtained when compared with SLURM (Section 5.5).
- An extensive simulated evaluation of our scheduling policy for larger machines and its comparison with the SLURM baseline scheduling policy. We achieve up to 5.2X speedup operating under a power budget of 4.75 MW (Section 5.6).

## 5.1 Related work

To the best of our knowledge, this work is the first to employ CPU power capping and job malleability for improving throughput of an overprovisioned HPC data center. Patki et al [14] proposed the idea of overprovisioning the compute nodes in power-constrained high performance computing data centers. They profile an application at different scales and different CPU power caps. Then they select the best operating configuration for the application for a given power budget. In Chapter 4 we extended this idea to include memory power caps and proposed a curve fitting scheme to get an exhaustive profile of an application at various scales of CPU and memory power caps (within the range of input data). This profile is then used to obtain the optimal operating configuration of the application under a strict power budget. Our work proposes a novel scheduling scheme to maximize throughput under a strict power budget for a data center scheduling *multiple* jobs simultaneously.

Performance modeling using DVFS has been studied previously [68]. Most of the existing research estimates execution time based on CPU frequency. These models cannot be used directly in the context of CPU power capping because applications have different memory/CPU characteristics can have cores working at different frequencies while operating under the same CPU power cap. The strong scaling power aware model proposed in this chapter differs from the work in the previous chapter as it estimates execution time of a job for a given *package* power cap that includes the power consumption of cores, caches and memory controller present on the chip. Researchers have also worked on developing performance models that capture the energy efficiency of an application [69]. Most of the energy efficiency work is focussed on optimizing energy consumption. Current data centers are overprovisioned with respect to power, i.e., each node can be supplied its maximum TDP power simultaneously, that is seldom needed. Adding more nodes and individually power capping each node puts the onus on the runtime to ensure that the total power consumption

of the data center does not exceed the maximum power that can be supplied to the entire machine. If the runtime fails to ensure the total power cap, this overdraw may cause the circuit breakers to trip, which can be costly. Treating power as a *constraint* can be a much harder problem than optimizing energy efficiency.

## 5.2 Data Center and Job Capabilities

In this section, we describe some of the capabilities or features that, according to our understanding, ought to be present in future HPC data centers. In the following sections, we highlight the role that these capabilities play for a scheduler that maximizes job throughput of a data center while ensuring fairness.

**Power capping:** This feature allows the scheduler to constrain the individual power draw of each node. Intel’s Sandy Bridge processor family supports on-board power measurement and capping through the RAPL interface [65]. RAPL is implemented using a series of Machine Specific Registers (MSRs) that can be accessed to read power usage for each power plane. RAPL supports power capping Package and DRAM power planes by writing into the relevant MSRs. Here, ‘Package’ corresponds to the processor chip that hosts processing cores, caches and memory controller. In this chapter, we use package power interchangeably with CPU power, for ease of understanding. RAPL can cap power at a granularity of milliseconds which is adequate given that the capacitance on the motherboard and/or power supply smoothes out the power draw at a granularity of seconds.

**Overprovisioning:** Capping CPU power below the TDP value using RAPL, allows us to use more nodes in an overprovisioned data center while staying within the power budget. An overprovisioned system is thus defined as a system that has more nodes than a conventional system operating under the same power budget. Due to the additional nodes, such a system cannot enable all of its nodes to function at their maximum TDP power levels simultaneously.

**Moldable jobs:** In these jobs, user specifies the range of nodes (the minimum and the maximum number of nodes) on which the job can run. The job scheduler decides the number of nodes within the specified range to be allocated to the job. Once decided, the number of nodes cannot be changed during job execution.

**Malleable jobs:** Such jobs can shrink to a smaller number of nodes or expand to a larger number of nodes upon instruction from an external command. Typically, the range of the nodes in which the job can run is dictated by its memory usage and strong scaling char-

acteristics. To enable malleable jobs, two components are critical – a *smart job scheduler*, that decides when and which jobs to shrink or expand, and a *parallel runtime system* that provides the dynamic contraction and expansion capability to the job. We rely on existing runtime support for malleable jobs in Charm++ [45]. In Charm++, malleability is achieved by dynamically exchanging compute objects between processors at runtime. Applications built on top of such an adaptive system have been shown to shrink and to expand with small costs [70]. Charm++ researchers are currently working on further improving the support for malleable jobs. Malleability support in MPI applications has been demonstrated in earlier work [71].

### 5.3 The Resource Manager

Figure 5.1 shows the block diagram of our online Power Aware Resource Manager, or PARM. It has two major modules: the scheduler and the execution framework. The scheduler is responsible for identifying which jobs should be scheduled and exactly what resources should be devoted to each job. We refer to the resource allocation for each job by the *resource combination* tuple,  $(n, p)$ , where  $n$  is the number of nodes and  $p$  is the CPU power cap for each of the  $n$  nodes. The scheduling decision is made based on the Integer Linear Program (ILP), and the job profiles generated by our strong scaling power aware model described in Section 5.4. The scheduler’s decisions are fed as input to the execution framework, which implements/enforces them by launching new jobs, shrinking/expanding running jobs, and/or setting the power caps on the nodes.

The scheduler is triggered whenever a new job arrives or when a running job ends or abruptly terminates due to an error or any other reason (‘Triggers’ box in Figure 5.1). At each *trigger*, the scheduler tries to re-optimize resource allocation to the set of pending as well as currently running jobs with the objective of maximizing overall throughput. Our scheduler uses both CPU power capping and moldability/malleability features for throughput maximization. We formulate this resource optimization problem as an Integer Linear Program (ILP). The relevant terminology is described in Table 5.1. Our scheduling scheme can be summarized as:

**Input:** A set of jobs that are currently executing or are ready to be executed ( $\mathcal{J}$ ) with their expected execution time corresponding to a set of resource combinations  $(n, p)$ , where  $n \in N_j$  and  $p \in P_j$ .

**Objective:** Maximize data center throughput.

**Output:** Allocation of resources to jobs at each trigger event, i.e., identification of the jobs



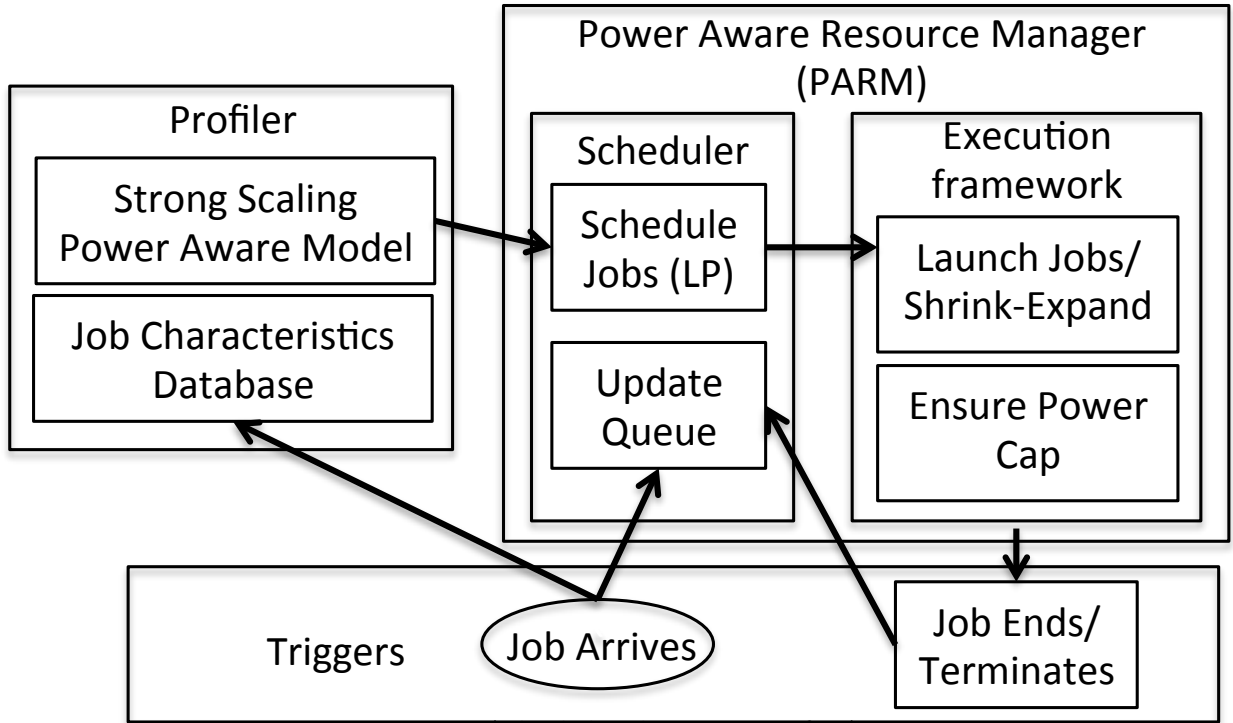


Figure 5.1: A high level overview of PARM

that should be executed along with their resource combination  $(n,p)$ .

### 5.3.1 Integer Linear Program Formulation

We make the following assumptions and simplifications in the formulation:

- All nodes of a given job are allocated the same power.
- We do not include cooling power of the data center in our calculations.
- Job characteristics do not change significantly during the course of its execution.
- Expected wall clock time and the actual execution time are equal for the purpose of decision making by the scheduler.
- $W_{base}$ , that includes power for all components of a node other than the CPU and memory subsystems, is assumed to be constant.
- A job once selected for execution is not stopped until its completion, although the resources assigned to it can change during its execution.

Variable	Description
$N$	total number of nodes in the data center
$J$	set of all jobs
$\mathcal{I}$	set of jobs that are currently running
$I$	set of jobs in the pending queue
$\mathcal{J}$	set of jobs that have already arrived and have not yet been completed, i.e., they are either pending or currently running, $\mathcal{J} = \mathcal{I} \cup I$
$N_j$	set of node counts on which job $j$ can be run
$P_j$	set of power levels at which job $j$ should be run or in other words, the power levels at which job $j$ 's performance is known
$n_j$	number of nodes at which job $j$ is currently running
$x_{j,n,p}$	binary variable, 1 if job $j$ should run on $n$ nodes at power $p$ , otherwise 0
$t_{now}$	current time
$t_j^a$	arrival time of job $j$
$W_{base}$	base machine power that includes everything other than CPU and memory
$t_{j,n,p}$	execution time for job $j$ running on $n$ nodes with a power cap of $p$
$s_{j,n,p}$	strong scaling power aware speedup of application $j$ running on $n$ nodes with a power cap of $p$
$\min(N_j)$	minimum number of nodes that can be assigned to job $j$
$\min(P_j)$	minimum amount of power that can be assigned to job $j$

Table 5.1: Integer Linear Program Terminology

- All jobs are from a single user (or have the same priority). This condition can be relaxed by introducing appropriate priority factors in the objective function of the ILP.

Scheduling problems are framed as ILPs and ILPs are NP-hard problems. Maximizing throughput in the objective function requires introducing variables for the start and end time of jobs. These variables make the ILP computationally very intensive and thus impractical for online scheduling in many cases. In this work, we propose to drop the job start and end time variables and take a greedy approach by selecting jobs and resource allocations that maximizes the sum of the power-aware speedup (described later) of selected jobs. This objective function improves the job throughput while keeping the ILP optimization computationally tractable for online scheduling.

*Objective Function*

$$\sum_{j \in \mathcal{J}} \sum_{n \in N_j} \sum_{p \in P_j} w_j * s_{j,n,p} * x_{j,n,p} \quad (5.1)$$

*Select One Resource Combination Per Job*

$$\sum_{n \in N_j} \sum_{p \in P_j} x_{j,n,p} \leq 1 \quad \forall j \in \mathcal{I} \quad (5.2)$$

$$\sum_{n \in N_j} \sum_{p \in P_j} x_{j,n,p} = 1 \quad \forall j \in \mathcal{I} \quad (5.3)$$

*Bounding total nodes*

$$\sum_{j \in \mathcal{J}} \sum_{p \in P_j} \sum_{n \in N_j} n x_{j,n,p} \leq \mathbf{N} \quad (5.4)$$

*Bounding power consumption*

$$\sum_{j \in \mathcal{J}} \sum_{n \in N_j} \sum_{p \in P_j} (n * (p + W_{base})) x_{j,n,p} \leq W_{max} \quad (5.5)$$

*Disable Malleability (Optional)*

$$\sum_{n \in N_j} \sum_{p \in P_j} n x_{j,n,p} = n_j \quad \forall j \in \mathcal{I} \quad (5.6)$$

Figure 5.2: Integer Linear Program formulation of PARM scheduler

We define the strong scaling power-aware speedup of a job  $j$  as follows:

$$s_{j,n,p} = \frac{t_{j,\min(N_j),\min(P_j)}}{t_{j,n,p}} \quad (5.7)$$

where  $s_{j,n,p}$  is the speedup of job  $j$  executing using resource combination  $(n, p)$  with respect to its execution with resource combination  $(\min(N_j), \min(P_j))$ . Objective function (Eq. 5.1) of the ILP maximizes the sum of the power-aware speedups of the jobs selected for execution at every trigger event. This leads to improvement in FLOPS/Watt (or power efficiency, as we define it). Improved power efficiency implies better job throughput (results discussed in Section 5.5, 5.6). Oblivious maximization of power efficiency may lead to starvation for jobs with low strong scaling power aware speedup. Therefore, to ensure fairness, we introduced a weighing factor ( $w_j$ ) in the objective function, which is defined as follows:

$$w_j = (t_{j,\min(N_j),\min(P_j)}^{rem} + (t_{now} - t_j^a))^\alpha \quad (5.8)$$

$w_j$  artificially boosts the strong scaling power aware speedup of a job by multiplying it to the job's completion time, where completion time is the sum of the time elapsed since the job's ar-

rival and the job’s remaining execution time with resource combination  $(\min(N_j), \min(P_j))$  i.e.  $(t_{j, \min(N_j), \min(P_j)}^{rem})$ . The percentage of a running job completed between two successive triggers is determined by the ratio of the time interval between the two triggers and the total time required to complete the job using its current resource combination. Percentage of the job that has been completed so far can then be used to compute  $t_{j, \min(N_j), \min(P_j)}^{rem}$ . The constant  $\alpha$  ( $\alpha \geq 0$ ) in Eq. 5.8 determines the priority given to job fairness against its strong scaling power aware speedup i.e. a smaller value of  $\alpha$  favors job throughput maximization while a larger value favors job fairness.

We now explain the constraints of our ILP (Figure 5.2):

- Select one resource combination per job (Eq. 5.2,5.3):  $x_{j,n,p}$  is a binary variable indicating if job  $j$  should run using resource combination  $(n, p)$ . This constraint ensures that at most one of the variables  $x_{j,n,p}$  is set to 1 for any job  $j$ . The jobs that are already running (set  $\mathcal{I}$ ) continue to run although they can be assigned a different resource combination (Eq. 5.3). The jobs in the pending queue ( $I$ ), for which at least one of the variables  $x_{j,n,p}$  is equal to 1 (Eq. 5.2), are selected for execution and moved to the set of jobs currently running ( $\mathcal{I}$ ).
- Bounding total nodes (Eq. 5.4): This constraint ensures that the number of active nodes does not exceed the maximum number of nodes available in the overprovisioned data center.
- Bounding power consumption (Eq. 5.5): This constraint ensures that power consumption of all nodes does not exceed the power budget of the data center.
- Disable Malleability (Eq. 5.6): To quantify the benefits of malleable jobs, we consider two versions of our scheduler. The first version supports only moldable jobs and is called as noSE (i.e. no Shrink/Expand), The second version allows both moldable and malleable jobs and is called as wSE (i.e. with Shrink/Expand). Malleability can be disabled by using Eq. 5.6. This constraint ensures that the number of nodes assigned to each running job does not change during the optimization process. However, it allows changing the power allocated to running jobs. In real-world situations, the jobs submitted to a data center will be a mixture of malleable and non-malleable jobs. The scheduler can apply Eq. 5.6 to disable malleability for non-malleable jobs.

## 5.4 Strong Scaling Power Aware Model

Recent processors allow power capping, which gives a new dimension to performance modeling. In this section, we propose a strong scaling power-aware model, by extending Downey's [72] strong scaling model and making it power aware. The goal is to develop a model that can estimate the execution time of an application for any given resource combination  $(n, p)$ .

### 5.4.1 Strong Scaling Model

We used Downey's [72] strong scaling model after modifying the boundary conditions. An application can be characterized by an average parallelism of  $A$ . The application's parallelism remains equal to  $A$ , except for a fraction  $\sigma$  of total execution time. The variance of parallelism, represented as  $V = \sigma(A - 1)^2$ , depends on  $\sigma$ , where  $0 \leq \sigma \leq 1$ . The execution time,  $t(n)$ , of an application can then be defined as follows:

$$t(n) = \begin{cases} \frac{T_1 - \frac{T_1\sigma}{2A}}{n} + \frac{T_1\sigma}{2A}, & 1 \leq n \leq A & (5.9) \\ \frac{\sigma(T_1 - \frac{T_1}{2A})}{n} + \frac{T_1}{A} - \frac{T_1\sigma}{2A} & A < n \leq 2A - 1 & (5.10) \\ \frac{T_1}{A}, & n > 2A - 1 & (5.11) \end{cases}$$

where  $n$  is the number of nodes and  $T_1$  is the execution time on a single node. Since we have to estimate execution time corresponding to different number of nodes  $n$  given  $t(1) = T_1$ , we had to modify Downey's model according to boundary condition  $t(1) = T_1$ . The first equation in this group represents the range of  $n$  where applications are most scalable. This is the range where the number of nodes is less than  $A$ , i.e., the average amount of parallelism. The application's scalability declines significantly once  $n$  becomes larger than  $A$  because some nodes are unable to do work in parallel owing to a lack of parallelism. Finally, for  $n > 2A$ , the execution time  $t(n)$  equals  $T_1/A$  and does not decrease. Given application characteristics  $\sigma$ ,  $A$ , and  $T_1$ , this model can be used to estimate execution time for any number of nodes  $n$ .

### 5.4.2 Adding Power Awareness to the Strong Scaling Model

The effect of increasing frequency on the execution time  $t$  varies from application to application [61]. In this section, we first describe a basic framework that models  $t$  as a function

of CPU frequency  $f$ . Since,  $f$  can be expressed as a function of CPU power  $p$ , we can finally express  $t$  in terms of  $p$ .

### Execution Time as a Function of Frequency

Existing work [61] indicates that an increase in CPU frequency beyond a certain threshold frequency,  $f_h$ , does not reduce the execution time  $t$ . The value of  $f_h$  depends on the memory bandwidth being used by the application. Since  $t \propto \frac{1}{f}$ , we can express  $t$  as [68]:

$$t(f) = \begin{cases} \frac{W}{f} + T, & \text{for } f < f_h \\ T_h, & \text{for } f \geq f_h \end{cases} \quad (5.12)$$

$$(5.13)$$

where  $W$  and  $T$  are constants that roughly correspond to the CPU and memory bounded work respectively.  $T_h$  is the execution time at frequency  $f_h$ . Given that  $f_l$  is the smallest possible frequency at which a CPU can operate, Equation 5.12 should obey the boundary conditions  $t(f_l) = T_l$  and  $t(f_h) = T_h$  where  $T_l$  is the execution time while operating at the minimum frequency level ( $f_l$ ).

We define parameter  $\beta$  that characterizes the frequency-sensitivity of an application and can be expressed as:

$$\beta = \frac{T_l - T_h}{T_l} \quad (5.14)$$

The range of  $\beta$  depends on the CPU's DVFS range. Given the DVFS range of  $(f_l, f_{max})$ ,  $\beta \leq 1 - \frac{f_l}{f_{max}}$ . Typically, CPU-bound applications have higher values for  $\beta$  whereas memory-intensive applications have smaller  $\beta$  values.

Using Equation 5.14 and subjecting Equation 5.12 to boundary conditions,  $t(f_l) = T_l$  and  $t(f_h) = T_h$ , gives us:

$$W = \frac{T_h \beta f_l f_h}{(1 - \beta)(f_h - f_l)} \quad (5.15)$$

$$T = T_h - \frac{T_h \beta f_l}{(1 - \beta)(f_h - f_l)} \quad (5.16)$$

### Execution Time as a Function of CPU Power

Although Intel has not released complete details of the CPU power capping functionality, it has been hinted that the power cap is ensured by using a combination of DVFS and CPU throttling. Core input voltage and frequency can be set within manufacturer defined ranges. This frequency-voltage range, in turn, defines a range over CPU power that can be achieved

using DVFS. Let  $p_l$  denote the CPU power corresponding to  $f_l$ , where  $f_l$  is the minimum frequency the CPU can operate at using DVFS. Beyond  $p_l$ , power is reduced by mechanisms other than DVFS, e.g., CPU throttling. The threshold  $p_l$ , where CPU throttling takes over from DVFS, can be determined by looking at the processor's operating frequency. CPU or package power includes the power consumption by its various components such as cores, caches, and memory controller. The value of  $p_l$  varies depending on an application's usage of these components. In a CPU bound application, a processor might be able to cap power to lower values using DVFS, since only the cores are consuming power. In contrast, for a memory intensive application,  $p_l$  might be higher, since the caches and memory controller are also consuming power in addition to the cores. Since core input voltage is proportional to  $f$ , power consumption of the cores,  $p_{core}$ , can be modeled as:

$$p_{core} = Cf^3 + Df \quad (5.17)$$

where  $C$  and  $D$  are constants. Since the number of cache and memory accesses are proportional to frequency, DVFS can change cache/memory controller power consumptions as well. The CPU power can then be expressed as [73]:

$$p = p_{core} + \sum_{i=1}^3 g_i L_i + g_m M + p_{base} \quad (5.18)$$

where  $L_i$  is accesses per second to level  $i$  cache,  $g_i$  is the cost of a level  $i$  cache access (in W),  $M$  is the number of memory accesses per second,  $g_m$  is the cost per memory access (in W), and  $p_{base}$  is the base package power consumption. Equation 5.18 can also be written as:

$$p = F(f) = af^3 + bf + c \quad (5.19)$$

where  $a$ ,  $b$ , and  $c$  are constants. In Equation 5.19, the term  $bf$  corresponds to the cores' leakage power and the power consumption of the caches and the memory controller. The term  $af^3$  represents the dynamic power of the cores, whereas  $c = p_{base}$  is the base CPU power. The constants  $a$  and  $b$  are application dependent since the cache and memory behavior can be different across applications. Equation 5.19 can be rewritten as a depressed cubic equation:

$$f^3 + \frac{b}{a}f + \frac{c-p}{a} = 0 \quad (5.20)$$

and solved using Fermat’s Last Theorem to get  $F^{-1}$ :

$$\begin{aligned}
 f = F^{-1}(p) &= \sqrt[3]{\frac{p-c}{2a} + \sqrt{\frac{(p-c)^2}{4a^2} + \frac{b^3}{27a^3}}} \\
 &+ \sqrt[3]{\frac{c-p}{2a} + \sqrt{\frac{(p-c)^2}{4a^2} + \frac{b^3}{27a^3}}}
 \end{aligned}
 \tag{5.21}$$

To express  $t$  in terms of  $p$ , we use Equation 5.21 to replace  $f$ ,  $f_l$ , and  $f_h$  in Equations 5.12, 5.15, 5.16. To combine our power aware model with the strong scaling model described in Section 5.4.1, we replace  $T_h$  in Equations 5.12, 5.15, 5.16 with  $t(n)$  from Equations 5.9, 5.10, 5.11.

**Summary:** We present a comprehensive model to estimate  $t$  for any resource combination  $(n, p)$ , given application parameters  $\sigma, T_1, A, p_l, p_h, \beta, a$  and  $b$ . We substitute parameters  $\sigma, T_1$  and  $A$  into Equations 5.9, 5.10, 5.11 to determine  $t = t(n)$ , i.e., execution time using  $n$  nodes working at maximum power. We then use  $T_h = t(n)$  and parameters  $p_l, p_h, \beta, a$  and  $b$  to determine  $t(n, p)$  using Equations 5.12, 5.15, 5.16, and 5.21, i.e., execution time using  $n$  nodes operating at  $p$  Watts each.

## 5.5 Experimental Results

In this section, we describe our experimental setup that includes applications, testbed, and job datasets. We obtain the application characteristics using the power-aware strong-scaling performance model and finally compare the performance of the noSE and wSE versions of PARM with SLURM.

### 5.5.1 Applications

We used five applications, namely, Wave2D, Jacobi2D, LeanMD, Lulesh, and Adaptive Mesh Refinement or AMR [74]. These applications have different CPU and memory usage:

- Wave2D and Jacobi2D are 5-point stencil applications that are memory-bound. Wave2D has higher FLOPS than Jacobi2D.
- LeanMD is a computationally intensive molecular dynamics application.
- CPU and memory usage of Lulesh and AMR lies in between the stencil applications and LeanMD.



### 5.5.2 Testbed

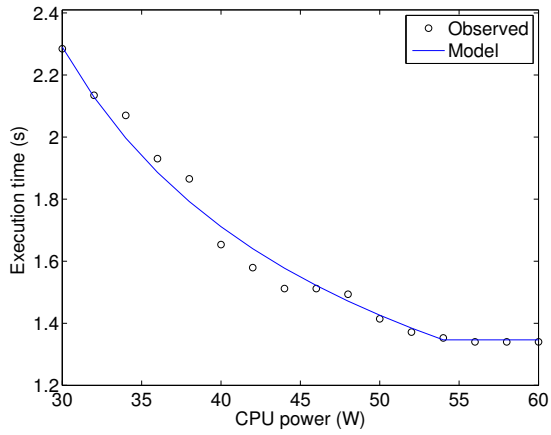
We conducted our experiments on a 38-node Dell PowerEdge R620 cluster (which we call the Power Cluster). Each node containing an Intel Xeon E5-2620 Sandy Bridge with 6 physical cores at 2GHz, 2-way SMT with 16 GB of RAM. These machines support on-board power measurement and capping through the RAPL interface [36]. The CPU power for our testbed can be capped in the range  $[25 - 95]W$ , while the capping range for memory power is  $[8 - 35]W$ .

### 5.5.3 Obtaining Model Parameters of Applications

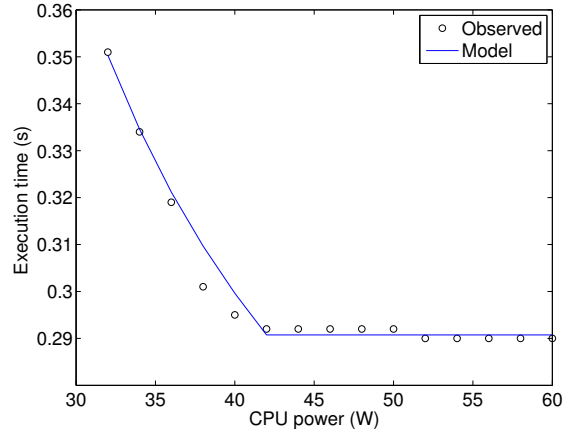
Application characteristics depend on the input type, e.g., grid size. We fix the respective input types for each application. Each application needs to be profiled for some (n,p) combinations to obtain data for curve fitting. 1 step/iteration is sufficient to get the performance for a given data point. Since, a step/iteration is usually of the order of milliseconds, the cost of profiling the application at several data points is negligible compared to the overall execution time of the application.

We use linear and non-linear regression tools provided by MATLAB to determine the application parameters by fitting the sampled application performance data to the performance model proposed in Section 5.4. Figure 5.3 (a-e) shows the observed (dots) and estimated (lines) execution time corresponding to different CPU power caps for all applications when run on 20 nodes of our Power Cluster. In all cases, the fitted curves match the observed data with a Root Mean Square Error (RMSE) percentage of less than 2%. The obtained parameter values for all applications are listed in Table 5.2 and are discussed here:

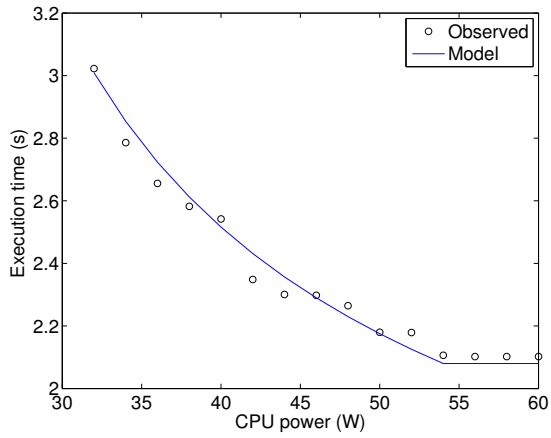
- The parameter  $c$  (CPU base power) lies in the range  $[13 - 14]W$  for all applications
- $p_l$  was 30W for LeanMD and 32W for rest of applications. For LeanMD, it is possible to cap the CPU power to a lower value just by decreasing the frequency using DVFS. This is because LeanMD is a computationally intensive application and therefore most of the power is consumed by the cores rather than caches and memory controller. On the contrary, for other applications, CPU throttling kicks in at a higher power level because of their higher cache/memory usage.
- value of  $p_h$  lies in the range of  $[37 - 54]W$  for applications under consideration.
- value of  $\beta$  lies in the range  $[0.08 - 0.40]$ . Higher value of  $\beta$  means higher sensitivity to CPU power.



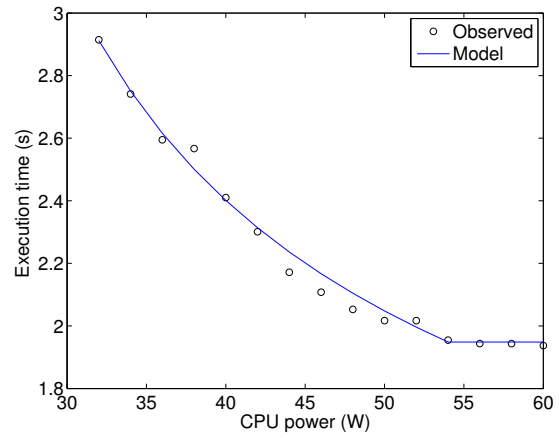
(a) LeanMD



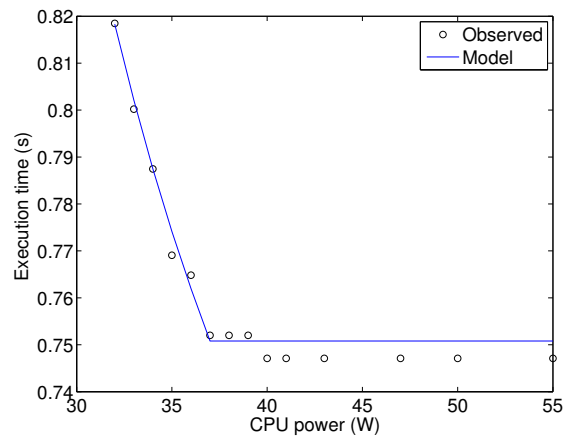
(b) Wave2D



(c) Lulesh



(d) AMR



(e) Jacobi2D

Figure 5.3: Model estimates (line) and actual measured (circles) execution times for all applications as a function of CPU power (a-e). Modeled power aware speedups for all applications (f).

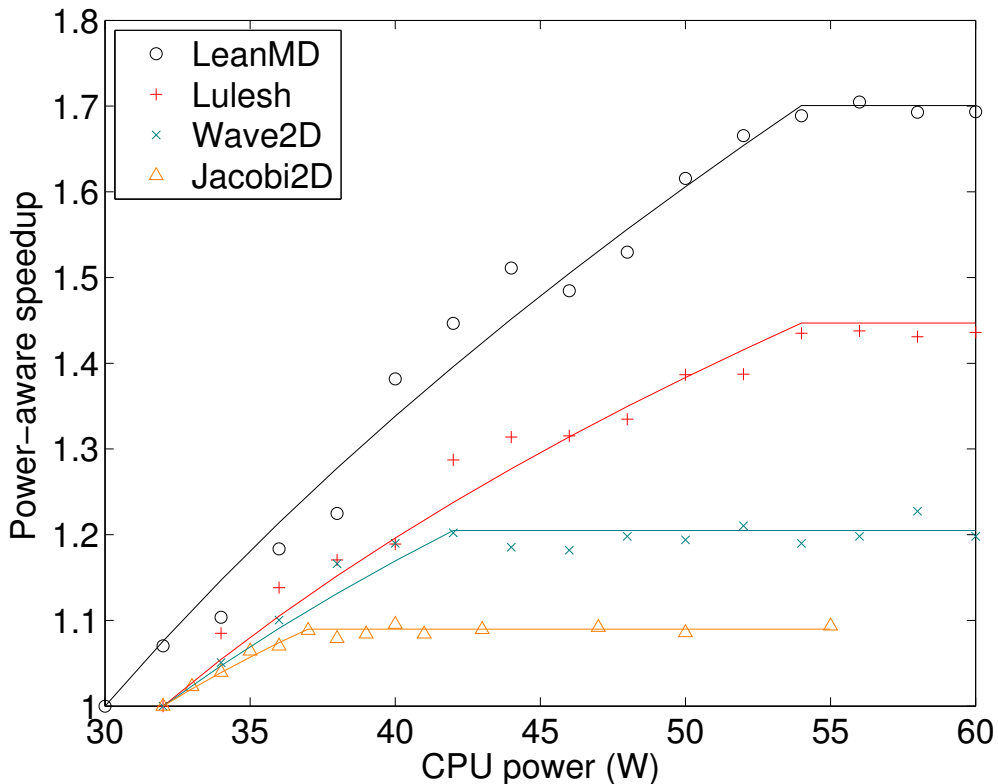


Figure 5.4: Modeled (lines) and observed (markers) power aware speedups for four applications

- Wave2D and Jacobi2D have the largest memory footprint that results in high CPU-cache-memory traffic. Therefore the value of  $b$  is high for these two applications.

Figure 5.4 shows the modeled (lines) as well as the observed (markers) power-aware speedups for 4 applications under consideration. Since *AMR*'s characteristics are very similar to *Lulesh*, we leave *AMR* out to improve the clarity of the figure. Each application's speedup was calculated with respect to the execution time when that application was executing at  $p = p_l$ . LeanMD has the highest power-aware speedup whereas Jacobi2D has the lowest.

#### 5.5.4 Power Budget

We assume a power budget of 3300W to carry out experiments using our Power Cluster. Although the vendor-specified TDP of CPU and memory of the Dell nodes was 95W and 35W, respectively, the actual power consumption of CPU and memory never went beyond 60W and 18W, respectively, when running any of the applications. Therefore, instead of

<b>Application</b>	<b>a</b>	<b>b</b>	$p_l$	$p_h$	$\beta$
<b>LeanMD</b>	1.65	7.74	30	52	0.40
<b>Wave2D</b>	3.00	10.23	32	40	0.16
<b>Lulesh</b>	2.63	8.36	32	54	0.30
<b>AMR</b>	2.45	6.57	32	54	0.33
<b>Jacobi2D</b>	1.54	10.13	32	37	0.08

Table 5.2: Obtained model parameters

the vendor-specified TDP, we consider 60W and 18W as the maximum CPU and memory power consumption and use them to calculate the number of nodes that can be installed in a traditional data center. The maximum power consumption of a node, thus, adds up to  $60W + 18W + 38W = 116W$ , where 38W is the base power of a node. Therefore, the total number of nodes that can be installed in a traditional data center with a power budget of 3300W will be  $\lfloor \frac{3300}{116} \rfloor = 28$  nodes. By capping the CPU power below 60W, the overprovisioned data center will be able to power more than 28 nodes.

### 5.5.5 Job Datasets

We constructed two job datasets by choosing a mix of applications from the set described in Section 5.5.1. All these applications are written using the Charm++ parallel programming model and hence support job malleability. Application’s power-response characteristics can influence the benefits of PARM. Therefore, in order to better characterize the benefits of PARM, these two job datasets were constructed such that they have very different average values of  $\beta$ . We name these datasets as SetL and SetH, with average  $\beta$  value of 0.1 and 0.27, respectively. For instance, SetH has 3 LeanMD, 3 Wave2D, 2 Lulesh, 1 Jacobi, and 1 AMR job, that gives us an average  $\beta$  value of 0.27. A mix of short, medium and long jobs were constructed by randomly generating wall clock times with a mean value of 1 hour. Similarly, the job arrival times were generated randomly. Each dataset spans over 5 hours of cluster time and approximately 20 scheduling decisions were taken (a scheduling decision is taken whenever a new job arrives or a running job terminates). The minimum and the maximum number of nodes on which a job can run was determined by the job’s memory requirements. We used 8 node levels (i.e.  $|N_j| = 8$ ) that are uniformly distributed between the minimum and maximum number of nodes on which the job can run. The memory power is capped at the fixed value of 18W whereas we used 6 CPU power levels - [30, 32, 34, 39, 45, 55]W.

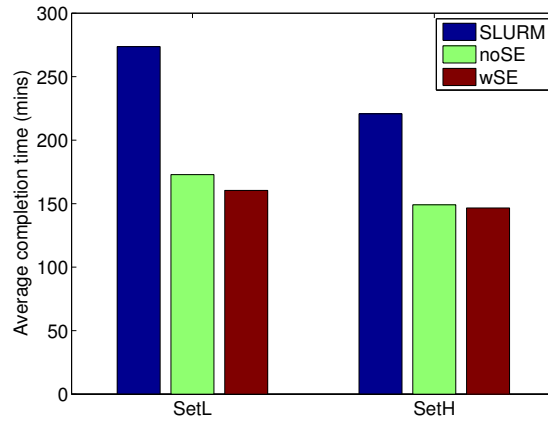
### 5.5.6 Performance Metric

We compare our scheduler with SLURM [75]: an open-source resource manager that allocates compute nodes to jobs and provides a framework for starting, executing and monitoring jobs on a set of nodes. SLURM provides resource management on many of the most powerful supercomputers of the world including Tianhe-1A, Tera 100, Dawn, and Stampede. We setup both PARM and SLURM on the testbed. For comparison purpose, we use SLURM’s baseline scheme in which the user specifies the exact number of nodes requested for the job and SLURM uses FIFO + backfilling for making scheduling decisions. We call this as the SLURM baseline scheme or just the baseline scheme. The number of nodes requested for a job submitted to SLURM is the minimum number of nodes on which PARM can run that job.

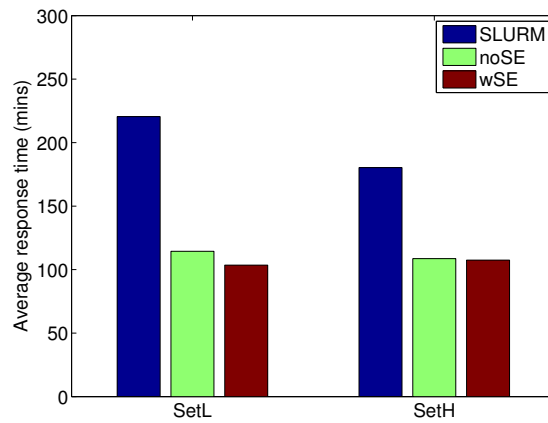
We use response time and completion time as the metrics for comparing PARM and SLURM. A job’s response time,  $t_{res}$ , is the time interval between its arrival and the beginning of its execution. Execution time,  $t_{exe}$ , is the time from start to finish of a job’s execution. Completion time,  $t_{comp}$ , is the time between a job’s arrival and the time that it finishes execution, i.e.,  $t_{comp} = t_{res} + t_{exe}$ . Job throughput is the inverse of the average completion time of jobs. In this study, we emphasize on completion time as the performance comparison metric, even though typically response time is the preferred metric. This is because unlike conventional data centers, where resources allocated to a job and hence the jobs execution time are fixed, our scheduler dynamically changes job configuration during execution which can vary job execution time significantly. Hence, response time is not a very appropriate metric for comparison in this study. Completion time includes both the response time and the execution time and is therefore the preferred metric of comparison.

### 5.5.7 Results

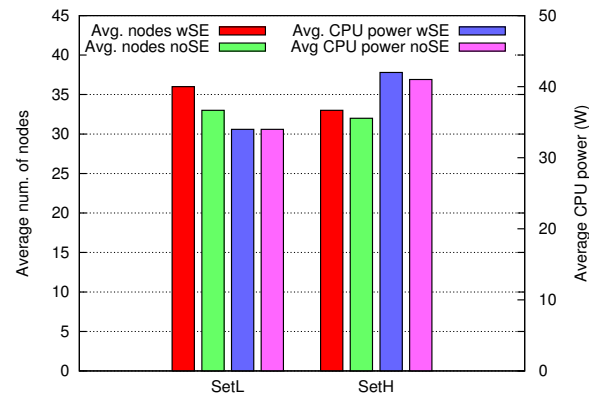
Figure 5.5(a) shows the average completion times of the two datasets with SLURM and the noSE and wSE versions of PARM. The completion times for *wSE* and *noSE* include all overhead costs including the ILP optimization time and the costs of constriction and expansion of jobs. As noted in the figure, PARM significantly reduces the average completion time for both the data sets. This improvement can mainly be attributed to the reduced average response times shown in Figure 5.5(b). Our scheduler intelligently selects the best power levels for each job which allows it to add more nodes to benefit from strong scaling and/or scheduling more jobs simultaneously. The completion times of wSE scheme are better than noSE. Job malleability allows wSE scheme to shrink and expand jobs at runtime. This



(a) Average completion time



(b) Average response time



(c) Average nodes and average power per node

Figure 5.5: (a) Average completion times, and (b) average response times for SetL and SetH with SLURM and noSE, wSE versions of PARM. (c) Average number of nodes and average CPU power in the wSE and noSE versions of PARM.

gives flexibility to the ILP to re-optimize the allocation of nodes to the running and pending jobs. On the other hand, noSE reduces the solution space of ILP by not allowing running jobs to change the number of nodes allocated to them. Additionally, wSE increases the machine utilization towards the tail of the job dataset execution when there are very few jobs left running. The wSE version can expand the running jobs to run on the unutilized machines. These factors reduce both the average completion and the average response time in wSE (Figure 5.5(a), 5.5(b)). As shown by Figure 5.5(c), wSE scheme utilizes 36 nodes on an average compared to an average of 33 nodes used in the case of noSE for SetL.

A smaller value of  $\beta$  means that effect of decreasing the CPU power on application performance is small. When  $\beta$  is small, the scheduler will prefer to allocate less CPU power and use more nodes. On the other hand, when  $\beta$  is large, the benefits of adding more nodes at the cost of decreasing the CPU power are smaller. The flexibility to increase the number of nodes gives PARM higher benefit over SLURM when  $\beta$  is small as compared to the case when  $\beta$  is large. Therefore, lower the sensitivity of applications to the allocated CPU power (i.e. smaller value of  $\beta$ ), higher will be the benefit of using PARM. This is corroborated with the observation (Figure 5.5) that the benefits of using PARM as compared to SLURM are much higher with dataset SetL ( $\beta = 0.1$ ) as compared to dataset SetH ( $\beta = 0.27$ ).

## 5.6 Large Scale Projections

After experimentally showing the benefits of PARM on a real cluster, we now analyze its benefit on very large machines. Since doing actual job scheduling on a large machine is practically infeasible for us, we use the SLURM simulator [76], which is a wrapper around SLURM. This simulator gives us information about SLURM’s scheduling decisions without actually executing the jobs. In the following subsections, we describe our shrink/expand cost model, give the experimental setup and then present a comparison of PARM scheduling with SLURM baseline scheduling policy.

### 5.6.1 Modeling Cost of Shrinking and Expanding Jobs

Constriction and expansion of jobs has an overhead associated with it. These overheads come from data communication done to balance the load across the new set of processors assigned to the job and from the boot time of nodes. A scheduler typically makes two decisions: 1) how many nodes to assign to each job, and 2) which nodes to assign to each job. We address the first decision in this paper and defer the second for future work. Let us say that job  $j$

with a total memory of  $m_j$  MB, has to expand from  $n_f$  nodes to  $n_t$  nodes. For simplification of analysis, we assume that each job is initially allocated a cuboid of nodes (with dimensions- $\sqrt[3]{n_f} \times \sqrt[3]{n_f} \times \sqrt[3]{n_f}$ ) interconnected through a 3D torus. After the expand operation, size of the cuboid becomes  $\sqrt[3]{n_f} \times \sqrt[3]{n_f} \times \frac{n_t}{\sqrt[3]{n_f}}$ . For load balance, the data in memory ( $m_j$  MB) will be distributed equally among the  $n_t$  nodes. Hence, the communication cost for the data transfer can be expressed as  $t_c$  (in seconds):

$$t_c = \frac{\left(\frac{m_j}{n_f} - \frac{m_j}{n_t}\right) * n_f}{2 * b * n_f^{\frac{2}{3}}} \quad (5.22)$$

where  $b$  is the per link bandwidth. The numerator in Eq. 5.22 represents the total data to be transferred whereas the denominator represents the bisection bandwidth of the cuboid. Similarly, the cost of shrinking a job is determined by computing the cost of distributing the data of  $n_f - n_t$  nodes equally across the final  $n_t$  nodes.

Boot times can be significant for some supercomputers. Since many supercomputers in Top500 [13] belong to the Blue Gene family, we include their boot time when evaluating our scheme. We adopt a simple linear model to calculate the boot time ( $t_b$ ) for expand operation. The following linear relationship is obtained by using the Intrepid boot time data [77]:

$$t_b(\text{in seconds}) = (n_t - n_f) * 0.01904 + 72.73 \quad (5.23)$$

In an expand operation, communication phase can start only after additional nodes become available. These additional nodes might have to be booted. Therefore the total cost of a shrink or expand operation is sum of the boot time and the data transfer time, i.e.,  $t_{se} = t_c + t_b$ . A job set for expansion might receive additional nodes from a job undergoing constriction in the same scheduling decision. Therefore, an expanding job has to wait until the shrinking job has released the additional resources. To simplify this analysis, we determine the maximum  $t_{se}$  from among the shrinking/expanding jobs ( $t_{se}^{max}$ ) and add  $2t_{se}^{max}$  to the execution times of all jobs that shrink or expand due to the current scheduling decision. To control the frequency of constriction or expansion of a job, and consequently its cost, we define a parameter  $f_{se}$  (in secs).  $f_{se}$  is the time after which a job can shrink or expand, i.e., if a job was shrunk or expanded at  $t$  secs, then it can be shrunk or expanded only after  $t + f_{se}$  secs. This condition is enforced using Eq. 5.6.



### 5.6.2 Experimental Setup

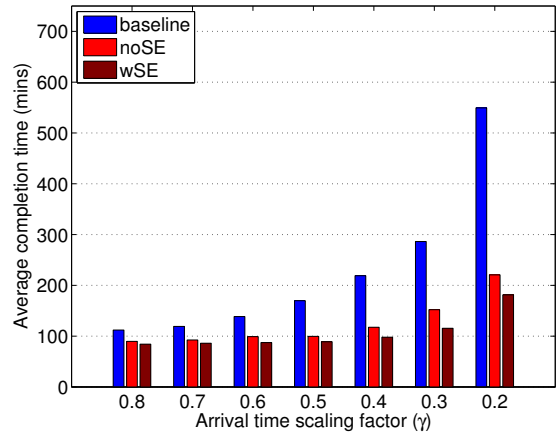
The results presented in this section are based on the job logs [78] of Intrepid. Intrepid is a IBM BG/P supercomputer with a total of 40,960 nodes, installed at Argonne National Lab. The job trace spans over 8 months and has 68,936 jobs. We extracted 3 subsets of 1000 successive jobs each from the trace file to conduct our experiments. These subsets will be referred to as Set1, Set2, and Set3 and the starting job id for these subsets are 1, 10500, and 27000, respectively. To measure the performance of PARM in the wake of diverse job arrival rates, we generated several other datasets from each of these sets by multiplying the arrival times of each job by  $\gamma$ , where  $\gamma \in [0.2 - 0.8]$ . Multiplication of the arrival times with  $\gamma$  increases the job arrival rate without changing the distribution of job arrival times.

As we do not know application characteristics ( $\sigma, T_1, A, f_t, f_h, \beta, a$  and  $b$ ) of the jobs in the Intrepid trace file, we take the parameter values from Section 5.5.3 and randomly assign values from these ranges to jobs in the Intrepid trace file. Since Intrepid does not allow moldable/malleable jobs, jobs request a fixed number of nodes instead of a range of nodes. For jobs submitted to the PARM scheduler, we consider this number as the maximum nodes that the job is allowed to use, i.e.,  $max(N_j)$  and set  $min(N_j) = \theta * max(N_j)$ , where  $\theta$  is randomly selected in the range  $[0.2 - 0.6]$ . The power consumption of Intrepid nodes is not publicly available, therefore we use the power values from our testbed cluster (described in Section 5.5.2). Hence, the maximum power consumption per node is taken to be 116W. The maximum power consumption of 40,960 nodes thus equals  $116 \times 40,960 = 4,751,360W$ . The SLURM scheduler schedules on 40,960 nodes with each node running at maximum power level. As in Section 5.5.5, PARM uses 6 CPU power levels,  $P_j = \{30, 33, 36, 44, 50, 60\}W$ .

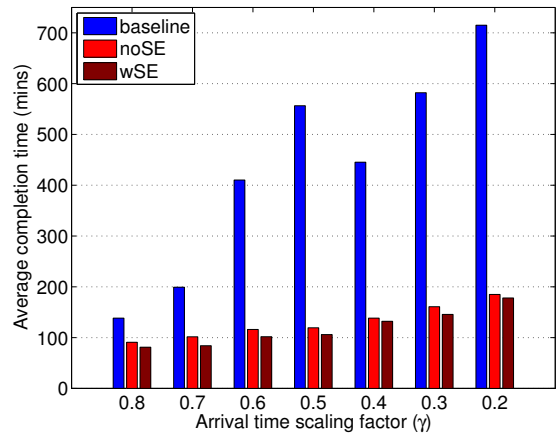
### 5.6.3 Performance Results

Both noSE and wSE significantly reduce average completion times compared to SLURM's baseline scheduling policy (Figure 5.6). As  $\gamma$  decreases from 0.8 to 0.2, the average completion time increases in all the schemes because the jobs arrive at a much faster rate and therefore have to wait in the queue for longer time before they get scheduled. However, this increase in the average completion times with both our schemes is not as significant as it is with the baseline scheme.

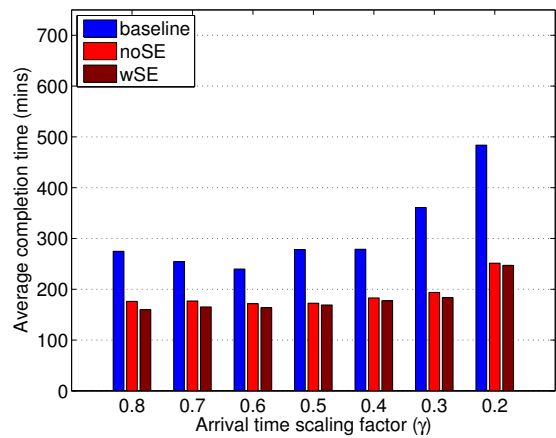
Both noSE and wSE have significantly improved average response times, with wSE outperforming noSE (Table 5.3). Execution time in wSE includes the costs of shrinking or expanding the job (Section 5.6.1). Despite this overhead, wSE outperforms noSE in average



(a) Set1



(b) Set2



(c) Set3

Figure 5.6: Average completion times of baseline, *noSE* and *wSE*. Job arrival times in all the sets (Set1, Set2, Set3) were scaled down by factor  $\gamma$  to get diversity in job arrival rate

Set	Avg Resp. Time (mins)			Avg Exe. Time (mins)			Avg. Num. of Nodes			Speedup	
	baseline	wSE	noSE	baseline	wSE	noSE	baseline	wSE	noSE	wSE	noSE
1 ( $\gamma = 0.5$ )	90	3	6	80	84	95	453	610	601	1.91	1.70
2 ( $\gamma = 0.5$ )	500	34	57	57	69	89	632	714	721	5.25	4.66
3 ( $\gamma = 0.5$ )	217	99	88	60	73	90	520	662	665	1.65	1.61
2 ( $\gamma = 0.7$ )	142	12	20	57	66	83	596	656	660	2.36	1.96
3 ( $\gamma = 0.7$ )	194	95	86	60	73	90	488	596	599	1.54	1.43

Table 5.3: Comparison of the baseline, wSE and noSE scheduling policies for different data sets.

execution time of jobs. wSE version consistently outperforms noSE in all data sets. The average completion times reported in Figure 5.6) includes cost of all overheads. In all the job datasets, the average overhead for shrinking and expanding the jobs was less than 1% of the time taken to execute the dataset. We controlled these costs by setting  $f_{se} = 500$  secs, i.e., the scheduler waited for at least 500 secs between two successive contraction and expansion operations for a job. We found the cost for solving the ILP to be small. The largest ILP that we solved took 15 secs which is negligible given the frequency at which the scheduler was invoked is much smaller. We use data from Table 5.3 to explain two observations related to the speedups of our schemes. The speedup in average completion time for both our policies is calculated relative to the baseline (shown in Table 5.3).

- Higher speedup in average completion time for  $\gamma = 0.5$  compared to  $\gamma = 0.7$  in Set2: The baseline case has a 4 fold increase in response time compared to just a 2 fold increase in response time for wSE when  $\gamma$  changes from 0.7 to 0.5. Average execution time in the wSE version increases only slightly after  $\gamma$  changes from 0.7 to 0.5 (Table 5.3), while it remains constant in the baseline scenario. Since, completion time is the sum of response and execution time, we observe higher speedups for smaller values of  $\gamma$  in Set2.
- Smaller speedups in Set3 as compared to Set2: Upon job trace inspection, we discovered that there are not enough jobs to keep the machine fully utilized during the first half of Set3. Therefore, even after reducing  $\gamma$  to small values, the response time is not significantly affected in Set3. In contrast, Set2 has a very high machine utilization which leads to a significant increase in the response time of the baseline scheduler as  $\gamma$  is reduced (from 0.5 to 0.7), resulting in higher speedups for both our scheduling policies.

To see the effectiveness of our scheme, we compared it with a baseline scheduler if it were to schedule jobs on an overprovisioned system. All CPUs in this system are power capped at the same value ( $< 60W$ ). This allows the baseline scheduler to add more nodes while remaining within the same power budget, e.g., setting the power cap for each CPU to 30W

CPU power cap (W)	30	40	50	60
Speedup	4.32	1.86	2.33	5.25
Avg number of nodes	50332	42486	39700	37956

Table 5.4: Comparison of *wSE* with the baseline scheduler running on an overprovisioned system (at different CPU power caps) using Set 2 ( $\gamma = 0.5$ )

allows baseline (SLURM) to use up to  $\lfloor \frac{4,751,360}{30+18+38} \rfloor = 55,248$  nodes. In Table 5.4, we present the speedup of *wSE* relative to a baseline scheduler operating on an overprovisioned system with different CPU power caps as the reference. Significant speedups in Table 5.4 emphasize the benefits of solving the ILP for determining optimal job configurations rather than using the baseline scheduler, which runs all jobs at the same node power. Table 5.4 shows that even after scheduling on an overprovisioned system and using greater than 40,960 nodes, the baseline scheduler still under performs our scheduler by a significant margin.

#### 5.6.4 Increasing Job Arrival Rate While Maintaining the Same QoS

For the purpose of this study we define the Quality of Service (QoS) for a data center to be determined by the average and maximum completion time of its jobs. To emphasize the usefulness of our schedulers, we increased the arrival rate of jobs (by multiplying the original arrival times by the constant  $\gamma$ ) as much as possible, so long as we maintain the same QoS as provided by the baseline schedule ( $\gamma = 1$ ). The results are presented in Figure 5.7). Consider the first group of bars: *wSE* allowed for arrival time of the last job of Set1 to be reduced to just 2.2 days and still provided the same QoS as the baseline scheduler whose last job arrived at 6.8 days (arrival times of other jobs are scaled down proportionately).. Similarly trends may be seen in Figure 5.7 for the other sets.

#### 5.6.5 Analyzing tradeoff between Fairness and Throughput

We introduced the term  $w_j$  in the objective function of the scheduler’s ILP (Equation 5.1) to prevent starvation of jobs with low power-aware speedup. In this section, we analyze the tradeoff between maximum completion time of any job (fairness) and the average completion time of jobs (equivalent to throughput). The parameter  $\alpha$  can be be tuned by the data center administrator to control fairness and throughput. We performed several experiments by varying  $\alpha$  and measured its impact on the average and maximum completion times. Figure. 5.8 and Figure. 5.8 plot the average and maximum completion times of Set2 for

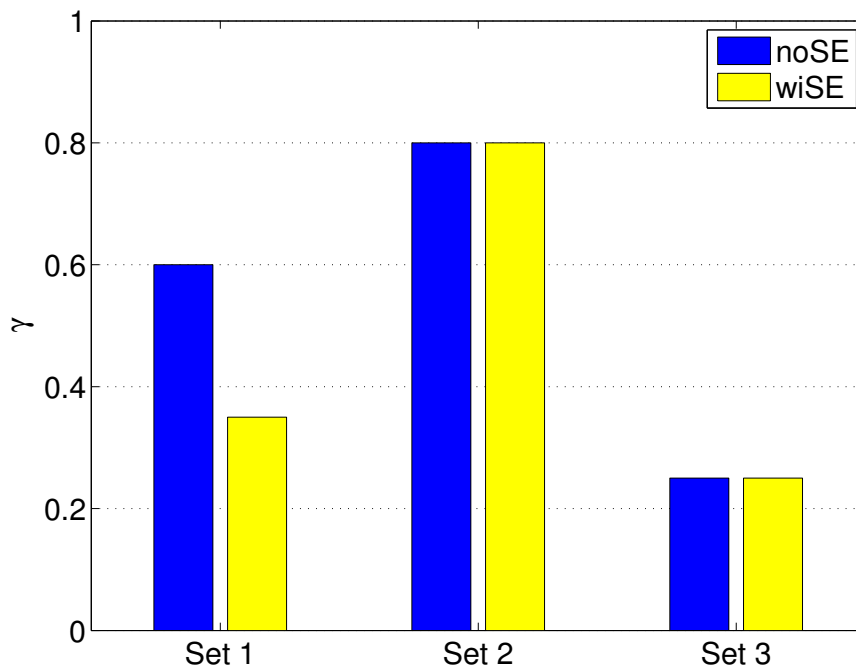


Figure 5.7: Reduction in job arrival times while maintaining the same QoS as the baseline scheduler

different values of  $\alpha$  using  $\gamma = 0.8$ . As the value of  $\alpha$  increases, the maximum completion time decreases at the cost of an increase in average completion time (Figure. 5.8 and Figure. 5.9).

We further compare completion times of our scheduler with the baseline. Figure. 5.10 plots the cumulative distribution frequency (CDF) of completion times of the 1000 jobs of Set 1 (with  $\gamma = 0.8$ ) for our wiSE scheduler and the baseline scheduler. For readability, wiSE’s performance is plotted with only two values of  $\alpha$ .

For both values of  $\alpha$ , wiSE is significantly better than the baseline. As  $\alpha$  is increased, the CDF for wiSE starts getting closer to the baseline’s CDF. Although this increase in  $\alpha$  increases the average completion time (decrease in slope), it reduces the maximum completion time from 71,644 secs to 62,061 secs. Figure. 5.10 shows that our scheduler, using  $\alpha = 0.28$ , finishes 90% of the jobs within 11,500 secs as compared to the baseline which takes 22,000 secs to finish 90% jobs.

### 5.6.6 How Much Profile Data is Sufficient?

Our scheduler’s ILP takes a job’s execution profile at different resource combinations as input. A Larger number of power levels  $|P_j|$ , will lead to better scheduling decisions compared

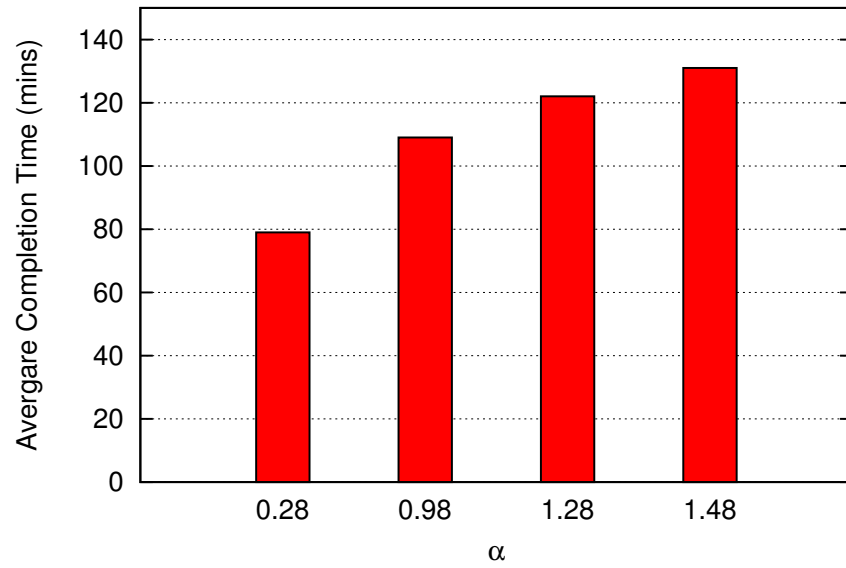


Figure 5.8: Average completion times for Set 1 for different values of ( $\alpha$ )

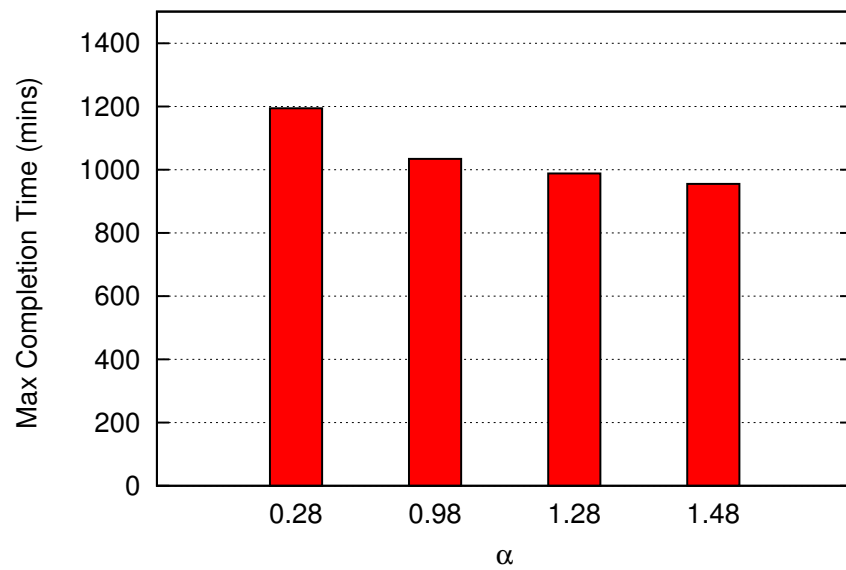


Figure 5.9: Maximum (worst) completion times for Set 1 for different values of ( $\alpha$ )

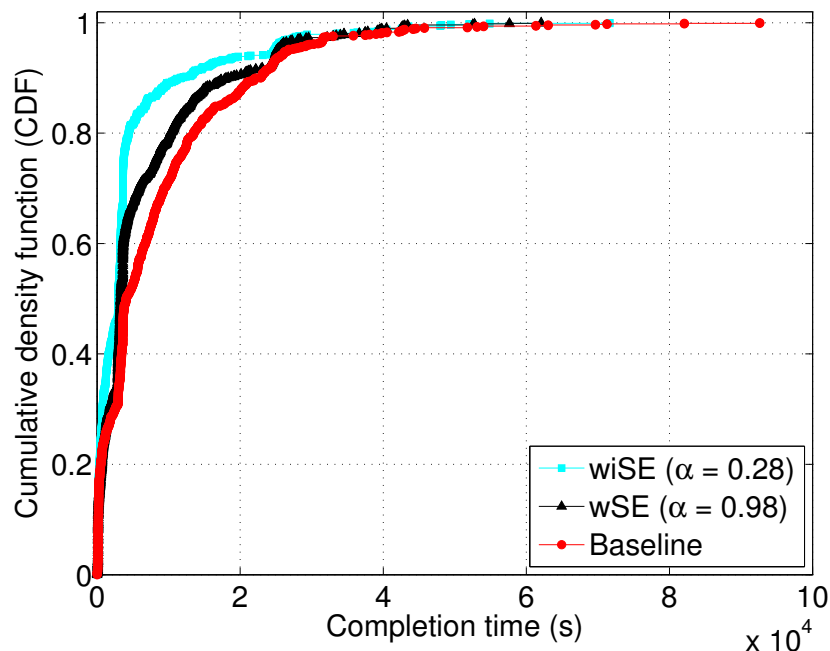


Figure 5.10: CDF for completion times for baseline and wiSE for different  $\alpha$  using SET1

to the case when fewer power levels are provided. However, the number of binary variables in the ILP ( $x_{j,n,p}$ ) are proportional to the number of power levels of the jobs. The larger the number of variables, the longer that it takes to solve the ILP. As mentioned earlier, the maximum cost of solving the ILP in all of our experiments was 15 secs where we used  $|P_j| = 6$  and the queue  $\mathcal{J}$  had 200 jobs. In this subsection, we see the impact of varying the number of power levels used per job. We did several experiments in which we scheduled Set1 with  $\gamma = 0.5$  using up to 8 different power levels,  $|P_j| = 8$ . For example, the case with 2 power levels means that all jobs can execute either at 30W or 60W. The average and maximum completion times with the baseline scheduler for Set1 ( $\gamma = 0.5$ ) were 170 mins and 1,419 mins, respectively. As we keep on increasing the number of power levels from 1 to 6, the solution space of the ILP increases and therefore we get better solutions, i.e., the average and maximum completion times decrease as the number of power levels increase (Figure 5.11 and Figure 5.12). However, the improvement in both the average and maximum completion times becomes negligible after 6 power levels. This insensitivity is due to huge increase in the number of available resource combinations that each new power level brings to the solution space. After 6 power levels, we can infer that the solution space has enough resource combinations to get a solution that is close the *best* solution. Hence, adding more power levels does not bring significant improvement.

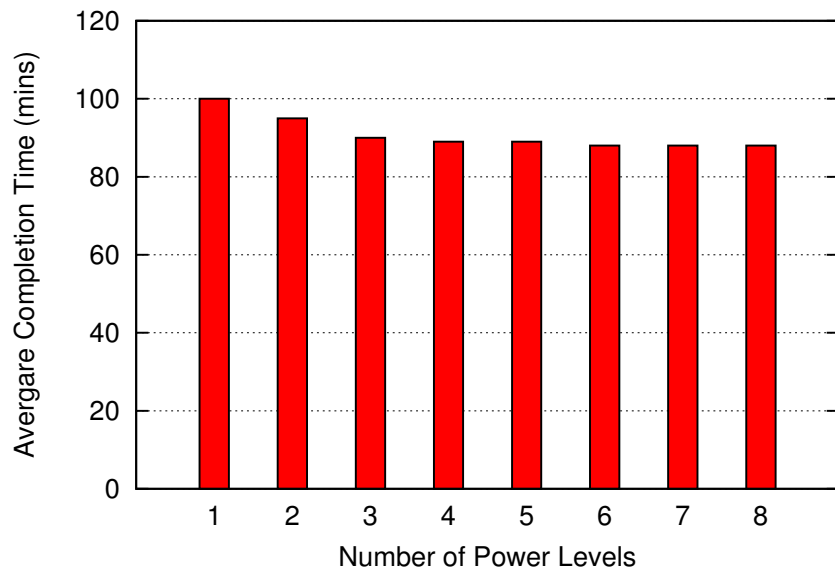


Figure 5.11: Effect of increasing the number of power levels ( $|P_j|$ ) on the average completion time of Set 1 ( $\gamma = 0.5$ ).

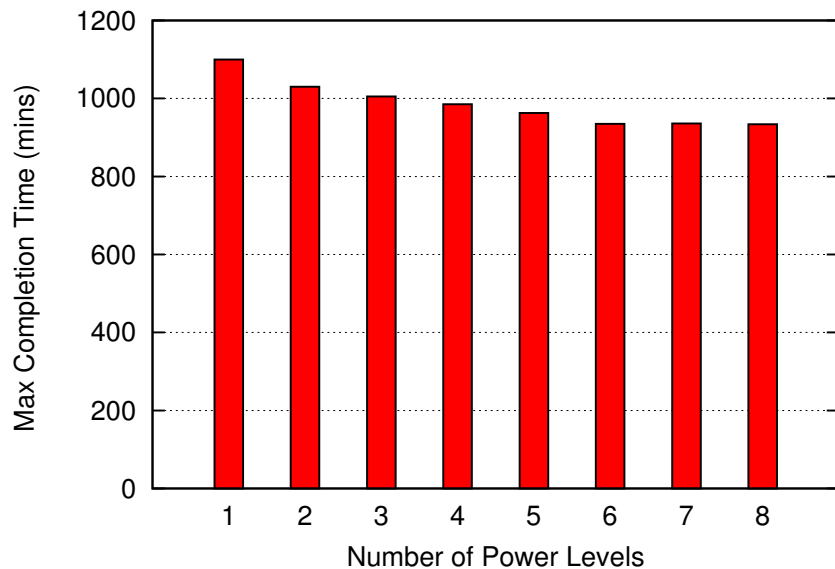


Figure 5.12: Effect of increasing the number of power levels ( $|P_j|$ ) on the maximum completion time of Set 1 ( $\gamma = 0.5$ ).



## Concluding Remarks

The research described in this thesis leverages hardware and software capabilities and makes a first attempt at solving three of the biggest challenges that the HPC community faces in moving to larger machines, i.e., energy, reliability and power. It uses Dynamic Voltage and Frequency Scaling (DVFS) and power capping of the CPU and memory subsystems in conjunction with an adaptive runtime system to optimize application performance under user specified thermal or power constraints. The proposed scheme can effectively restrain CPU temperatures leading to a reduction in the cooling energy consumption of a data center. This thesis also estimates the improvement in machine reliability resulting from applying the proposed thermal restraint scheme. The later part of the thesis presents power-aware scheduling, which can significantly improve the throughput of an HPC data center by intelligently assigning power levels to all nodes in the data center. In this chapter, we highlight the findings of this dissertation and outline an incomplete list of promising ideas derived from it. This chapter is divided into two sections. Section 6.1 summarizes the conclusions that result from applying thermal constraints along with potential directions for future work. Section 6.2 states some conclusions and mentions potential future work for power-constrained data centers.

### 6.1 Thermal Restraint

The following conclusions can be made from the first part of this thesis, which uses thermal restraint to reduce cooling energy, improve reliability and optimize application performance:

- Cooling energy can be reduced by restraining processor temperatures. Our scheme shown in Chapter 2 uses DVFS and demonstrates reduction of up to 63% in the

cooling energy consumption of a cluster.

- Naive use of DVFS can restrain processor temperatures but not without significantly impacting the performance of parallel applications. Our scheme from Chapter 2 combines DVFS with a dynamic runtime system that supports object migration to alleviate the impact of DVFS. Our frequency-aware load balancing scheme from Chapter 2 shows significant improvement in execution time over the baseline scheme that naively uses DVFS.
- DVFS can be used to restrain processor temperatures for any application below a reasonable threshold. However, the impact temperature restraint has on the execution time of an application varies. Applications having lower FLOP/s rate can significantly benefit from temperature restraint as their execution time is less affected by temperature control which in turn helps in reducing energy consumption. Chapter 2 shows that restraining processor temperatures with a memory bound application (*Jacobi2D*) can reduce the total energy consumption by as much as 18% while increasing the execution time by only 3%.
- Restraining processor temperatures and hot spot avoidance can significantly improve the reliability of an HPC machine. Chapter 3 outlines a model that relates processor temperature to Mean Time Between Failures (MTBF) of a machine. It uses this relationship to estimate the improvement in MTBF resulting from restraining processor temperatures.
- Restraining processor temperatures can significantly improve the performance of an HPC machine in a faulty environment. Chapter 3 builds a comprehensive model that estimates execution time by combining thermal restraint with checkpoint/restart.

The following is an incomplete list of promising ideas derived from the contributions in this thesis related to thermal restraint:

**Sequential Execution Block Optimization:** Our recent work [61] proposes and evaluates a runtime technique for MPI that reduces both machine and cooling energy consumption on a single node. By dividing the computation into different Sequential Execution Blocks (SEBs) depending on their sensitivity to frequency, and running them at different levels of frequency, we were able to reduce machine energy consumption by 17% with as little as 0.9% increase in execution time while restraining core temperatures below 60° C. In the future, one can extend our SEB-based work to handle multiple nodes, i.e., combine it with *CoolLB*. Such a scheme will reduce both the

machine and cooling energy consumption of a data center while constraining core temperatures under a user defined threshold. Different nodes, when capped under a given temperature threshold, might have to operate at different frequencies due to thermal variations. Hence, this difference in frequencies can cause load imbalance which needs to be fixed based on processor frequencies. Difference in the sensitivities of multiple SEBs to frequency can be leveraged to reduce the impact of DVFS on execution time. By migrating the sensitive SEBs to cooler processors (operating at higher frequencies) and keeping the insensitive SEBs on the hotter processors (operating at lower frequencies), our proposed scheme would be able to reduce the execution time penalty as well as total energy consumption. However, this work requires the ability of per-core-DVFS which is currently not available. Implementing such a technique on existing hardware, i.e., with processor-wide DVFS, limits its applicability significantly.

**Thermal restraint for message-logging and parallel recovery:** Chapter 3 combined thermal restraint with checkpoint/restart protocol for fault tolerance to improve the reliability of an HPC machine. Since thermal restraint increases the Mean Time Between Failure (MTBF) of the system, it should benefit any fault tolerance protocol. Extending our work by implementing thermal capping in other fault tolerance protocols could be an interesting future work, e.g., message logging and parallel recovery [49], and comparing their benefits to our current scheme.

**Reducing thermal throttling:** Earlier studies show that large temperature variations can decrease the reliability of a processor [79]. Estimating the effects of such variations on MTBF of a processor by looking at real temperature data of a processor for various workloads could be an interesting future work. Based on the thermal profiles of different applications that capture thermal throttling, application performance can be improved by *controlling* processor temperature and reducing any large temperature variations.

## 6.2 Power Constraint

The second part of this thesis optimizes performance under a strict power constraint and makes the following conclusions:

- CPU and memory power capping can be used to constrain the power drawn by each node of an HPC machine. This feature comes with a performance impact for the

application. Chapter 4 describes a curve fitting scheme that can capture the relation between execution time and CPU power.

- Power capping the CPU and memory subdomains in the context of an overprovisioned system can significantly improve the performance of an application. Capping the CPU and memory power subsystems allows us to add additional nodes that speedup the computation while staying within the power budget. Chapter 4 demonstrates that our overprovisioning scheme improves application performance under a strict power budget.
- Base/idle power of a machine can significantly effect the usefulness of an overprovisioned system. It acts as a fixed cost for adding more nodes and hence determines the ease with which additional nodes can be added by capping the CPU/memory power of other nodes. Chapter 4 shows how lower base/idle power can improve application performance in an overprovisioned system.
- Depending on application characteristics, CPU power capping can degrade performance differently. Chapter 5 captures the sensitivity of application performance to CPU power by describing a comprehensive model that takes into account the power consumed by various subcomponents of the CPU.
- CPU power capping can be used for improving the throughput of an entire data center by using an efficient resource management system. Chapter 5 describes our scheduling scheme that takes into account application characteristics to determine the best set of jobs to execute along with an optimum resource combination for each of the selected jobs.

The work described in the second part of this thesis presents the following interesting ideas to explore in the future:

**Power capping induced heterogeneity:** Two compute nodes operating under the same CPU power cap might end up working at different *frequencies* due to different thermal conditions [80]. Such frequencies can get exaggerated for very low power caps. This *heterogeneity* can be addressed by using dynamic load balancing capabilities of a system that supports dynamic object migration [81]. Our frequency-aware load balancer can be used to fix such heterogeneity. The frequency-aware load balancer should load balance and hence improve performance.

**Thermal and power constraints:** Applying a thermal constraint can reduce cooling costs (Chapter 2) and improve reliability (Chapter 3) of an HPC data center. In the future,

one can combine our power capping work with temperature restraint to combine the benefits of both the schemes. Such a solution would efficiently operate an overprovisioned data center under fixed power *and* temperature constraints.

**Fine grained power capping:** RAPL supports individually power capping both the PP0 (only the cores) and PKG (the entire processor including the cores, caches and the memory controller) subdomains. So far, we have applied power capping at the PKG level. Benefits of individually capping the PP0 and PKG subdomains would be an interesting work to follow.

## Machine Descriptions

To evaluate the schemes proposed in this thesis, we required machines that allowed DVFS or CPU power capping. We used two different Dell clusters located at the Computer Science Department of the University of Illinois at Urbana Champaign. Table A.1 summarizes the two clusters i.e. Energy Cluster and Power Cluster.

<b>Component</b>	<b>Energy Cluster</b>	<b>Power Cluster</b>
Processor	Intel Xeon X3430	Intel Xeon E5-2620
Processor frequency (GHz)	2.4	2.0
Turbo frequency (GHz)	2.8	2.5
Cores per processor	4	6
TDP (W)	95	95
Interconnect switch	Gigabit ethernet	Gigabit ethernet
Memory per node (GB)	4	16

Table A.1: Summary of features of clusters used in this thesis.

### Energy Cluster

Energy Cluster consists of 40 nodes (160 cores) installed in the Department of Computer Science of the University of Illinois at Urbana-Champaign. Each node has a single socket with a four-core Intel Xeon X3430 processor chip. Each chip can be set to 10 different frequency levels (‘P-states’) between 1.2 GHz and 2.4 GHz. It also supports Intel’s TurboBoost [82], allowing some cores to overclock up to 2.8 GHz. The operating system on the nodes is CentOS 5.7 with `lm-sensors` and `coretemp` module installed to provide core temperature readings, and the `cpufreq` module installed to enable software-controlled

DVFS. The cluster nodes are connected by a 48-port gigabit ethernet switch. We use a Liebert power distribution unit installed on the rack containing the cluster to measure the machine power after a 1 second interval on a per-node basis. We gather these readings for each experiment and integrate them over the execution time to come up with the total machine energy consumption.

The Computer Room Air Conditioner (CRAC) is an air cooler fed by chilled water from a campus plant. It achieves the temperature set-point prescribed by the operator by manipulating the flow of chilled water. The temperature of the exhaust air coming from the machine room is compared to the set-point and the water flow is adjusted accordingly.

## Power Cluster

This testbed is a 20-node Dell PowerEdge R620 cluster installed at the Department of Computer Science, University of Illinois at Urbana-Champaign. Each node is an Intel® Xeon® E5-2620 Sandy-bridge server with 6 physical cores @ 2GHz, 2-way SMT with 16GB of DRAM. The package/CPU corresponds to the processor die that also includes the cores, L1,L2 and L3 caches amongst other components. The package power for this cluster can be capped in the range 25W to 95W (71 integer power levels) while the memory power can be capped between 8W to 35W (28 integer power levels).

# APPENDIX **B**

## Benchmark Descriptions

To evaluate the benefits of the schemes proposed in this dissertation, we used a variety of parallel applications. These applications come from various domains and are implemented using different languages. This appendix describes each of the applications used in this thesis.

### Jacobi2D

A 5-point stencil application that computes the transmission of heat over a discretized 2D grid. The global 2D grid is divided into smaller blocks that are processed in parallel. It is an iterative application where all processors synchronize at the end of each iteration. As is the case in a stencil computation, each grid point is the average of the neighboring 5 points. Neighboring blocks communicate the *ghost* layers with each other so that averaging computations are done for all cells inside each block. This application is implemented in Charm++ using a 2D chare array.

### Wave2D

This benchmark is a finite differencing method that computes the pressure information over a discretized 2D grid. The entire space is divided into smaller blocks that are divided among the processors. As in any other parallel stencil computation, neighboring blocks exchange ghost layers to do computation. The computation updates all cells in the grid using the previous two values of the neighboring cells using a 5-point stencil. This benchmark is



implemented using Charm++ where each block is represented as an array element of a 2D chare array.

## Mol3D/LeanMD

This mini-application is a molecular dynamics application that emulates the communication pattern of a real world application NAMD [83]. It computes the interaction forces based on Lennard-Jones forces amongst particles in a 3D space. It does not include any long range force calculation. The object decomposition is achieved using a scheme similar to NAMD. The 3D space is divided into hyperrectangles, called *cells* or *patches* in NAMD's nomenclature, each containing a subset of particles. A *compute* object is responsible for the force calculations between each pair of cells. In each computation of the application, each cell sends its particle data to all *computes objects* attached to it and receives the updates from those computes objects. This mini-application is implemented using Charm++ where the set of cells and *computes objects* are represented by chare arrays.

## Lulesh

Livermore Unstructured Lagrangian Explicit Shock Hydrodynamics (LULESH) was originally defined and implemented by Lawrence Livermore National Laboratory (LLNL) as one of five challenge problems in the DARPA UHPC program and has since become a widely studied proxy application in DOE co-design efforts for exascale [56]. LULESH is a highly simplified application, hard-coded to only solve a simple Sedov blast problem with analytic answers. It represents the numerical algorithms, data motion, and programming style typical in scientific C or C++ based applications. It approximates the hydrodynamics equations discretely by partitioning the spatial problem domain into a set of volumetric elements defined by a mesh. Each node represents a point of intersection on the mesh. It is an iterative application that exchanges ghost layers with neighboring elements. Although LULESH is implemented using many parallel programming models, we use a Charm++ implementation that uses a 3D chare array.

## NPB Parallel Benchmarks

The NAS Parallel Benchmarks (NPB) are a small set of programs designed to help evaluate the performance of parallel supercomputers. The benchmarks are derived from computational fluid dynamics (CFD) applications and consist of five kernels and three pseudo-applications in the original "pencil-and-paper" specification (NPB 1) [84–86]. Problem sizes in NPB are predefined and indicated as different classes. In this thesis we use AMPI implementations of FT and MG.

**FT:** This benchmark is a 3D partial differential solver that uses FFT. It is a communication intensive code that does several long distance communication operations. The benchmark problem is to solve a discrete version of the original PDE by computing the forward 3-D discrete Fourier transform (DFT) of the original state array.

**MG:** is a simplified multigrid kernel, that solves a 3-D Poisson PDE. The Class B problem uses the same size grid as Class A but a greater number of inner loop iterations.

## Adaptive Mesh Refinement (AMR)

We use an efficient oct-tree based Charm++ implementation of AMR. This implementation is fully distributed and highly asynchronous which removes several centralized bottlenecks and synchronization overheads present in competing implementations [74]. Instead of a process, it models a block as a basic schedulable unit that acts as a virtual processor. This virtualization allows overlap of communication and computation. This benchmark allows dynamic placement of a block on any physical processor that facilitates dynamic load balancing.

# REFERENCES

- [1] T. Renzenbrink, “Data Centers Use 1.3% of Worlds Total Electricity. A Decline in growth.” [Online]. Available: <http://www.techthefuture.com/energy/>
- [2] B. Rountree, D. K. Lowenthal, S. Funk, V. W. Freeh, B. R. de Supinski, and M. Schulz, “Bounding Energy Consumption in Large-scale MPI Programs,” in *Proceedings of the ACM/IEEE conference on Supercomputing*, 2007, pp. 49:1–49:9.
- [3] R. Springer, D. K. Lowenthal, B. Rountree, and V. W. Freeh, “Minimizing execution time in MPI programs on an energy-constrained, power-scalable cluster,” in *Proceedings of the eleventh ACM SIGPLAN symposium on Principles and practice of parallel programming*, ser. PPOPP '06. New York, NY, USA: ACM, 2006. [Online]. Available: <http://doi.acm.org/10.1145/1122971.1123006> pp. 230–238.
- [4] R. F. Sullivan, “Alternating cold and hot aisles provides more reliable cooling for server farms,” White Paper, Uptime Institute, 2000.
- [5] C. D. Patel, C. E. Bash, R. Sharma, M. Beitelmal, and R. Friedrich, “Smart cooling of data centers,” *ASME Conference Proceedings*, vol. 2003, no. 36908b, pp. 129–137, 2003.
- [6] R. Sawyer, “Calculating total power requirements for data centers,” *White Paper, American Power Conversion*, 2004.
- [7] S. Lacey, “Data center efficiency may be getting worse.” [Online]. Available: <http://www.greentechmedia.com/articles/read/are-data-centers-getting-less-energy-efficient>
- [8] Ericsson, “Reliability Aspects on Power Supplies,” *Technical Report Design Note 002, Ericsson Microelectronics, April 2000*.
- [9] J. Srinivasan, S. Adve, P. Bose, and J. Rivers, “The impact of technology scaling on lifetime reliability,” in *Dependable Systems and Networks, 2004 International Conference on*, 2004, pp. 177–186.
- [10] J. A. Chung H. Hsu, W. Feng, “Towards Efficient Supercomputing: A Quest for the Right Metric.” [Online]. Available: <http://sss.cs.vt.edu/presentations/hppac05.ppt.pdf>
- [11] P. Kogge, K. Bergman, S. Borkar, D. Campbell, W. Carlson, W. Dally, M. Denneau, P. Franzon, W. Harrod, J. Hiller, S. Karp, S. Keckler, D. Klein, R. Lucas, M. Richards, A. Scarpelli, S. Scott, A. Snavey, T. Sterling, R. S. Williams, and K. Yelick, “Exascale computing study: Technology challenges in achieving exascale systems,” 2008.

- [12] K. Ferreira, J. Stearley, J. H. Laros, III, R. Oldfield, K. Pedretti, R. Brightwell, R. Riesen, P. G. Bridges, and D. Arnold, “Evaluating the viability of process replication reliability for exascale systems,” in *SC 2011*. New York, NY, USA: ACM, 2011. [Online]. Available: <http://doi.acm.org/10.1145/2063384.2063443> pp. 44:1–44:12.
- [13] “Top500 supercomputing sites,” <http://top500.org>, 2013.
- [14] T. Patki, D. Lowenthal, B. Rountree, S. Martin, and B. Supinski, “Exploring Hardware Overprovisioning in Power-Constrained, High Performance Computing,” in *Proceedings of the 27th International Conference on Supercomputing, ICS*, 2013.
- [15] O. Sarood, A. Gupta, and L. V. Kale, “Temperature aware load balancing for parallel applications: Preliminary work,” in *The Seventh Workshop on High-Performance, Power-Aware Computing (HPPAC’11)*, Anchorage, Alaska, USA, 5 2011.
- [16] C. Bash and G. Forman, “Cool job allocation: measuring the power savings of placing jobs at cooling-efficient locations in the data center,” in *2007 USENIX Annual Technical Conference on Proceedings of the USENIX Annual Technical Conference*. Berkeley, CA, USA: USENIX Association, 2007, pp. 29:1–29:6.
- [17] L. Wang, G. von Laszewski, J. Dayal, and T. Furlani, “Thermal aware workload scheduling with backfilling for green data centers,” in *IEEE 28th International Performance Computing and Communications Conference (IPCCC)*, 2009, pp. 289–296.
- [18] L. Wang, G. von Laszewski, J. Dayal, X. He, A. Younge, and T. Furlani, “Towards thermal aware workload scheduling in a data center,” in *10th International Symposium on Pervasive Systems, Algorithms, and Networks (ISPAN)*, 2009, pp. 116–122.
- [19] Q. Tang, S. Gupta, D. Stanzione, and P. Cayton, “Thermal-aware task scheduling to minimize energy usage of blade server based datacenters,” in *2nd IEEE International Symposium on Dependable, Autonomic and Secure Computing*, 2006, pp. 195–202.
- [20] D. Rajan and P. Yu, “Temperature-aware scheduling: When is system-throttling good enough?” in *The Ninth International Conference on Web-Age Information Management*, july 2008, pp. 397–404.
- [21] S. Li, H. Le, N. Pham, J. Heo, and T. Abdelzaher, “Joint optimization of computing and cooling energy: Analytic model and a machine room case study,” in *Proceedings of the 2012 IEEE 32Nd International Conference on Distributed Computing Systems*, ser. ICDCS ’12. Washington, DC, USA: IEEE Computer Society, 2012. [Online]. Available: <http://dx.doi.org/10.1109/ICDCS.2012.64> pp. 396–405.
- [22] M. Y. Lim, V. W. Freeh, and D. K. Lowenthal, “Adaptive, transparent CPU scaling algorithms leveraging inter-node MPI communication regions,” *Parallel Computing*, vol. 37, no. 10-11, pp. 667–683, 2011.
- [23] S. Huang and W. Feng, “Energy-efficient cluster computing via accurate workload characterization,” in *Proceedings of the 2009 9th IEEE/ACM International Symposium on Cluster Computing and the Grid*. IEEE Computer Society, 2009, pp. 68–75.

- [24] H. Hanson, S. Keckler, R. K. S. Ghiasi, F. Rawson, and J. Rubio, “Power, performance, and thermal management for high-performance systems,” in *IEEE International Parallel and Distributed Processing Symposium (IPDPS)*, 2007, pp. 1–8.
- [25] A. Banerjee, T. Mukherjee, G. Varsamopoulos, and S. Gupta, “Cooling-aware and thermal-aware workload placement for green HPC data centers,” in *International Green Computing Conference*, 2010, pp. 245–256.
- [26] Q. Tang, S. Gupta, and G. Varsamopoulos, “Energy-efficient thermal-aware task scheduling for homogeneous high-performance computing data centers: A cyber-physical approach,” *IEEE Transactions on Parallel and Distributed Systems*, vol. 19, no. 11, pp. 1458–1472, 2008.
- [27] A. Merkel and F. Bellosa, “Balancing power consumption in multiprocessor systems,” in *Proceedings of the 1st ACM SIGOPS/EuroSys European Conference on Computer Systems*, ser. EuroSys. ACM, 2006.
- [28] V. W. Freeh and D. K. Lowenthal, “Using multiple energy gears in MPI programs on a power-scalable cluster,” in *Proceedings of the 10th ACM SIGPLAN Symposium on Principles and Practice of Parallel Programming*, ser. PPOPP ’05. New York, NY, USA: ACM, 2005. [Online]. Available: <http://doi.acm.org/10.1145/1065944.1065967> pp. 164–173.
- [29] L. Kalé and S. Krishnan, “CHARM++: A Portable Concurrent Object Oriented System Based on C++,” in *Proceedings of OOPSLA ’93*, A. Paepcke, Ed. ACM Press, September 1993, pp. 91–108.
- [30] R. K. Brunner and L. V. Kalé, “Handling application-induced load imbalance using parallel objects,” in *Parallel and Distributed Computing for Symbolic and Irregular Applications*. World Scientific Publishing, 2000, pp. 167–181.
- [31] P. Jetley, F. Gioachin, C. Mendes, L. V. Kale, and T. R. Quinn, “Massively parallel cosmological simulations with ChaNGa,” in *Proceedings of IEEE International Parallel and Distributed Processing Symposium 2008*, 2008.
- [32] G. Zheng, A. Bhatele, E. Meneses, and L. V. Kale, “Periodic Hierarchical Load Balancing for Large Supercomputers,” *International Journal of High Performance Computing Applications (IJHPCA)*, March 2011.
- [33] O. Sarood and L. V. Kalé, “A ‘cool’ load balancer for parallel applications,” in *SC 2011*, Seattle, WA, November 2011.
- [34] L. Kalé and A. Sinha, “Projections : A scalable performance tool,” in *Parallel Systems Fair, International Parallel Processing Symposium*, Apr. 1993, pp. 108–114.
- [35] R. Kufirin, “PerfSuite: An Accessible, Open Source Performance Analysis Environment for Linux,” in *In Proceedings of the Linux Cluster Conference*, 2005.

- [36] Intel, “Intel-64 and IA-32 Architectures Software Developer’s Manual , Volume 3A and 3B: System Programming Guide, 2011.”
- [37] K. Sato, N. Maruyama, K. Mohror, A. Moody, T. Gamblin, B. R. de Supinski, and S. Matsuoka, “Design and modeling of a non-blocking checkpointing system,” in *Proceedings of the International Conference on High Performance Computing, Networking, Storage and Analysis*, ser. SC ’12. Los Alamitos, CA, USA: IEEE Computer Society Press, 2012. [Online]. Available: <http://dl.acm.org/citation.cfm?id=2388996.2389022> pp. 19:1–19:10.
- [38] C.-H. Hsu, W.-C. Feng, and J. S. Archuleta, “Towards efficient supercomputing: A quest for the right metric,” in *Proceedings of the HighPerformance Power-Aware Computing Workshop*, 2005.
- [39] W.-c. Feng, “Making a case for efficient supercomputing,” vol. 1, no. 7. New York, NY, USA: ACM, Oct. 2003. [Online]. Available: <http://doi.acm.org/10.1145/957717.957772> pp. 54–64.
- [40] W.-c. Feng, “The Importance of Being Low Power in High-Performance Computing,” *Cyberinfrastructure Technology Watch Quarterly (CTWatch Quarterly)*, vol. 1, no. 3, August 2005.
- [41] G. Zheng, L. Shi, and L. V. Kalé, “FTC-Charm++: An In-Memory Checkpoint-Based Fault Tolerant Runtime for Charm++ and MPI,” in *2004 IEEE Cluster*, San Diego, CA, September 2004, pp. 93–103.
- [42] P. Lemarinier, A. Bouteiller, T. Herault, G. Krawezik, and F. Cappello, “Improved message logging versus improved coordinated checkpointing for fault tolerant MPI,” *IEEE Cluster*, pp. 115–124, 2004.
- [43] G. Bosilca, A. Bouteiller, F. Cappello, S. Djilali, G. Fedak, C. Germain, T. Herault, P. Lemarinier, O. Lodygensky, F. Magniette, V. Neri, and A. Selikhov, “Toward a scalable fault tolerant MPI for volatile nodes,” in *Proceedings of SC 2002*. IEEE, 2002.
- [44] D. Buntinas, C. Coti, T. Héroult, P. Lemarinier, L. Pilard, A. Rezmerita, E. Rodriguez, and F. Cappello, “Blocking vs. non-blocking coordinated checkpointing for large-scale fault tolerant MPI protocols,” *Future Generation Comp. Syst.*, vol. 24, no. 1, pp. 73–84, 2008.
- [45] L. Kalé, “The Chare Kernel parallel programming language and system,” in *Proceedings of the International Conference on Parallel Processing*, vol. II, Aug. 1990, pp. 17–25.
- [46] O. Sarood, P. Miller, E. Totoni, and L. V. Kale, “Cool load balancing for high performance computing data centers,” *IEEE Transactions on Computers*, pp. 1752–1764, 2012.
- [47] A. Moody, G. Bronevetsky, K. Mohror, and B. R. de Supinski, “Design, modeling, and evaluation of a scalable multi-level checkpointing system,” in *SC*, 2010, pp. 1–11.

- [48] E. Meneses, X. Ni, and L. V. Kale, “A Message-Logging Protocol for Multicore Systems,” in *Proceedings of the 2nd Workshop on Fault-Tolerance for HPC at Extreme Scale (FTXS)*, Boston, USA, June 2012.
- [49] S. Chakravorty and L. V. Kale, “A fault tolerance protocol with fast fault recovery,” in *Proceedings of the 21st IEEE International Parallel and Distributed Processing Symposium*. IEEE Press, 2007.
- [50] E. Meneses, O. Sarood, and L. V. Kale, “Assessing Energy Efficiency of Fault Tolerance Protocols for HPC Systems,” in *Proceedings of the 2012 IEEE 24th International Symposium on Computer Architecture and High Performance Computing (SBAC-PAD 2012)*, New York, USA, October 2012.
- [51] F. Petrini, K. Davis, and J. Sancho, “System-level fault-tolerance in large-scale parallel machines with buffered coscheduling,” in *Proceedings of 18th International Parallel and Distributed Processing Symposium*, 2004.
- [52] J. T. Daly, “A higher order estimate of the optimum checkpoint interval for restart dumps,” *Future Generation Comp. Syst.*, vol. 22, no. 3, pp. 303–312, 2006.
- [53] J. W. Young, “A first order approximation to the optimal checkpoint interval,” *Commun. ACM*, vol. 17, no. 9, pp. 530–531, 1974.
- [54] L. Bautista-Gomez, D. Komatitsch, N. Maruyama, S. Tsuboi, F. Cappello, and S. Matsuoka, “FTI: High performance fault tolerance interface for hybrid systems,” in *Supercomputing*, Nov. 2011, pp. 1–12.
- [55] P. H. Hargrove and J. C. Duell, “Berkeley lab checkpoint/restart (blcr) for linux clusters,” in *SciDAC*, 2006.
- [56] “Lulesh,” <http://computation.llnl.gov/casc/ShockHydro/>.
- [57] B. Schroeder and G. A. Gibson, “Understanding failures in petascale computers.”
- [58] D. Fiala, “Detection and correction of silent data corruption for large-scale high-performance computing,” in *IEEE International Symposium on Parallel and Distributed Processing Workshops and Phd Forum (IPDPSW)*, 2011, pp. 2069–2072.
- [59] P. Ramachandran, S. Adve, P. Bose, and J. Rivers, “Metrics for architecture-level lifetime reliability analysis,” in *IEEE International Symposium on Performance Analysis of Systems and Software. ISPASS*, 2008, pp. 202–212.
- [60] J. Srinivasan, S. V. Adve, P. Bose, and J. A. Rivers, “The case for lifetime reliability-aware microprocessors,” in *Proceedings of the 31st Annual International Symposium on Computer Architecture*, ser. ISCA '04. Washington, DC, USA: IEEE Computer Society, 2004. [Online]. Available: <http://dl.acm.org/citation.cfm?id=998680.1006725> pp. 276–.

- [61] O. Sarood and L. Kale, “Efficient cool down of parallel applications,” *Workshop on Power-Aware Systems and Architectures in conjunction with International Conference on Parallel Processing*, 2012.
- [62] B. Behle, N. Bofferding, M. Broyles, C. Eide, M. Floyd, C. Francois, A. Geissler, M. Hollinger, H.-Y. McCreary, C. Rath et al., “IBM Energyscale for POWER6 Processor-based Systems,” *IBM White Paper*, 2009.
- [63] M. Broyles, C. Francois, A. Geissler, M. Hollinger, T. Rosedahl, G. Silva, J. Van Heuklon, and B. Veale, “IBM Energyscale for POWER7 Processor-based Systems,” *white paper, IBM*, 2010.
- [64] “Advanced Micro Devices. BIOS and Kernel Developers guide (BKDG) for AMD Family 15h Models 00h-0fh Processors,” January 2012. [Online]. Available: [http://support.amd.com/TechDocs/42301\\_15h\\_Mod\\_00h-0Fh\\_BKDG.pdf](http://support.amd.com/TechDocs/42301_15h_Mod_00h-0Fh_BKDG.pdf)
- [65] B. Rountree, D. H. Ahn, B. R. de Supinski, D. K. Lowenthal, and M. Schulz, “Beyond DVFS: A First Look at Performance Under a Hardware-enforced Power Bound,” in *Parallel and Distributed Processing Symposium Workshops & PhD Forum (IPDPSW), 2012 IEEE 26th International*. IEEE, 2012, pp. 947–953.
- [66] Intel, “Intel Power Governor.” [Online]. Available: <http://software.intel.com/en-us/articles/intel-power-governor>
- [67] R. Kumar, D. M. Tullsen, N. P. Jouppi, and P. Ranganathan, “Heterogeneous Chip Multiprocessors,” *Computer*, vol. 38, no. 11, pp. 32–38, 2005.
- [68] C.Hsing Hsu and W.Chun Feng, “Effective dynamic voltage scaling through CPU-boundedness detection,” in *Proceedings of the 4th International Conference on Power-Aware Computer Systems*, ser. PACS’04. Berlin, Heidelberg: Springer-Verlag, 2005. [Online]. Available: [http://dx.doi.org/10.1007/11574859\\_10](http://dx.doi.org/10.1007/11574859_10) pp. 135–149.
- [69] R. Ge, X. Feng, and K. Cameron, “Modeling and evaluating energy-performance efficiency of parallel processing on multicore based power aware systems,” in *IEEE International Symposium on Parallel Distributed Processing, 2009. IPDPS 2009*, 2009, pp. 1–8.
- [70] L. V. Kalé, S. Kumar, and J. DeSouza, “A malleable-job system for timeshared parallel machines,” in *2nd IEEE/ACM International Symposium on Cluster Computing and the Grid (CCGrid 2002)*, May 2002.
- [71] M. C. Cera, Y. Georgiou, O. Richard, N. Maillard, and P. O. A. Navaux, “Supporting malleability in parallel architectures with dynamic cpusets mapping and dynamic MPI,” in *Proceedings of the 11th International Conference on Distributed Computing and Networking*, ser. ICDCN’10. Berlin, Heidelberg: Springer-Verlag, 2010. [Online]. Available: <http://dl.acm.org/citation.cfm?id=2018057.2018090> pp. 242–257.
- [72] A. B. Downey, “A model for speedup of parallel programs,” Tech. Rep., 1997.



- [73] X. Chen, C. Xu, and R. Dick, “Memory access aware on-line voltage control for performance and energy optimization,” in *Computer-Aided Design (ICCAD), 2010 IEEE/ACM International Conference on*, 2010, pp. 365–372.
- [74] A. Langer, J. Lifflander, P. Miller, K.-C. Pan, , L. V. Kale, and P. Ricker, “Scalable Algorithms for Distributed-Memory Adaptive Mesh Refinement,” in *Proceedings of the 24th International Symposium on Computer Architecture and High Performance Computing (SBAC-PAD 2012)*, New York, USA, October 2012.
- [75] M. A. Jette, A. B. Yoo, and M. Grondona, “Slurm: Simple linux utility for resource management,” in *In Lecture Notes in Computer Science: Proceedings of Job Scheduling Strategies for Parallel Processing (JSSPP) 2003*. Springer-Verlag, 2002, pp. 44–60.
- [76] A. Lucero, “Slurm Simulator,” <http://www.bsc.es/marenostm-support-services/services/slurm-simulator>, Tech. Rep.
- [77] ANL, “Running jobs on BG/P systems,” <https://www.alcf.anl.gov/user-guides/bgp-running-jobs#boot-time>.
- [78] Computer Science and Engineering Department, The Hebrew University of Jerusalem, “Parallel Workloads Archive,” <http://www.cs.huji.ac.il/labs/parallel/workload/>, Tech. Rep.
- [79] J. Srinivasan, S. Adve, P. Bose, and J. Rivers, “Lifetime reliability: Toward an architectural solution,” *Micro, IEEE*, vol. 25, no. 3, pp. 70–80, 2005.
- [80] B. Rountree, D. Ahn, B. De Supinski, D. Lowenthal, and M. Schulz, “Beyond dvfs: A first look at performance under a hardware-enforced power bound,” in *Parallel and Distributed Processing Symposium Workshops PhD Forum (IPDPSW), 2012 IEEE 26th International*, May 2012, pp. 947–953.
- [81] L. Kalé and S. Krishnan, “Charm++ : A portable concurrent object oriented system based on C++,” in *Proceedings of the Conference on Object Oriented Programming Systems, Languages and Applications*, September 1993.
- [82] “Intel turbo boost technology,” <http://www.intel.com/technology/turboboost/>.
- [83] L. V. Kalé, M. Bhandarkar, R. Brunner, N. Krawetz, J. Phillips, and A. Shinozaki, “A case study in multilingual parallel programming,” in *10th International Workshop on Languages and Compilers for Parallel Computing*, Minneapolis, Minnesota, June 1997.
- [84] R. F. V. der Wijngaart and H. Jin, “NAS Parallel Benchmarks, Multi-Zone Versions,” Tech. Rep. NAS Technical Report NAS-03-010, July 2003.
- [85] D. Bailey, E. Barszcz, L. Dagum, and H. Simon, “NAS parallel benchmark results,” in *Proc. Supercomputing*, Nov. 1992.

- [86] D. H. Bailey, E. Barszcz, J. T. Barton, D. S. Browning, R. L. Carter, R. A. Fatoohi, P. O. Frederickson, T. A. Lasinski, H. D. Simon, V. Venkatakrisnan, and S. K. Weeratunga, "The NAS Parallel Benchmarks," *The International Journal of Supercomputer Applications*, Tech. Rep., 1991.